

**Coatings with Inversely Switching Behavior.
New Applications of Core-Shell Hydrogel Particles.**

D I S S E R T A T I O N

zur Erlangung des akademischen Grades

Doctor rerum naturalium

(Dr. rer. nat.)

vorgelegt

**der Fakultät Mathematik und Naturwissenschaften
der Technischen Universität Dresden**

von

HORECHA MARTA

geboren am 04 August 1976 in Lviv, Ukraine

Eingereicht am 22.07.2010

Die Dissertation wurde in der Zeit von Oktober 2006 bis
Juli 2010 im Institut für Polymer Forschung, Dresden angefertigt

1.	INTRODUCTION	1
1.1	PROLOGUE AND MOTIVATION	1
1.2	GOAL OF THE WORK: CREATION OF SURFACES WITH INVERSELY SWITCHABLE WETTING BEHAVIOUR	5
1.3	OUTLINE	9
2.	THEORETICAL BACKGROUND AND LITERATURE OVERVIEW	10
2.1	WETTING PHENOMENA	10
2.2	SWITCHING OF SURFACE PROPERTIES BY MEANS OF RESPONSIVE SUBSTANCES AT INTERFACE	20
2.3	CONCEPTS TO OBTAIN AN INVERSE SWITCHING EFFECT OF SURFACE WETTABILITY	25
2.4	HYDROGELS AS A “SMART” MATERIAL FOR SURFACE MODIFICATION.....	29
3.	EXPERIMENTAL TECHNIQUES.....	37
3.1	ATOMIC FORCE MICROSCOPY.....	37
3.2	SCANNING ELECTRON MICROSCOPY	43
3.3	DYNAMIC LIGHT SCATTERING.....	46
3.4	DROP SHAPE ANALYSIS TECHNIQUE (DSA)	51
3.5	OTHER METHODS.....	53
4.	RESULTS AND DISCUSSIONS	54
4.1	EVALUATION OF PARAMETERS OF INVERSE SWITCHING.	54
4.2	SYNTHETIC APPROACHES TO OBTAIN THE CORE-SHELL STRUCTURES HAVING HYDROGEL CORE AND HYDROPHOBIC SHELL	65

4.2.1	SUBSTRATE SELECTION AND CHARACTERIZATION	68
4.2.2	“ONE-POT” SYNTHETIC ROUTE TO CORE-SHELL PARTICLES VIA INVERSE SUSPENSION POLYMERIZATION	70
4.2.2.1	<i>Synthesis and characterization of shell-forming polymeric surfactant</i>	<i>73</i>
4.2.2.2	<i>Selection of the monomer for the formation of inner part of core-shell particles</i>	<i>75</i>
4.2.2.3	<i>Synthesis of core-shell particles via inverse suspension polymerization and their characterization</i>	<i>78</i>
4.2.2.4	<i>“Contraphilic” surfaces prepared using core-shell particles synthesized by “one-pot” approach.....</i>	<i>83</i>
4.2.3	PREPARATION OF THE CORE-SHELL PARTICLES VIA “BOTTOM-UP” APPROACH.....	93
4.2.3.1	<i>Synthesis, characterization and tuning the composition of core-forming microgels with suitable swelling effect.</i>	<i>95</i>
4.2.3.2	<i>Formation of loose periodic arrays of microgels on the substrate</i>	<i>102</i>
4.2.3.3	<i>Surface density as a function of swelling effect</i>	<i>107</i>
4.2.3.4	<i>Measurements of the maximal pressure developing upon the swelling of the microgels</i>	<i>108</i>
4.2.3.5	<i>Chemical modification of hydrogel microparticles.....</i>	<i>110</i>
4.2.3.6	<i>Confined swelling of the microgels.....</i>	<i>115</i>
4.2.3.7	<i>Adsorption of oppositely charged nanoparticles on the surface of microgels.....</i>	<i>124</i>
4.2.3.8	<i>Grafting-from polymerization of shell on the microgels surface.....</i>	<i>128</i>
4.2.3.9	<i>Utilization of polyisoprene latex for PI shell formation</i>	<i>134</i>
4.2.3.10	<i>Cross-linking of the shell.....</i>	<i>142</i>

4.2.4 SWITCHING PROPERTIES OF HYDROPHILIC SURFACES COVERED WITH HYDROPHOBIC CORE-SHELL MICROGELS SWELLABLE IN WATER	146
4.2.4.1 <i>Responsive surfaces fabricated via “bottom-up” approach: in-situ AFM monitoring of the water-induced change of the surface coverage.....</i>	<i>146</i>
5. SUMMARY	153
6. REFERENCES	159

LIST OF ABBREVIATIONS

AA -	acrylic acid	PAA -	poly(acrylic acid)
AAM -	acrylamide	PAAM -	polyacrylamide
AEMA -	2-aminoethyl methacrylate	PBPA -	poly(benzophenone acrylate)
AFM -	Atomic Force Microscopy	PDEA -	poly(2-(diethylamino)ethyl methacrylate)
AIBN -	azo-bis-(isobutyronitril)	PDI -	polydispersity index
BP -	4-hydroxybenzophenone	PE -	polyethylene
BPA -	4-acryloyloxybenzophenone	PEG -	poly(ethylene glycol)
DAIB -	(diacetoxy) iodobenzene	PEO -	poly(ethylene oxide)
DCC -	<i>N,N</i> -dicyclohexylcarbodiimid	PGMA -	poly(glycidyl methacrylate)
DLS -	Dynamic Light Scattering	PI -	polyisoprene
DMAP -	4-(dimethylamino)pyridin	PMMA -	poly(methyl methacrylate)
DMF -	<i>N,N</i> -dimethylformamide	PNIPAM -	poly(<i>N</i> -isopropylacrylamide)
DSA -	Drop Shape Analysis	PS -	polystyrene
EDC -	1-ethyl-3-[3-dimethyl aminopropyl] carbodiimide hydrochloride	PTFE -	polytetrafluoroethylene
GPC -	Gel Permeation Chromatography	PVA -	poly(vinyl alcohol)
HEMA -	2-hydroxyethyl methacrylate	P4VP -	poly(4-vinylpyridine)
HLB -	hydrophilic-lipophilic balance	RMS -	root mean square
KPS -	potassium persulfate	SAM -	self-assembled monolayer
LCST -	low critical solution temperature	SDS -	sodium dodecylsulfate
MAA -	methacrylic acid	SEC -	Size Exclusion Chromatography
MBA -	<i>N,N</i> -methylenebisacrylamide	SEM -	Scanning Electron Microscopy
NaHSS -	<i>N</i> -hydroxysulfosuccinimide	TGA -	Thermogravimetric Analysis
NBA -	4-Nitrobenzaldehyde	TMP -	trimethylpentane
NIPAM -	<i>N</i> -isopropylacrylamide	tBA -	tertbutylacrylate
NMR -	Nuclear Magnetic Resonance	VA -	vinylamine
		VPT -	volume phase transition
		WCA -	water contact angle

1. INTRODUCTION

1.1 PROLOGUE AND MOTIVATION

Surface wettability has been a topic of scientific investigation for over 60 years. This great level of interest has been fueled by the fundamental importance of wetting phenomena in various technological applications, e.g. textile technology, production of water-repellant materials^[1], spraying of paints and agricultural chemicals^[2], penetration of ink in paper, impart to fabrics adsorbing and desorbing properties^[3], etc. Hydrophobic and superhydrophobic materials are widely used for many functions including the design and manufacture of self-cleaning panes^[4], waterproof textiles, microfluidic devices^[5], hydroprotection of reinforced concrete constructions, corrosion protection^[6], biofouling protection^[7], prevention of capillary condensation and icing, shielding of surfaces against radioactive, organic, and inorganic contaminations and many others.

With such a high degree of applications in modern technologies, the materials used are themselves the subject of modification with the purpose of controlling their surface properties. It is noteworthy to mention that the cost of materials being modified is an extremely important factor for the evaluation of their innovative potential. Usually, high costs of raw materials are the main limiting factor, which restrict manufacture of the final product with desired technical properties. Fortunately, wettability is a surface feature, which is mainly defined by the structure and properties of a few nanometers thick superficial layer rather than by the characteristics of the bulk material as a whole. Therefore, one of the most productive and cost-efficient methods for the creation of novel materials is to develop an

external coating on the surface of existing ones. substances with dissimilar properties are usually used as coatings in order to correct or totally change the surface properties of the raw material.

As a practical aspect of a material usage is often defined by its physical and chemical surface properties, numerous tasks could not be realized without the use of surface modifications, coatings and thin film technology. Coating techniques can be used to improve a material technical feature, look and performance. Routinely used examples of such materials applications include wear-resistant coatings, which are used on tools or machine parts, or thin films on paned glass which optimize the transmission or reflection of selected parts of the electromagnetic spectrum. Many innovative products would not even exist without the special properties provided by thin films. Prominent examples are computer hard disc drive, optical data storage media like CDs, DVDs and Blue-ray disks, flat displays and thin-film solar cells. Therefore, the need for efficient and effective methods of surface modification becomes increasingly important in allowing the production of far superior products in terms of altered mechanical (wear, friction resistance,) chemical (corrosion protection, permeation control, enhanced biocompatibility, thermal insulation), electrical (improved conductivity) or optical (transmission, reflection, absorption, colour adjustment) properties.

Coatings can provide complex functionalities to surfaces, significantly changing their properties, compared to uncoated material. Many coating deposition techniques and surface treatments are available for this purpose. If secondary material is added to the surface, the process is referred to as coating deposition process; however, if the surface microstructure and / or chemical composition are altered, then the process is referred to as a surface modification process. Selection of the coating deposition or surface modification techniques depends on the functional requirements, shape, size and

properties of the substrate, nature of the coating material, compatibility, adhesion, coating equipment and cost.

Coatings applied by deposition techniques are basically of two types - decorative and functional. Decorative coatings are widely used in the automotive, home appliances, hardware, costume, jewellery etc. Functional coatings can improve adhesion, wettability, corrosion resistance, wear and scratch resistance, chemical stability of a raw materials, they can also provide conductive properties to a surface, correct reflection or modify optical properties, etc.

Recently, the process of development and the improvement of modern coatings quality have turned to an idea of creation of adaptive or sensitive (also called “smart” or “intelligent”) surfaces. Based on dynamically active systems, usually achieved by a combination of materials with opposite properties, such sensitive surfaces are able to adapt their structure by the rearrangement of interfacial components under the changing of environment in order to minimize surface energy. A number of switchable or adaptive coatings, which react to different stimuli from the environment, can be created using this principle.

Surfaces with switchable wetting behaviour, able to change their properties from hydrophilic to hydrophobic and vice versa, are of considerable interest because of their potential applications including tissue engineering and cell growth, creation of “intelligent” breath-active and water-repelling textiles, self-regulating valves. In particular, the design of a new generation of such “smart” materials and surfaces is required for new concepts of sensors^[8], drug delivery systems^[9], microfluidic devices^[10], and colloidal assembly techniques^[11].

Since the wetting behaviour of material is strongly dependent on the surface structure and chemical composition, it is possible to prepare the surface as a dynamic system that consists of two

components having opposite properties and with components ratio alterable with the environmental changes. As environmental conditions change, the ratio of the components will adjust. The application of such responsive materials presents the possibility to create tailored surfaces designed to adapt to environmental conditions. Altering the balance between two components of the system shifts the system properties toward an energetically favourable component what enables the temporary stabilization of the system until next stimuli is applied.

It was shown that the modulation of surface hydrophilicity could be triggered by light irradiation^[12], temperature^[13], electric field^[14, 15], pH^[8] or mechanical stress^[16]. A general approach to create smart surfaces that become hydrophilic in polar and hydrophobic in apolar solvents has been already developed using above described principle^[17]. However, for many practical applications, e.g. air breath-active but water repellent textile or dynamic self-cleaning surfaces, the inverse or “contraphilic” response to external stimuli is desired.

1.2 GOAL OF THE WORK: CREATION OF SURFACES WITH INVERSELY SWITCHABLE WETTING BEHAVIOUR

This thesis has been focused on the design and development of the concept of an inversely switchable surface coating, which becomes *hydrophobic in aqueous media* that is opposite to the reaction of the conventional responsive systems (as discussed in Chapter 2.2). The swelling property of hydrogels was exploited as a driving force to change the components ratio in presence of water.

In order to realize the inverse switching of surface wettability or in other words to achieve the “contraphilic” behaviour of the surface, it was suggested to cover the hydrophilic substrate with loosely packed *core-shell particles*, which have *water swellable cores* and *hydrophobic elastic shells*. The shell should not prevent the water penetration to the core but has to be hydrophobic enough for providing the surface hydrophobic effect of whole particle.

Schematically the suggested principle of inverse switching of surface wettability is represented on the Fig.1-1.

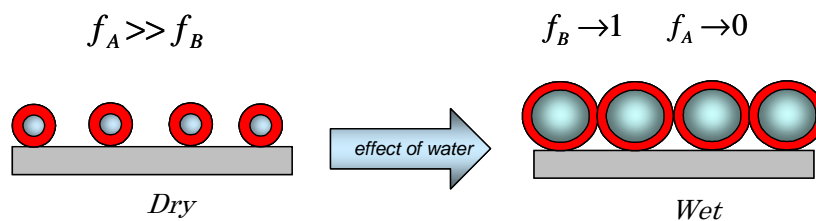


Figure 1-1 Schematically represented principle of inversed switching of wettability. The effect of increase of hydrophobicity caused by swelling of core-shell hydrogels having hydrophobic shell on the surface; the fractions of hydrophilic surface and hydrophobic particles are f_A and f_B respectively.

According to the Cassie’s equation, the wetting behavior of the two-component heterogeneous surface depends on the coverage ratio of both

components (f_A and f_B) and their own contact angles (Θ_A and Θ_B) (discussed in details in Chapter 2.2). Therefore, the contact angle of the described complex system in a dry state (Fig.1-1, left) can be estimated as:

$$\cos \Theta = f_A \cos \Theta_A + f_B \cos \Theta_B \quad [1-1]$$

f_A, f_B - the fractions of particles on the surface (A) and free surface area (B), Θ_A and Θ_B - the contact angles of material of particles shell and substrate respectively.

After the particle swelling, resulted in an increase of the surface coverage of up to 100% (Fig.1-1, right), the surface properties, in particular the contact angle, will be determined only by the properties (wettability) of the particles surface itself and presented as:

$$\cos \Theta = \cos \Theta_A \quad [1-2]$$

In this state the intrinsic properties of the substrate are not important because the underlying substrate will not interact with water.

Therefore, to achieve the maximal switching effect, occupation of the surface with hydrophobic core-shell particles has to be minimal in their dry state. With the reasonably small fraction of hydrophobic surface area, the resulting wettability of the composite surface will be largely defined by the properties of the hydrophilic substrate (Fig.1-1, left). However, upon exposure to water, particles' cores will swell and expand the hydrophobic shells over the whole surface, causing the surface properties to be determined only by the properties of the hydrophobic shell (Fig.1-1, right).

However, this facile approach of inverse switching would work only with the proper optimization of all parameters of the system, which is the main subject of this work.

The prerequisite of the desired opposite-switching behaviour is dependent on the intrinsic material properties of the core-shell particles as well as on the construction, quality and optimal placement and arrangement of the particles on the surface. The following important issues must be settled in order to achieve the proposed task:

- **Swellability of the Hydrogel Core**

The core of the core-shell particles must be able to undergo *reversible* swelling in specific range in such a way that in their dry state the microgels have to occupy a minor part of the surface, whereas upon contact with water they have to swell up to a certain volume limit, sufficient to cover the whole surface. In this case, the “under-swelling” is strongly undesired since it will reduce the switching range. On the other hand, the “over-swelling” is also unfavourable due to possible disturbance of the surface properties of particles and increase of coating roughness.

- **Shell Properties of the Microgels**

The shell of the microgels must provide specific hydrophobic properties to the surface and follow the changing of microgels size upon swelling-collapsing process by changing its thickness. The shell must also be permeable for water and minimally impede the process of particle swelling.

- **Three-Dimensional Swelling-Deswelling of Microgels on the Substrate**

The core-shell particles must undergo three-dimensional (3D) swelling-deswelling on the substrate since alternative one-dimensional (normal to the substrate plane) collapse will

lead to a projection of the particles upon drying without recovering the hydrophilic surface.

- **Homogeneous Distribution**

The core-shell particles must be homogeneously distributed over the whole surface without clustering to ensure uniform and adequate surface coverage.

- **Attachment of Core-Shell Particles to the Substrate**

The core-shell particles must be firmly attached to the substrate to avoid washing away during the contact with water, having in the same time a certain degree of spatial freedom for reversible swelling-deswelling.

1.3 OUTLINE

The thesis is organized in 5 major Chapters. In Chapter 1, the general introduction has been given on surface coatings, which allow to adjust the surface properties in predictable way. The peculiarities of switchable surfaces are pointed out, as well as motivation and goal of current work were defined.

Chapter 2 represents theoretical background of wetting phenomena and literature overview of existing approaches about switchable surfaces accenting the hydrogels as a promising material for responsive surface coatings.

Descriptions of experimental techniques and methods used in current work are given in Chapter 3.

Chapter 4 is devoted to theoretical prerequisites and the progress in achievement of inversely switchable wettability (“contraphilic” behaviour) of the surfaces using hydrogel particles with hydrophobic shell as coating building blocks. The essential parameters of target system were evaluated, including microgels properties and shell material requirements, as well as the achievable change of surface coverage due to the swelling of core-shell particles deposited on the surface and, thereafter, the potential change of the surface contact angle. The main part consist of experimental results related to the development of two basic strategies of preparation of desired core-shell particles with hydrogels core and water permeable hydrophobic shell, namely “one-pot” and “bottom-up” approaches. The developed ways to obtain the “contraphilic” switchable surface coatings are presented. Hereafter, the results concerning the wettability of obtained surfaces are shown and possible courses of systems optimizations are traced.

Finally, the summary of the work and possible directions of further investigations and applications of developed materials are given in Chapter 5.

2. THEORETICAL BACKGROUND AND LITERATURE OVERVIEW

2.1 WETTING PHENOMENA

Wetting is the ability of a liquid to maintain contact with a solid surface, resulting from intermolecular interactions. The term “wettability” means degree of wetting and is determined by the balance between adhesive and cohesive forces. Adhesive forces between liquid and solid cause a liquid drop to spread across the surface. Meanwhile, cohesive forces within the liquid cause the drop to ball up and avoid contact with the surface. At thermal equilibrium, a discrete and a measurable contact angle is observed between the horizontal surface and the droplet exactly at the circular solid/liquid/vapour three-phase contact line. Depending on the type of surface and liquid used this angle (Θ_{eq}) creates a cone (or a cylinder if the contact angle is 90°) with a tip on the water side of the surface if $\Theta_{eq} < 90^\circ$ (high wettability) or with a tip on the solid side of the surface if $\Theta_{eq} > 90^\circ$ (low wettability) (Figure 2-1).

Contact angles substantially less than 90° (low contact angles) usually indicate that wetting of the surface is favourable and the liquid will spread over the surface. Contact angles greater than 90° (high contact angles) generally

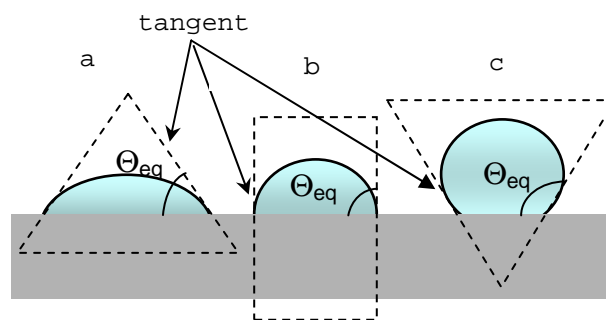


Figure 2-1 Determination of contact angle and schematic representation of different degree of wettability. (a) $\Theta_{eq} < 90^\circ$, (b) $\Theta_{eq} = 90^\circ$, (c) $\Theta_{eq} > 90^\circ$.

mean that wetting of the surface is unfavourable and the liquid will minimize contact with the surface and form a compact droplet.

The thesis that there is an “appropriate angle of contact” between the liquid exposed to the air and the solid for every solid/liquid pair was first suggested in 1804 by Thomas Young in his “An Essay on the Cohesion of Fluids”^[18]. Later, this angle was re-termed as the “contact angle”, related to the surface tension at the meeting point of the three-phase junction and expressed as a

relationship in mathematical form. It is known now as Young-Laplace Equation (Eq.2-1) and describes the static wetting phenomena on a macroscopic scale. Equation 2-1, written in terms of forces (or interface tensions) is general and valid for all types of surfaces: smooth,

rough, clean, dirty, homogeneous or heterogeneous. It considers all forces (simple or complex), which act on the droplet at the point of junction of three phases (solid, liquid, gas), and consequently determines the resulting shape of the droplet on the solid surface (Fig.2-2).

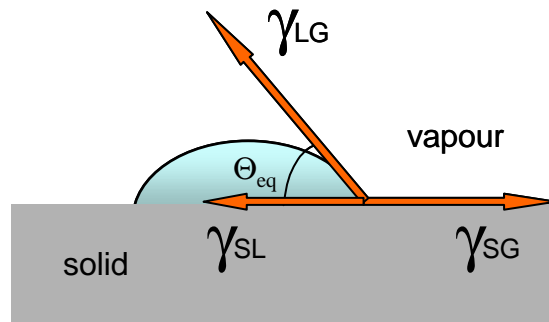


Figure 2-2 Schematic representation of forces balance acting on a liquid droplet on a solid surface.

$$\cos \theta_{eq} = \frac{\gamma_{SG} - \gamma_{SL}}{\gamma_{LG}} \quad [2-1]$$

γ - the surface tension at corresponding interface (S-solid, L-liquid, G-gas),

θ_{eq} - Young's equilibrium contact angle.

Later, Wenzel and Cassie described the interactions between the three phases in contact in terms of energies^[19, 20] connecting in such a way surface free energies of phases with the equilibrium contact angle θ_{eq} .

In many publications^[20-25] these terms are used interchangeably because the interfacial surface tension is numerically equal to the characteristic interfacial specific surface energy and both values are related to the one unit of actual surface area. To clarify, these terms are not identical and difference between them should be taken into consideration when dealing with precise calculations. Surface tension is a tensor that acts perpendicularly to a line on a surface and represents a force per unit length (dyn/cm). Surface tension can be figured as a force that contracts the surface of a drop at a contact line. The surface energy, in one's turn, is a scalar nondirectional property of surface area, which constitutes the energy per unit area (erg/cm²) and can be realized as a work required for creation of additional surface area.

Since the values of γ_{SG} and γ_{SL} are not directly assessable from the experimental data, the Young equation is often used for determination of the difference ($\gamma_{SG} - \gamma_{SL}$), which is referred as wetting tension or adhesive tension, by means of the experimental values of θ_{eq} and γ_{LG} . Here, the Young equation assumes that the solid surface is smooth, homogeneous, isotropic, non reactive and non deformable.

Empirical equation of state for correlation between interfacial tensions γ_{SL} , γ_{LG} and γ_{SG} was proposed by Good et.al^[26] (Eq.2-2):

$$\gamma_{SL} = \gamma_{SG} + \gamma_{LG} - 2\phi(\gamma_{SG}\gamma_{LG})^{1/2} \quad [2-2]$$

where ϕ is a Good's adjustable parameter. By Neumann et al^[27] parameter ϕ was calculated as a function of γ_{SG} and γ_{LG} (Eq.2-3):

$$\phi = e^{-\beta(\gamma_{LG}-\gamma_{SG})^2} \quad [2-3]$$

where β is a constant which was experimentally found of 0.0001247 (mJ/m²)⁻².

The combination of this equation with the Young relation results in Equation 2-4:

$$1 + \cos \theta = 2 \sqrt{\frac{\gamma_{SG}}{\gamma_{LG}}} e^{-\beta(\gamma_{LG} - \gamma_{SG})^2} \quad [2-4]$$

Thus, knowing the liquid surface tension γ_{LG} and contact angle θ , solid surface tension γ_{SG} can be easily calculated.

Taking into account that real surfaces are far from ideal (no perfect smoothness, rigidity or chemical inhomogeneity), in dynamic wetting process the contact angle passes through a number of metastable states at the solid-liquid-gas interface while the droplet changes. The contact angles of all these states have their own values, differing from an ideal equilibrium static state. Whereas the equilibrium contact angle describes static wetting conditions, dynamic wetting is usually discussed in terms of spreading coefficients and contact angle hysteresis^[23, 28-31], defined as a difference between advancing (θ_a) and receding (θ_r) contact angles^[24] (Eq.2-5).

$$\Delta\theta = \theta_a - \theta_r \quad [2-5]$$

To clarify, the angle formed when the drop front advances is called advancing contact angle and characterize the ability of the liquid to wet the surface. The angle formed when the drop front recedes is known as receding contact angle and describes the ability of the liquid to dewet from the surface.

Liquid which advance over the solid surface provides a higher contact angle than when it recedes (Fig.2-3, adapted from Ref. [32]).

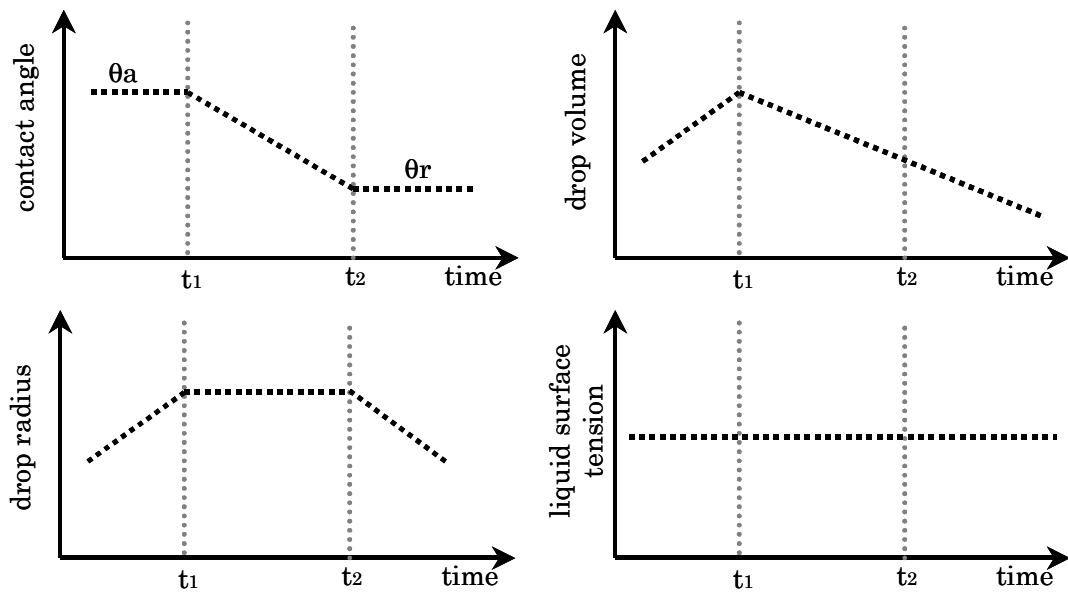


Figure 2-3. Schematic representation of liquid drop development on non-ideal surface in a typical wetting experiment. Starting from the time 0 liquid is continuously added to the drop through the vertically positioned thin needle. While the drop advances over the surface, its radius and volume increase. At the time t_1 liquid starts to be removed from the drop, causing the decrease of the drop volume. The drop radius remains constant for the time from t_1 to t_2 and then decreases. Initially constant contact angle θ_a start to decrease to the value of θ_r , and then remains constant till the end of receding of the drop.

The deviation of the intrinsic contact angle from the apparent one depends on a number of different factors. Among them surface composition (e.g. chemical heterogeneities) and physical properties (such as roughness, geometry) are considered by many researcher as critical parameters [19, 20, 24, 33-42].

One of the most known and studied deviations from the ideal state is the surface's rough texture. The roughness of the surface causes different competitive regimes of wetting, otherwise called homogeneous and heterogeneous wetting regimes. A homogeneous wetting regime was described by Wenzel's theory of wetting^[19, 43]. In Wenzel model it is assumed that liquid is in complete contact with a rough surface, totally filling its grooves and covering the surface ledges without any trapped air

in the grooves of the surface (Fig.2-4, a). The Wenzel contact angle, θ_w , is described by Equation 2-6:

$$\cos \theta_w = r \cos \theta_{eq} \quad [2-6]$$

r - the surface roughness, defined as the ratio of actual surface area to the geometrically projected surface area.

Since the roughness factor is greater than 1, Equation 2-6 predicts an increase of the Wenzel contact angle with roughness if the equilibrium contact angle of surface is greater than 90° and decrease if lower than 90°. It should be mentioned that this conclusion not always agree with experimental observations, in fact with increase of roughness advancing contact angle increases but receding one decreases. Wenzel equation did not distinguish between advancing and receding contact angles, therefore any correlation between roughness and hysteresis cannot be predicted.

When dealing with a heterogeneous wetting regime, the Wenzel model is not sufficient. A more complex model is needed to describe how the apparent contact angle changes when various materials are involved. The heterogeneous wetting regime could be described by Cassie-Baxter model^[33], which assumes that air is trapped between surface features and the liquid droplet laying on the top of the features at the solid-air interface (Fig.2-4, b).

Cassie-Baxter contact angle, θ_c , is defined by the Equation 2-7:

$$\cos \theta_c = f(r \cos \theta_{eq} + 1) - 1 \quad [2-7]$$

f - the fraction of a solid area on the mixed solid-air surface.

The model of Cassie-Baxter is a development of Wenzel’s model, which takes into account two possible surface defects: roughness and porosity. If the surface is rough, but not porous, the fraction of solid area f will be equal to 1 and Cassie–Baxter equation adopts the form of Wenzel equation.

Later, Cassie extended his analysis of rough surfaces to chemically heterogeneous surfaces composed of geometrical areas f_1 and f_2 of different materials having different contact angles^[22]. He stated that the resulting contact angle of composite surface is defined by surface area fraction and contact angle of each component (Eq.2-8).

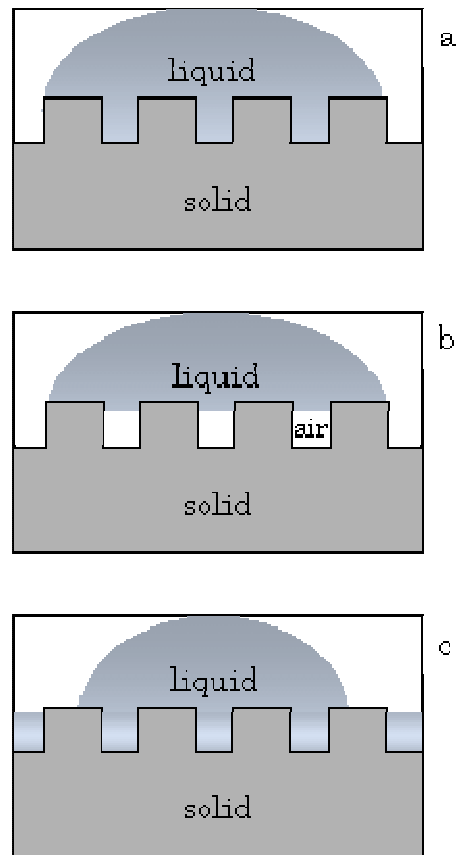


Figure 2-4 Schematic representation of liquid/solid interface for Wenzel (a), Cassie-Baxter (b) and wicking (c) wetting regimes.

$$\cos \theta = f_1 \cos \theta_1 + f_2 \cos \theta_2$$

[2-8]

f_1, f_2 - fractions of a surface area on the mixed surface with different contact angles θ_1 and θ_2 .

The wicking regime (Fig.2-4, c) valid when the drop sits on the surface composed with solid and liquid. Bico et al^[44] showed that in this case contact angle could be described by the Equation 2-9.

$$\cos \theta = 1 - f(1 - \cos \theta_{eq}) \quad [2-9]$$

In this regime, liquid fills the grooves of the rough surface remaining only small fraction f of the upper part of the structures contacting with a gas phase. At these conditions $\theta_{eq} < \theta_c$, where θ_c is a critical value of contact angle when $\cos \theta_c = (1-f)/(r-f)$.

After works of Wenzel and Cassie, Johnson and Dettre^[23] extended the model of wetting and postulated that surface roughness and chemical heterogeneity permit the existence of a large number of metastable configurations. For rough surface, the number of such configurations depends on the number of crests under the droplet, and therefore, are a function of drop size and roughness factor (r). The contact angle, which is observed in a real system, is considered to be dependent on the energy barriers levels between the metastable states and on the ability of a droplet to cross over these barriers. The height of this barrier was found to be approximately directly proportional to the height of the grain and approximately independent of their separation distance. The energy barriers for composite heterogeneous surfaces (Cassie regime) are much lower than for homogeneous non-composite ones (Wenzel regime). The absolute energetic minimum occurs in this case at the Wenzel's angle (stable equilibrium). The energy barriers are higher near Wenzel's angle (θ_w) and approach zero at the maximum advancing and the minimum receding angles. The energy barriers increase with increasing ridge height and ridge slope. Therefore hysteresis increases with an increasing roughness. It has also been demonstrated that at contact angles $< 90^\circ$ Wenzel's angle decreases with an increase of surface roughness, while for the contact angles $> 90^\circ$, Wenzel's angle increases with an increase of surface roughness.

Ideal heterogeneous surface hysteresis was explained by the same authors as a balance between the vibrational (mechanical) energy of a

drop and the energy barriers levels between allowed metastable states^[31]. The absolute minimum of drop free energy for such type of surfaces occurs at the Cassie's angle (θ_C). The energy barrier in this state is maximal and approaches zero at contact angles θ_1 and θ_2 , corresponding to the contact angles of fraction on the mixed surface. The authors predicted the sharp transition from the Wenzel regime to the Cassie regime with an increase of roughness. At the same time, the contact angle hysteresis increases until the critical value of roughness and then decreases. There were also made experimental confirmation of these conclusions^[45, 46].

Accordingly, both surface roughness and heterogeneity can cause contact angle hysteresis. Generally, hysteresis will be negligible when the roughness (r) is below 0.1-0.5 μm , or when the lateral dimensions of heterogeneous phase is smaller than 0.1 μm ^[47]. As demonstrated for a sinusoidal surface, and postulated that above a certain value of r , the Cassie-Baxter contact angle is the preferred equilibrium state (i.e. the Gibbs free energy is lower in the Cassie-Baxter state). Above this value of r , a further increase in the roughness ratio seems to be inefficient, since the slope of the increase in θ_C with the r value is much lower than that of θ_W .

Recently, based on experimental data possibility of existence of two contact angles (Wenzel and Cassie) on the same rough surface was demonstrated^[41, 48]. Dependence of the conditions of drop formation on its resulting state was found. The effect of surface geometry on the transition, which can occur between the Wenzel and Cassie states, was discussed. The energy balance was proposed as a criterion, which estimate the possibility of the transition of droplet from Cassie to Wenzel regime. The authors stated that even if the Wenzel state is an energetically more efficient, it does not surely mean that drop will get to this state. The transition can only occur if the energy barrier between two states can be overcome.

Wenzel and Cassie-Baxter equations were also reviewed by Marmur^[29] from a proper mathematical-thermodynamic perspective. This allowed the conditions for determining the transition between the homogeneous and heterogeneous wetting regimes to be defined. In particular, he added a new condition (an occurrence of the local minimum of Gibbs free energy) that is necessary for existence of the heterogeneous wetting regime and demonstrated that when this condition is violated, the homogeneous wetting regime is the natural state, even though the Cassie-Baxter equation may be satisfied.

It was also shown ^[29, 49] that the above-mentioned equations Eq.2-6, Eq.2-7 and Eq.2-8 are valid only if the droplet size is sufficiently large compared to the typical roughness scale.

The above theories state the roughness and heterogeneity of the solid substrate and correlation between the surface energies of three coexisting phases as milestones of wettability. On the contrary, some scientists provide the arguments that not the liquid-solid interface, but the three-phase structure at the contact line controls the contact angle ^[50, 51]. They stress that the contact angle and hysteresis are the functions of the contact line structure and the kinetics of drop movement, rather than thermodynamics dictates wettability^[52-55]. The reasons for such conclusions were the facts that the surfaces with completely different topographies can have the same fraction of solid area in contact with liquid, but absolutely different contact line structures. Depending on either continuous (pinned drop) or discontinuous (unstable drop) contact line is formed, the advancing and receding contact angles can significantly differ from the calculated equilibrium Cassie angle^[54].

2.2 SWITCHING OF SURFACE PROPERTIES BY MEANS OF RESPONSIVE SUBSTANCES AT INTERFACE

The wetting behavior of polymer surfaces is of fundamental importance for diverse applications such as paints and coatings, microfluidics, cosmetics or biomaterials. The outermost molecular layer controls the surface response to external stimuli such as initial wetting response to water. Thus, changes on the micro- to nanoscale may be employed to control macroscale wetting behavior^[56, 57].

Advances in materials science requirements have created a need for dual surface properties that frequently are in conflict. For example a given material, depending on the conditions under which it is used, must be hydrophobic or hydrophilic, acidic or basic, conductive or non-conductive, adhesive or repellent, or must be able to release or absorb chemical compounds. Investigation into systems, which are able to change material surface properties began a few decades ago as a response to rising interest in “smart” or “intelligent” materials. Since 1975, when one of the first investigations into the reformation of hydrogel polymer chains at the interface had been done^[58], hundreds of theoretical and experimental studies in this field have been performed. Different strategies have been utilized for the creation of the systems, which are able to change the surface properties including wettability, adhesion and lubrication, biological compatibility and others, as a response to the variations in environmental stimuli^[12, 15]. The major response mechanisms are based on a fundamental tendency of a system to minimize the interfacial energy between the surface and the environment that causes, for example, the reorientation of amphiphilic polymer chains. Thus, homopolymers, end-functionalized polymers, random copolymers, block copolymers, graft-copolymers, mixed polymer brushes, and other surface systems have already been employed in the fabrication of

switchable surfaces. To illustrate this further, the restructuring of the surface of the homopolymer poly(2-hydroxyethyl methacrylate) during its exposure to different solvents was reported in previous scientific studies^[59, 60]. By treating the polymer with a polar solvent an increase of the surface polarity was observed changing its original properties, as intended. Inversely, treatment of the same polymer with a non-polar solvent resulted in a decrease of the surface polarity. Based on the reaction of the material it becomes apparent that the hydrophobic backbone and hydrophilic side groups of the polymer are made to act as the amphiphilic system.

A similar phenomenon was also observed for random copolymers. Hopken and Moller studied reorganization of styrene-based polymers containing perfluorocarbon segmented side groups during annealing^[61]. They reported a drastic reduction of the surface tension when only a few percent of the fluorocarbon-containing monomers were incorporated into the polymer.

Switching behaviour has also been observed for various segmented polymers, block copolymers and graft copolymers^[62]. For instance, segmented polyurethanes having perfluoropolyether, poly(dimethylsiloxane) and poly(ethylene glycol) segments, exhibited a range of oleophobic, hydrophobic, and hydrophilic properties in response to the polarity of the contacting medium, which was used as an environmental stimuli. The contact angle was observed to decrease from 120° to 34° when the polymer came into a contact with water. Due to this response, it was argued that the oleophobic and hydrophobic properties of polyurethane caused by the segregation of hydrophobic segments at the polymer-air interface. It was revealed that the same surface became hydrophilic, presumably due to the segregation of the PEG segments at the polymer-water interface^[63].

In contrast to the above described switchable surface systems, where adaptive properties of the surface are inherited from the bulk material,

purposeful modification of the surface is a more elegant and, in some cases, a more effective way to introduce the adaptive properties to the material. The term “modification” in this context means either changing the chemistry of the very top layer of the bulk material, or covering the substrate with a thin layer of switchable surface system.

Thus, the oxidation of low-density polyethylene (PE) film with chromic acid resulted in the material bearing hydrophilic carboxylic and ketone groups in a thin oxidatively functionalized surface layer. This interface, which was hydrophilic and indefinitely stable at room temperature, became hydrophobic and similar in the wettability to the non-functionalized polyethylene film upon heating under vacuum^[56]. The changing of polarity of the surface was explained by migration of the carboxylic groups away from the interface.

Responsive surface systems can be designed by using a number of approaches including reversible swelling/collapse of water-soluble grafted polymers, phase separation in grafted di-block copolymers and polymer layers, consisting of two different kinds of end-tethered polymer chains (mixed brushes).

On particular surface coating system showing reversible switching between superhydrophobic and superhydrophilic state^[57] was recently reported. Poly(N-isopropylacrylamide) (PNIPAM) undergoes a phase transition at lower critical solution temperature (LCST) close to 32°. The layer of PNIPAM was prepared by surface-initiated atom-transfer radical polymerization. When the sample was heated above LCST, the water contact angle increased from 63,5° to 93° for the flat surface and from 0° to 149,3° for the rough one. Some surfaces have been designed to change wetting behaviour in response to an electrical potential^[15]. Here nanofilms undergo conformational transitions between a hydrophilic and moderately hydrophobic state in response to an electrical stimulus.

Another switchable surface coating system, able to change the wetting properties of the surface, was created by deposition of a

monolayer of photocromic monodendron polymer^[64]. UV-irradiation caused a microstructural reorganization of the polymer film, detectable with *Atomic Force Microscopy* (AFM), resulting in an increase of the water contact angle from 56° to 79°.

Switching of end-grafted monolayers of block copolymers, induced by treatment with the solvents, selective for each block, was theoretically predicted^[65, 66] and experimentally proved for the first time for the tethered PS-*b*-PMMA layer^[67]. The tethered di-block copolymer underwent reversible changes of water contact angles as the film was treated with different solvents. Initially, the film exhibited a contact angle characteristic for PMMA (75°). However, treatment with methylcyclohexane created an increase in contact angle characteristic for PS (98°). Finally, a subsequent treatment of the same sample with dichloromethane reversed this change.

Coatings able to reversibly switch their surface properties as a response to environmental stimuli, based on mixture of two different polymers at the surface have been designed and created^[68, 69]. For this purpose, polymers were chemically bonded to a solid substrate by one end to ensure stability of the surface system, while the properties (hydrophilic and hydrophobic) of the two grafted polymer species determined the switching range of the brush surface properties. If a binary brush is exposed to a polar solvent, selective for the hydrophilic polymer, it swells and occupies the top layer of the brush while the second hydrophobic polymer collapses and occupies the bottom layer. The opposite state of a brush surface can be obtained upon its exposure to a nonpolar solvent or upon annealing in vacuum (Fig.2-5, adapted from the Ref. [69]).

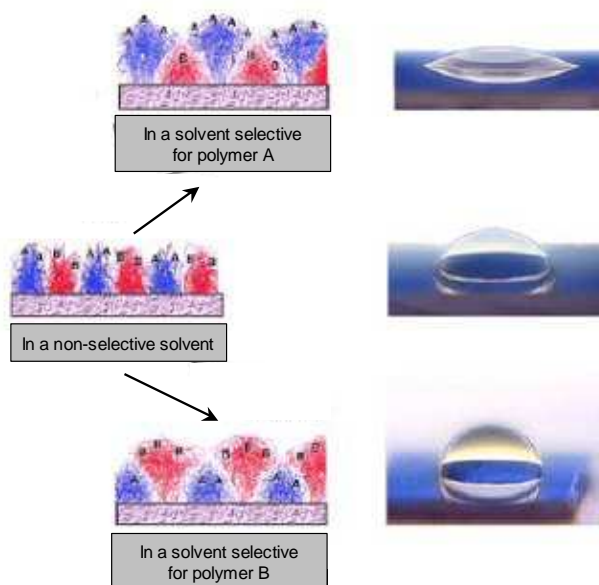


Figure 2-5 Switching behavior of the physico-chemical properties of the surface modified with a binary polymer brush upon exposure to the different solvents.

A binary brush, consisting of fluorinated polystyrene and poly(2-vinyl)pyridine was prepared on a plasma etched PTFE substrate. Sequential treatment of the samples with the solvents, selective for one of the components of the brush followed by a rapid drying of the surface, allowed the surface system to switch the wetting properties of the surface from superhydrophilic to superhydrophobic^[69].

2.3 CONCEPTS TO OBTAIN AN INVERSE SWITCHING EFFECT OF SURFACE WETTABILITY

From all examples described above, it is evident that amphiphilic surfaces become more hydrophilic in a polar medium and more hydrophobic if exposed to an apolar environment. This rather “natural” phenomenon, also known as self-adaptation, is based on the reorientation of polymer chains or segments in order to minimize the interfacial energy between the polymer surface and environment. However, for many practical applications opposite and less “natural” responses to external stimuli would be desired. Frustratingly, the designs of surface systems, which become *hydrophobic* upon treatment with *water* and hydrophilic upon treatment with apolar solvents (inverse switching or “contraphilic” behaviour), is still challenging task.

To the best of my knowledge, there has been only several successful examples in literature which reported the inverse or “contraphilic” switching of surface wetting properties^[70-72].

An unexpected case of increased hydrophobicity for oxidized 1,2-polybutadiene surfaces exposed to hot water was revealed recently by Ferguson et al.^[70] It was suggested that in lightly cross-linked systems rubber elasticity competes with the thermodynamic tendency of the surface to minimize surface free energy. As a consequence, the functional groups attached to the mobile segments stretch out of their random coil conformations. When the temperature is increased, the entropic loss translates into a restoring force and the chains recoil, pulling the hydrophilic functional groups away from the air-polymer interface and gradually increasing the advancing contact angle. On cycling, the surface eventually remains hydrophilic independent of temperature.

The “opposite switching” was also demonstrated for the polyurethane coating, containing semifluorinated and 5,5-dimethylhydantoin segments in a soft block^[71, 72]. The term “contraphilic” was suggested for this new wetting behavior because the surface coatings behave in a way opposite to the anticipated amphiphilic response. A difference of 27°, and after annealing even 38° in advancing contact angles for dry (68°) and wet (106°) states was measured using *Drop Shape Analysis Technique* (DSA) by static sessile drop and dynamic measurements. The “contraphilic” effect was found completely reversible upon drying the coating at 50°C in vacuum. The polyurethane having the highest semifluorinated-to-5,5-dimethylhydantoin ratio had the lowest initial contact angle and the “contraphilic” effect was maximized for this composition.

The mechanism of “contraphilic” wetting was also discussed in this work (Fig.2-6, adapted from the Ref. [72]). For the dry surface enthalpically driven hydrogen bonding of 5,5-dimethylhydantoin amide groups to acidic methylene hydrogens of semifluorinated groups disrupts the normal surface concentration of semifluorinated groups whereas the geometric arrangement of hydantoin N-H results in availability for hydrogen bonding with water (Fig.2-6, a). This accounts for the hydrophilic surface of the dry state. Upon exposure to water amide groups switch from hydrogen bonding with fluorinated moieties to stronger hydrogen bonding with water. As a result, semifluorinated groups are “released”, and the surface becomes hydrophobic (Fig.2-6, b). Upon dehydration of the surface, the initial hydrophilic wetting character is restored.

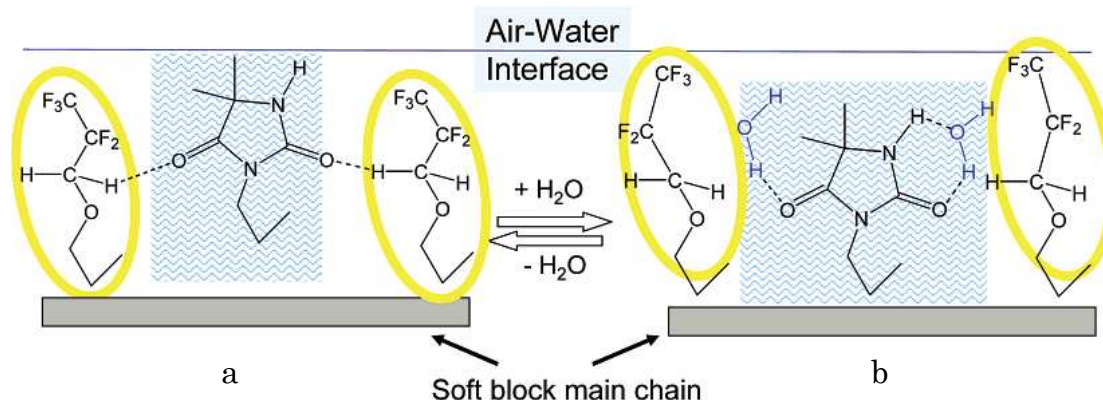


Figure 2-6 Mechanism of contraphilic wetting proposed by J. Wynne et al.
a – hydrophilic dry state, b – hydrophobic wet state.

Although this approach is very elegant, the “contraphilic” effect is provided by a delicate (and fortuitous) balance of hydrophobic interactions and hydrogen bonds in the amphiphilic network and thus this principle might be difficult to implement in other systems with an aim to optimize the “contraphilic” effect. The authors themselves concluded the obtained “contraphilic” effect as quite robust. One of the reasons is that the reaction-on-polymer approach, which was used to obtaining the 5,5-hydantoin-substituted soft blocks, was the only tractable method to obtain the desired soft block compositions. Unfortunately, this reaction has several significant disadvantages. First of all, the precursor polyurethane soft blocks are derived from relatively low molecular weight telechelics. The reaction-on-polymer method produces a soft block with residual initial groups and a chain architecture of unknown sequence distribution, and after substitution, the soft blocks have T_g (glass transition temperature) barely below ambient. Another shortcoming of switching system described above is its instability. If such coating is left at ambient humidity, the contact angle becomes a value that is intermediate between those of the dry and wet state. Therefore, the authors stated that simpler preparative method for creating soft block structures with better defined compositions and chain architectures is

still needed for making their approach of “contaphilic” surface behavior more reliable and predictable.

In the present work the main interest was to design a new switchable surface systems in which the ability to become more hydrophobic upon the contact with water can be modulated in a well predictable and precise way. These systems would be very promising candidates for many practical applications, for example, for fabrication of breathable (permeable for water-vapours) textiles, which become water-repelling (and as a result, a self-cleaning) in water, or for designing of “green” paints, which do not degrade the properties of natural building materials and are able to clean themselves in the rain.

2.4 HYDROGELS AS A “SMART” MATERIAL FOR SURFACE MODIFICATION

From the common point of view, a gel (from the lat. *gelu*—freezing, cold, ice or *gelatus*—frozen, immobile) is a semi-solid, jelly-like material, which has properties ranging from soft and weak to hard and tough. Gels, in technical terms, are defined as substantially dilute cross-linked systems, which exhibit no flow in the steady-state^[73] and can be considered as an intermediate state between solids and liquids. Gels also exhibit rather complex mixtures of properties from the two limiting states of solids and liquids^[74]. Any gel, within which the liquid medium is water, can be classified as a hydrogel.

A hydrogel, in common definition, is a hydrophilic polymer network. It can be built from synthetic or natural polymers, and be able to absorb and retain large amount of water, sometimes up to thousands of times of its own dry weight^[75, 76].

According to the cross-linking nature the hydrogels can be classified as physically or chemically cross-linked gels. The first category of hydrogels is defined by polymeric networks that are bound together by entanglements or other non-covalent attractive interactions between the polymer chains, such as hydrogen bonds, chelating ions or electrostatic interactions^[77-79]. Physically cross-linked gels can be dissolved under conditions that weaken the attractive forces between the polymer chains. Many types of such gels can be formed from biopolymers. For example, hydrogel particles of amine-containing chitosan or its derivatives can be obtained by polymer cross-linking either with multifunctional inorganic compounds, such as sodium tripolyphosphate^[80, 81], or with an oppositely charged polymer, such as DNA^[82]. Typical examples of other physical biomicrogels include alginate^[83], agarose^[84], and carrageenan^[85]. Other

examples of low-molecular-weight compounds, which can form a gel, are organogelators.^[86] These organic molecules are capable to grow from homogeneous solution into fine fibrillar dendritic structures within the solvent. Such fibrillar structures build a continuous three-dimensional network resulting in a macroscopic gel formation. This self-assembly-type gelation process is driven by specific noncovalent intermolecular interactions and, therefore, is thermoreversible.

The second category of hydrogels are chemically cross-linked gels. These hydrogels exhibit improved structural stability compared to the physically cross-linked analogues. In chemically cross-linked gels covalent bonds between polymer chains are formed throughout the entire network and lead to permanent stability with respect to the network structure. Chemically cross-linked materials are commonly prepared by copolymerization of a mono-functional monomer with a cross-linking monomer, having at least two polymerizable groups.

Apart from the separate structural classifications, hydrogels can be further distinguished by their responsive behavior to changes in their immediate environment. Non-responsive gels simply swell upon the uptake of water. In contrast, responsive gels display structural changes as a reaction to certain stimuli, such as temperature^[87-89], pH^[90], radiation^[91], electromagnetic field^[92], solvent composition or salt concentration^[93], due to the functional moieties incorporated into the polymer network.

The materials response arises from competing mechanisms of solvation within the swollen polymer networks. External stimuli can lead to attractive polymer-polymer interactions, which then dominate over the polymer-solvent interaction. This causes aggregation of the polymer chains and shrinkage of the network, accompanied by expelling of the solvent, ultimately causing the dimensions of the entire polymer network to be reduced. Due to their ability to react to environmental changes

stimuli-responsive hydrogels are often referred to as “smart” or “intelligent” materials.

Hydrogels can be prepared in different forms and sizes. Many studies have, so far, been focused on bulk gels, larger than one millimeter in diameter. These so-called macrogels can be made on length scale, which range from millimeters to centimeters. However, bulk gels requires a long time to reach an equilibrium of swelling because the time interval of swelling (or shrinking) of a gel (t) is proportional to the square of the characteristic length (l) of a gel such as radius for a spherical or cylindrical gel^[94] or thickness for a slab gel^[95] (Eq.2-10).

$$t = (l^2) / D_c \quad [2-10]$$

The diffusion coefficient, D_c , of a gel is usually considered to be constant and of the order of 10^{-7} cm²/s if the initial and final states of the swelling change are fixed^[96-98]. Therefore, the time needed for volume changes reduces with the geometrical size of the gel sample.

To determinate the physical properties and the technological applications of a gel, it is desirable for its response time to be as short as physically possible. Thus, minigels having diameter in range of 1-10 μ m satisfy this requirement and so have attracted constant scientific attention over the past 20 years^[99-103].

The sizes of microgels are even smaller, and lie on a colloidal length scale with typical dimensions ranging from a few tens to several hundreds of nanometers. Since physical dimensions affect the time in which a responsive hydrogels can react to environmental changes, microgels have a reaction time in the range of 10^{-5} - 10^{-2} s. This time scale is much shorter compared to the macrogels, which have relatively long reaction times, often in order of minutes, and therefore are limited in use for applications requiring short time of response^[104, 105].

Macro- as well as microgels may consist of identical or different monomer units and cross-linkers that can change their internal structure according to the preparation procedure and initial composition of synthetic material.

One of the most widely investigated stimuli-responsive polymers is poly(N-isopropylacrylamide) (PNIPAM). Below LCST ($\sim 31\text{-}32\text{ }^\circ\text{C}$)^[106, 107], PNIPAM exists in a highly solvated state. At these conditions water molecules form hydrogen bonds with amide groups of polymer chains. Upon heating, the interaction between the water and nitrogen of the amide groups get weaker, and above LCST the interaction between neighboring amides in polymers becomes preferable, resulting in collapsing of the polymer chains (Fig.2-7). This macromolecular shrinkage of PNIPAM also releases a large amount of structured water resulting in an increasing of entropy.

This process is referred to as the coil-to-globule transition^[108], where the polymer undergoes a switching from solvated to collapsed state.

Similarly, PNIPAM-based microgels undergo a reversible volume phase transition (VPT)^[109], where the cross-linked particles retain their shape upon the summation of the swelling-deswelling process. The particles adopt a swollen conformation at low temperatures due to hydrophilic interactions between water molecules and amide groups along

the polymer chains. As the temperature is increased above the LCST,

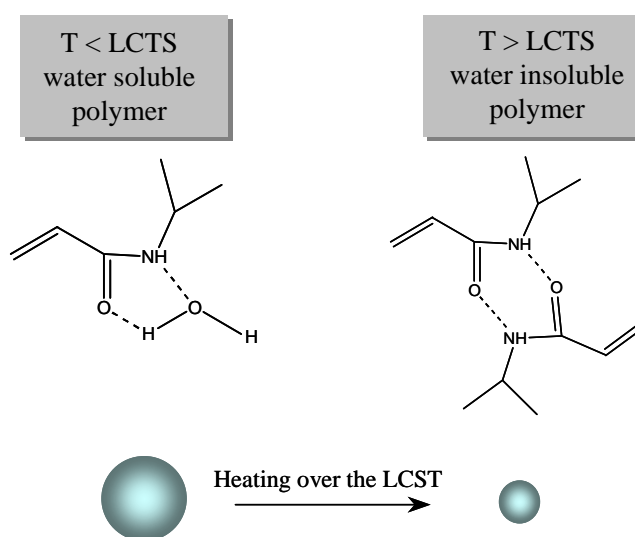


Figure 2-7 Schematic representation of LCST behaviour of PNIPAM leading to volume phase transition of cross-linked microgels.

hydrogen bonding with water is disrupted, resulting in an entropically favored expulsion of water from the polymer matrix. At the same time, hydrophobic interactions occur between neighboring polymer chains, inducing the particles to undergo a volume change as a function of temperature. Thus, PNIPAM particles are highly swollen with a solvent at temperatures lower than the LCST, but turn into their deswollen state above LCST when polymer-polymer interactions dominate.

The versatility of this material can be enhanced even further with the incorporation to the polymer network components sensitive to a second stimulus. Copolymerization of NIPAM with different ionic monomers such as acrylic (AA)^[90] or methacrylic acid (MAA)^[110], vinyl pyridine^[111], vinyl imidazole^[112], aminoethylmethacrylate (AEMA)^[113] make the resulting materials tunable, with multi-responsive properties.

Functionalization of PNIPAM microgels with carboxylic groups, generally provided via copolymerization of NIPAM with acrylic or methacrylic acid is of particular interest. The resulting polyelectrolyte microgels undergo volume phase transition as response to changes of temperature, pH and ionic strength. Many applications of polyelectrolyte gels are derived from their ability to bind oppositely charged species and form resulting complexes. Most hydrogels, used for metal ions removal, are able to develop negative charges to form complexes with metal cations^[114]. Positively charged hydrogels, containing amine-groups in their structure, can successfully remove from aqueous media negatively charged species such as dyes or arsenic compounds, a dangerous environment contaminant^[115].

The dependence of swelling behavior on pH and ionic strength in polyelectrolyte microgels predominantly originate from electrostatic interactions between ionic groups. For example, poly(NIPAM-co-AA) microgels undergo a sharp increase in size at pH \sim 4,5 due to deprotonation of the carboxylic groups and, as a result, electrostatic repulsion between the negatively charged carboxylate residues

(pKa of AA \sim 4,25)^[116]. Inversely, an increase of ionic strength of the medium causes a decrease of microgel size.

The swelling ability of polyelectrolyte, or charged microgels significantly differs from uncharged microgels. Functional groups of polyelectrolyte polymer chains can interact selectively with a single solute species and bind the oppositely charged ions to the gel network, increasing the total charge of the cross-linked system. Gel swelling mainly results from an increased osmotic pressure within the network, while an increasing of local charge density leads to repulsion between the chains giving an additional contribution to the swelling effect. In ionized form, the polyelectrolyte charge is determined only by a number of ion species and, therefore, the degree of swelling of such types of hydrogels increases with the number of incorporated charged groups.

Copolymerization of NIPAM with non-charged monomers, such as styrene^[113] or acrylamide^[117] (AAm), is also known as a method of tuning the LCST and introducing new properties to PNIPAM-based hydrogels.

Several studies in the past few decades dealing with microgels have attracted a lot of attention in the theoretical studies of soft matter^[118] and in its relevant applied fields^[119, 120]. In particular, there has been rapidly gained importance in materials science owing to its potential applications in drug delivery^[121], environmental sensing^[122], fabrication of photonic crystals^[123], template-based syntheses of inorganic nanoparticles^[124] and in separation and purification technologies^[125]. Due to the significant water uptake ^[126, 127], hydrogels possess a degree of flexibility very similar to natural tissue. Thus, hydrogels are some of the most promising materials in biology and medicine science today with an almost immeasurable economic potential^[120].

Over the past few years, several research groups have attempted the microgels for material surfaces modification^[128-130]. One example was the deposition of microgel particles on a poly(ethylene terephthalate) surface by spin coating followed by their covalent tethering, done by Lyon and co-

workers^[131]. A 2D monolayer of PNIPAM microgel beads was prepared by Yoshida and co-workers via double-template polymerization^[132]. Interestingly, fabrication of 2D colloidal lattices of particles with controlled distances between them is of special interest due to the potential optical applications (e.g. for surfaces with specific reflecting properties)^[133]. Unfortunately, the use of microgels for photonic materials is impeded by their inherent softness. However, microgels, filled with nanoparticles are attractive as a functional building block for the fabrication of photonic crystals^[123] due to improvements in mechanical properties. Microgels are also ideal candidates for the fabrication of microlense arrays with dynamically tunable focal lengths, which can be prepared in an inexpensive and scalable fashion. Kawaguchi and co-workers prepared films of PNIPAM particles upon air-drying and obtained highly ordered 2D colloidal crystals with a controllable interparticle distance^[134]. They claim a balance between capillary attraction and steric repulsion as a reason of the regular distance between the particles. Electrostatic repulsion between particles whose charge originates only from the negatively charged initiator is assumed to be minor. An increase of a particles charge, by means of incorporation of charged moieties, helps to control the density of adsorbed hydrogels in a reproducible fashion^[135]. Tuning of particle-particle and substrate-particle interaction is a way to design 2D colloidal crystals with regular particles distribution and obtain desired film properties.

Alternatively to self-assembled ordered particles arrays, patterned hydrogel structures have been obtained through the use of the soft lithography^[136], double-templating method^[137] as well as polymerization of hydrogel-forming monomers from the surface, patterned by microcontact printing^[138].

Coating of surfaces with hydrogel film has been proposed to improve the properties of substrates for tissue engineering^[139], drug-eluting contact lenses production^[140], enhancing of surface properties of artificial

medical devices^[141] or for derivatization and changing the wettability of organic solids^[142]. Volume transition as a controllable parameter of polymeric hydrogel films has been used in chemomechanical systems^[143], separation devices^[144] as well as various sensors^[103].

Due to versatility of the composition, morphologies and “smart” behavior of hydrogels to response on different external stimuli, they can be exploited to create materials with precisely tunable properties, such as, wettability, permeability, flexibility, refractive index, dimensions, etc. They are extremely attractive building blocks for nano- and micro-structured materials, for the evolution of new functional material, as well as for creation of novel composite materials. Attempts at such material development and the investigation of possible applications in surface modification process are being carried out in research labs around the world.

3. EXPERIMENTAL TECHNIQUES

3.1 ATOMIC FORCE MICROSCOPY

The scanning tunnelling microscope (STM) is the ancestor of all scanning probe microscopes. Gerd Binnig and Heinrich Rohrer at IBM Zurich invented it in 1982. Five years later they were awarded the Nobel Prize in Physics for their invention.

The atomic force microscopy (AFM) was also introduced by Binnig et al^[145] in 1986. While the STM measures the tunnelling current (conducting surface), the AFM measures the forces acting between a fine tip and a sample. The tip is attached to the free end of a cantilever and is brought very close to a surface. Attractive or repulsive forces resulting from interactions between the tip and the surface will cause a positive or negative bending of the cantilever. The bending is detected by means of a laser beam, which is reflected from the backside of the cantilever (Fig.3-1).

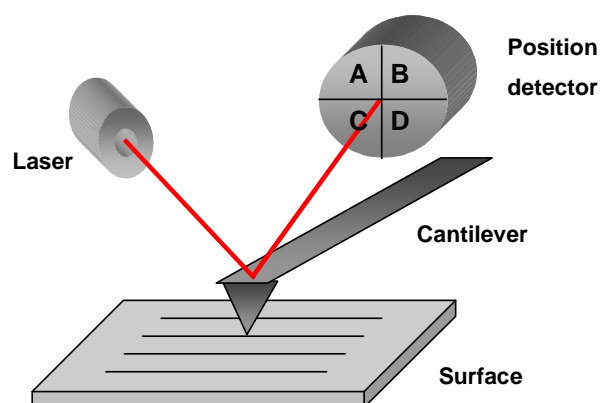


Figure 3-1 Schematic representation of detection of deflected laser beam in AFM imaging.

Components of the Microscope

Piezocrystals are ceramic materials that expand or contract in the presence of voltage gradient and conversely, they develop an electrical potential in response to mechanical pressure. In this way, movements in x, y and z direction are possible.

The probe represents a micromachined cantilever typically fabricated from Si or Si₃N₄ with a sharp tip (radius is a few to tens of nanometers) at one end, which is brought into interaction with the sample surface. Cantilevers size range from 100 to 200 μm in length (l), 10 to 40 μm in width (w), and 0,3 to 2μm in thickness (t). Typically cantilevers are characterized by their force constant and resonant frequency, which have to be chosen according to the requirements of sample to be studied.

Laser Beam Deflection Detector

To detect the displacement of the cantilever, a laser is reflected off the back of the cantilever and collected in a photodiode. The diode is divided into four parts, as seen in Figure 4-1. When the laser is displaced vertically along the positions top (B-A) and bottom (D-C), there exists a bending due to topography, while if this movement is horizontal left (B-D) and right (A-C), it produces a torsion due to “friction” (lateral force).

Force vs. Distance Curve

A force sensor in an AFM can only work if the probe interacts with the force field associated with the sample surface. The dependence of the van der Waals force upon the distance between the tip and the sample is shown in Figure 3-2.

In the contact regime, the cantilever is held less than a few angstroms from the sample surface, and the interatomic force between the cantilever and the sample is repulsive. This causes the cantilever to bend up. In the non-contact regime, the cantilever is held on the order of

tens to hundreds of angstroms from the sample surface, and the interatomic force between the cantilever and sample is attractive (largely a result of the long-range Van der Waals interactions).

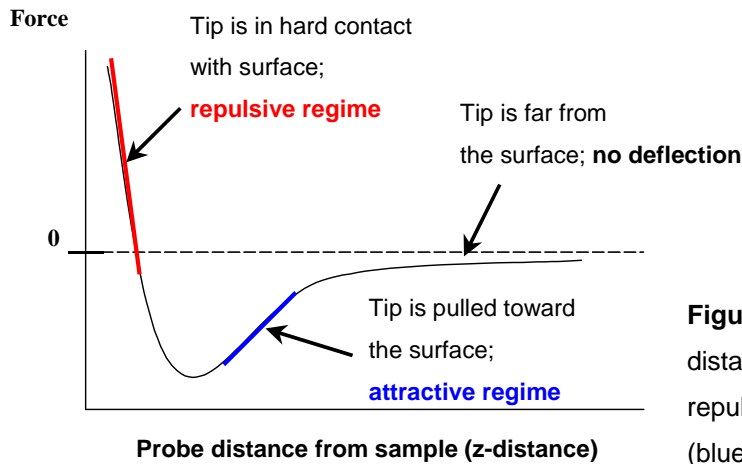


Figure 3-2 Typical force-distance curve with indicated repulsive (red) and attractive (blue) regimes of AFM imaging.

The force is not measured directly, but calculated by measuring the deflection of the lever, and knowing the stiffness of the cantilever. The deflection of the cantilever Δx is proportional to the force acting on the tip, according to the Hook's law, $F = -k\Delta x$, where k is the spring constant of the cantilever.

Modes of Operation

Contact Mode

In contact-AFM mode, the tip makes soft “physical contact” with the surface of the sample. The tip either scans at a constant small height above the surface or is under the conditions of applied constant force. In the constant-height mode the height of the tip is fixed, whereas in the constant-force mode the deflection of the cantilever is fixed and the motion of the scanner in z-direction is recorded. By using contact-mode AFM, even “atomic resolution” images are obtained.

Because the tip is in hard contact with the surface, for contact mode AFM imaging it is necessary to have a cantilever, which is soft enough to be deflected by very small forces, and has a resonant frequency high enough to be unsusceptible to vibrational instabilities. Silicon Nitride tips having a spring constant of $< 1\text{N/m}$ are used for the contact mode imaging.

Non Contact Mode

In this mode, the probe operates in the attractive force region and the tip-sample interaction is minimized. The cantilever is instead oscillated at a frequency slightly above its resonance frequency where the amplitude of oscillation is typically a few to ten nanometers. The van der Waals forces, which are strongest from 1 nm to 10 nm above the surface, or any other long-range forces which extend above the surface acts to decrease the resonance frequency of the cantilever. This decrease in resonance frequency combined with the feedback loop system maintains a constant oscillation amplitude or frequency by adjusting the average tip-to-sample distance. Measuring the tip-to-sample distance at each (x, y) data point allows the scanning software to construct a topographic image of the sample surface. The use of non-contact mode allows scan the sample without influencing of its the shape by the tip-sample forces.

In most cases, the cantilever of choice for this mode is the one having high spring constant of 20-100 N/m so that it does not stick to the sample surface at small amplitudes. The tips mainly used for this mode are silicon probes.

Tapping Mode (Intermittent Contact Mode)

The forces measured by AFM can be classified into long-range and short-range forces. The long range forces dominate when scan is performed at large distances from the surface and are usually related to Van der Waals or capillary forces (due to the water layer often present in an ambient environment).

In tapping mode-AFM the cantilever is driven to oscillate up and down at frequency close to resonant by a small piezoelectric element mounted in the AFM tip holder. The oscillation amplitude is typically 100 to 200 nm. Due to the interaction with sample and forces acting on the cantilever when the tip comes close to the surface (Van der Waals, electrostatic or dipole-dipole interaction) the amplitude of this oscillation decreases. An electronic servo uses the piezoelectric actuator to control the height of the cantilever above the sample. The servo adjusts the height to maintain set oscillation amplitude as the cantilever scans over the sample, such that a constant tip-sample interaction is maintained during scanning.

Forces that act between the sample and the tip will cause not only changes in the oscillation amplitude, but also changes in the resonant frequency and phase of the cantilever. The amplitude is used for the feedback and the vertical adjustments of the piezoscanner are recorded as a height image. Simultaneously, the phase changes are displayed in the phase image.

The advantages of the tapping mode are the elimination of a large part of permanent shearing forces and, as a result, less damage to the soft samples surface, even with stiffer probes. Different components of the sample, which exhibit difference adhesive and mechanical properties, will show a phase contrast, allowing compositional analysis to be performed. For a good phase contrast, larger tip forces are of advantage, while minimization of this force reduces the contact area and facilitates high-resolution imaging. So in applications it is necessary to choose the right values matching the objectives. Silicon probes are used primarily for Tapping Mode applications.

Tapping mode operation in liquid has the same advantages over contact mode as in the air or vacuum. However, imaging in a liquid media tends to damp the cantilever own resonant frequency. In this case, the entire fluid cell can be oscillated to drive the cantilever into oscillation.

This differs from the tapping or non-contact operation modes in air or vacuum where the cantilever oscillates itself. Alternatively, very soft cantilevers can be used to get the adequate results during the scanning in fluids. The spring constants are usually used of 0.1 N/m compared to the cantilevers for tapping mode in air where the constants are typically in the range of 1-100 N/m.

AFM is a promising surface analytical technique for studying mechanical and structural properties of hydrogels^[146, 147]. Determination of the size, geometry of hydrogels deposited on the substrate as well as measuring of interaction forces between microgels and surfaces were already reported^[148]. Elastic properties of hydrogels could be also estimated from the force-distance curves analysis. Structural studies of hydrogel films including investigations of surface roughness^[149], hydrogels surface packing density^[135] were also performed by AFM technique. Investigation of swelling ability and thermoresponce of hydrogels deposited on the substrate can be also found in the literature^[150].

In this work, AFM studies of individual hydrogel microparticles as well as particles assemblies have been done.

For all AFM investigations *DI Scanning Probe Microscope* NanoScope IV-D3100 (Digital Instruments, Santa Barbara, CA) was used. This instrument is applicable for scanning of both dry surfaces and surfaces wetted with fluids (in our case – with water). For the last case special fluid cell (*Fluid Imaging Cell*) was installed onto the scanner head. The cantilever holder was protected from the contact with water by using the elastic protective skirt. Such system allows to perform both Contact and Tapping Mode AFM imaging in fluid environment after simple placement of water droplet between the scanner and substrate.

Tapping mode AFM was used for recording of the images of hydrogels in their dry state in air. Imaging was performed using silicon

cantilevers with radius of 10-20 nm, spring constant of 30 N/m and resonance frequency of 250-300 kHz.

For scanning surfaces in fluids contact mode AFM is usually used, but in case of hydrogels it has one considerable limitation. It is possible to measure properly the size of hydrogel particles in their dry state, but in water, when particles are swollen and became very soft, they are easily damaged during the scanning procedure.

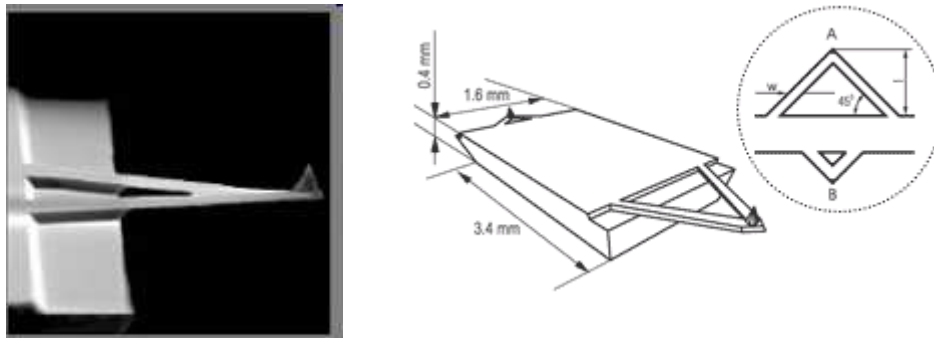


Figure 3-3 SEM image of the triangular cantilever (left) and schematic draw of the probe chip (right). Adapted from the <http://www.spmtips.com>

In contrast to this, more delicate tapping mode in combination with soft ultra sharp silicon tips with triangle cantilever configuration (Fig.3-3), resonant frequency of 30 kHz and force constant 0.35 N/m, is the best to my knowledge for proper measurements of the size of hydrogels both in the dry state as well as under water.

3.2 SCANNING ELECTRON MICROSCOPY

Scanning Electron Microscopy (SEM) can be used for qualitative surface topography analysis, primary based on the fact that it allows excellent visualization. Possible magnification levels in modern SEMs are

from less than 100X up to 100000X. This means that the imaged area can be scaled from 1 μm^2 to 1 mm^2 . At high magnification, the ultimate resolution is as good as about 2 nm on a conductive surface.

Although SEM images obtained by detecting secondary electrons have a striking three-dimensional appearance (due to shadowing effect), they are still inherently 2-D. There are several techniques how to reconstruct 3D structure of surface features, but the simplest method of topography evaluation is imaging the sample under different visual angles, performing the stepwise tilting of the specimen.

In a typical SEM, an electron beam is thermionically emitted from an electron gun fitted with a tungsten filament cathode. Tungsten is normally used in thermionic electron guns because it has the highest melting point and lowest vapour pressure of all metals, thereby allowing it to be heated for electron emission, and because of its low cost. A high-resolution SEM is typically equipped with a field-emission gun. The field-emission gun is a heated tungsten crystal with a very fine tip (tip diameter ~ 100 nm), from which the electrons are emitted with assistance of a strong electric field.

The electron beam, which typically has an energy ranging from a few hundred eV to 40 keV, is focused by one or two condenser lenses to a spot about 0.4 – 5 nm in diameter. The beam passes through pairs of scanning coils or deflector plates in the electron column, which deflect the beam in the x and y axes so that it scans in a raster fashion over a rectangular area of the sample surface. When the primary electron beam interacts with the sample, the electrons lose energy by repeated random scattering and absorption within a teardrop-shaped volume of the specimen known as the interaction volume, which extends from less than 100 nm to around 5 μm into the surface. The size of the interaction volume depends on the electron's landing energy, the atomic number of the specimen and the specimen's density. The energy exchange between the electron beam and the sample results in the reflection of high-energy

electrons by elastic scattering, emission of secondary electrons by inelastic scattering and the emission of electromagnetic radiation, each of those could be detected by specialized detectors. The beam current passed through the specimen can also be detected and used to create images of the distribution of specimen current.

Electronic amplifiers of various types are used to enhance the signals, which are displayed as variations in brightness on a cathode ray tube. The raster scanning of the CRT display is synchronised with that of the beam on the specimen in the microscope, and the resulting image is therefore a distribution map of the intensity of the signal being emitted from the scanned area of the specimen. The image may be captured by photography from a high resolution cathode ray tube, but in modern machines is digitally captured and displayed on a computer monitor and saved to a computer's hard disc.

In this work scanning electron microscopy was carried out using Ultra 55 (Carl Zeiss NTS, Oberkochen, Germany) operating at 3 kV in the secondary electron (SE) mode. For conventional imaging with SEM, specimens must be electrically conductive, at least at the surface, and electrically grounded to prevent the accumulation of electrostatic charge at the surface. Nonconductive specimens (like most of polymers and, in particular, hydrogels) tend to charge when scanned by the electron beam, and especially in secondary electron imaging mode, this causes scanning faults and other image artefacts. Therefore they are usually coated with an ultrathin layer of electrically conductive material. In this work all samples before SEM imaging were coated with 5-10 nm of platinum layer using low vacuum sputter coater.

3.3 DYNAMIC LIGHT SCATTERING

In Dynamic Light Scattering (DLS) (also known as Photon Correlation Spectroscopy (PCS) or Quasi-Elastic Light Scattering (QELS)) scattering of monochromatic light (laser beam) is used for measuring of the particles diffusion coefficient and hence, their hydrodynamic radius. This technique is one of the most widely used methods to determine the size of sub micron particles suspended within a liquid.

When light beam passes through the colloidal dispersion, the particles or droplets scatter the part of the light in all directions. When the particles are very small compared to the wavelength of the light (below approximately 250 nm in diameter), the intensity of the scattered light is uniform in all directions (Rayleigh scattering); for larger particles the intensity is angle dependent (Mie scattering).

If the light is coherent and monochromatic, like in laser beam, it is possible to observe time-dependent fluctuations in the scattered intensity using a suitable detector such as a photomultiplier capable for operation in photon counting mode.

The fluctuations arise from the fact that the particles are small enough to undergo random thermal (Brownian) motion and the distance between them is therefore constantly varying. Constructive and destructive interference of light scattered by neighbouring particles within the illuminated zone gives rise to the intensity fluctuation at the detector plane, which, as it arises from particle motion, contains information about this motion. Analysis of the time dependence of the intensity fluctuation can therefore yield the diffusion coefficient of the particles from which, via the Stokes-Einstein equation (Eq.3-1), knowing the viscosity of the medium, the hydrodynamic diameter of the particles can be calculated.

$$d(H) = \frac{kT}{3\pi\eta D} \quad [3-1]$$

$d(H)$ - hydrodynamic diameter of particles, D - translation diffusion coefficient, k - Boltzmann constant, T - absolute temperature, η - the viscosity of the medium.

An accurately controlled temperature is necessary for a DLS experiments, because the viscosity of a liquid, required for calculations is related to its temperature. The temperature also needs to be stable; otherwise convection currents in the sample will cause non-random movements that will ruin the correct interpretation of size.

The time dependence of the intensity fluctuation is most commonly analysed using a digital correlator. It determines the intensity autocorrelation function, which can be described as the ensemble average of the product of the signal with a delayed version of itself as a function of the delay time. The "signal" in this case is the number of photons counted in one sampling interval. At short delay times correlation is high and, over time as particles diffuse, correlation diminishes to zero with the exponential decay of the correlation function characterising the diffusion coefficient of the particles. Data are typically collected over a delay range of 100 ns to several seconds depending on the particle size and viscosity of the medium.

In other words the correlator used in a DLS instrument constructs the correlation function $G(\tau)$ of the scattered intensity, which fluctuates as a function of time:

$$G_\tau = \langle I(t)I(t+\tau) \rangle \quad [3-2]$$

τ - the time difference (the sample time) of the correlator.

For a large number of monodisperse particles in Brownian motion, the correlation function is an exponentially decaying function of the correlator time delay τ .

$$G_{\tau} = A[1 + B \exp(-2\Gamma \tau)] \quad [3-3]$$

A - the baseline of the correlation function, B - the intercept of the correlation function.

$$\Gamma = Dq^2 \quad [3-4]$$

D - the translational diffusion coefficient, q - the scattering vector

In scattering experiments the magnitude of scattering vector is one of the most important parameters, which is given by

$$q = (4\pi n / \lambda_0) \sin(\Theta / 2) \quad [3-5]$$

n - refractive index of dispersant, λ_0 - the wavelength of the laser, Θ - the scattering angle.

Thus, knowing q and Γ one can obtain the value of D , and returning back to the Stokes-Einstein equation it is easy to calculate $d(H)$. The diameter that is measured by DLS is a value that refers to how the particles diffuse within the fluid so it is called a hydrodynamic diameter. This value is also known as Stokes diameter and this is a diameter of a sphere having the size hydrodynamically equivalent (the same translational diffusion coefficient) to the sample particles.

For polydisperse samples, the equation of correlation function can be written as:

$$G_{\tau} = A[1 + Bg_1(\tau)^2] \quad [3-6]$$

$g_1(\tau)$ - the sum of all the exponential decays contained in the correlation function.

Analysis of the autocorrelation function in terms of particle size distribution is done by numerically fitting the data with calculations based on assumed distributions. There are two approaches that can be used in order to obtain the mean size (z-average diameter) and estimate the width of the distribution (polydispersity index). A truly monodisperse sample would give rise to a single exponential decay to which fitting a calculated particle size distribution is relatively straightforward (Cumulants analysis)^[151]. In practice, polydisperse samples give rise to a series of exponentials and several quite complex schemes have been devised for the fitting process in order to obtain the distribution of particle sizes. One of the methods most widely used for this purpose is known as Non-Negatively Constrained Least Squares (NNLS) or CONTIN^[152].

The size distribution obtained is a plot of the relative intensity of light scattered by particles in various size classes and is therefore known as an intensity size distribution.

A typical dynamic light scattering system comprises of six main components (Fig.3-4).

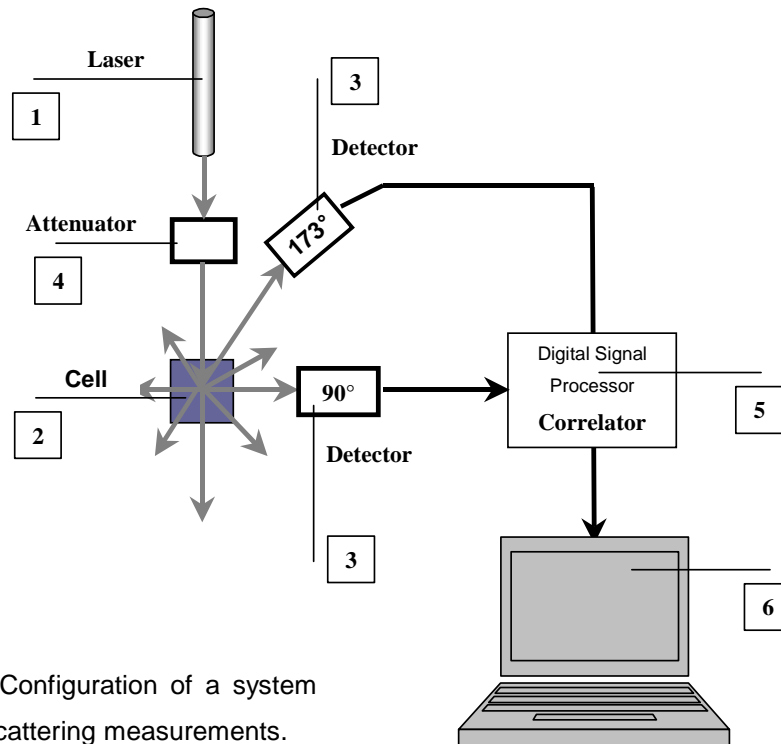


Figure 3-4 Configuration of a system for dynamic light scattering measurements.

A laser (1) provides a light source to illuminate the sample contained in a cell (2). For dilute concentrations, most of the laser beam passes through the sample, while small part is scattered by the particles within the sample in all directions. Detector (3) is used to measure the intensity of scattered light. Typically the detector position is at either 173° or 90° , depending upon the particular model. The intensity of scattered light must be within a specific range for the detector for successful measurement. If too much light is detected, then the detector will become saturated. To overcome this, an attenuator (4) is used to reduce the intensity of the laser source and hence reduce the intensity of scattered light. For samples that do not scatter much light, such as very small particles or samples with low particles concentrations, the amount of scattered light must be increased. In this situation, the attenuator will allow more laser light pass through the sample. For samples that scatter more light, such as large particles or samples at higher concentration, the intensity of scattered light must be decreased. The appropriate

attenuator position is automatically determined by the software and covers a transmission range from 0.0003 to 100%.

The scattering intensity signal from the detector is passed to a digital processing board called a correlator (5). The correlator compares the scattering intensity at successive time intervals to derive the rate at which the intensity is varying. This correlator information is then passed to a processor (6), where the software will analyze the data and derive size information.

In this work dynamic light scattering (DLS) measurements were performed using Zetasizer Nano S, (He-Ne-laser 4 mW, 632,8 nm), collecting the scattering information at 173° (back scattering), NIBS®-Technology, Malvern Instruments. Each sample was allowed to equilibrate at each particular temperature for 10 min before measurement. At each measuring point 3 consecutive runs were performed where each run was composed of 15 individual measurements using a 20 sec integration time for each measurement.

3.4 DROP SHAPE ANALYSIS TECHNIQUE (DSA)

The contact angle between solid and liquid can be measured with a static drop. The drop is produced before the measurement and has a constant volume during the measurement. Angle between the baseline of the drop (three-phase contact line) and the tangent at the drop boundary is measured. This method is used to estimate wetting properties of a localized region on a solid surface.

An alternative approach that allows to obtain the information about contact angle is a shape determination of a sessile drop. The shape of the drop could be determined through combination of surface tension and gravity effects.

The balance between surface tension of drop and external forces, such as gravitation, could be represented by Laplace equation of capillarity, which describes the condition of equilibrium of two phases separated by interface^[153, 154].

$$\Delta p = \gamma \left(\frac{1}{R_1} + \frac{1}{R_2} \right) \quad [3-7]$$

Δp - the pressure difference across the interface, γ - the surface tension,
 R_1, R_2 - two principal radii of curvature.

In the case of absence of any additional forces other than gravity, Δp can be expressed as a linear function of the elevation:

$$\Delta p = \Delta p_0 + (\Delta \rho)gz \quad [3-8]$$

Δp_0 - the pressure difference at the reference plane, $\Delta \rho$ - the density difference between two phases, g - the gravitational acceleration, z - the height of the drop from the reference plane.

The strategy of measurement is to find the function that expresses the deviation of physically observed curve from theoretical curve satisfying the Laplace equation.

Krüss DSA 10 drop shape analyzer (Germany) was used to determine liquid contact angles of volume about 10-20 μl . To produce a drop on the surface, a manually controlled microsyringe was used to push liquid into the drop from above. At least 5 separate measurements for each sample were used in averaging the contact angle. All contact angle measurements were carried out at $24 \pm 0.5^\circ\text{C}$ and relative humidity of $40 \pm 3\%$.

3.5 OTHER METHODS

Electrophoretic mobility was measured as a function of pH using Electrokinetic Analyzer (EKA) (Anton Paar GmbH, Graz, Austria). The pH of the prepared suspensions was controlled by adding 0.1M KOH or HCl aqueous solutions. The samples have been prepared by the dilution of concentrated hydrogels with 10^{-3} M KCl to final concentration of about 0.001mg/ml. Three measurements were recorded for each sample at each value of pH. The zeta potentials were calculated from the electrophoretic mobility using the Smoluchowsky equation^[155].

UV/Vis measurements were carried out using UV/vis Spectrometer Lambda 800 (Perkin-Elmer, Germany).

¹H-NMR spectra were recorded on a Bruker DRX-500 spectrometer operating at 500.13 MHz for ¹H using CDCl₃ as solvent. The spectra were referenced on the solvent peak ($\delta(^1\text{H})=7.26$ ppm).

GPC measurements were carried out on Agilent 1100 Series (Agilent) normal-temperature size exclusion chromatograph, equipped with refractive index detector and one column PL Gel MIXED-B (Polymer Laboratories, U.K.) using chloroform as eluent and flow rate of 1 ml/min. Calibration was based on polystyrene standards obtained from Polymer Standards Service (PSS, Germany).

Ellipsometric measurements were carried out on a rotating-analyzer ellipsometer SE400 (SENTECH Instruments GmbH, Germany). The instrument uses a He-Ne laser as the light source ($\lambda = 632.8$ nm) and is equipped with focusing optics collimating the laser beam in a 30 μm size spot on sample surface. The incident angle was fixed at 70°. The thickness of the polymer films was calculated using a three-layer model: Si-SiO₂ / polymer / air. The ellipsometric parameters were fitted using the Elli program developed by Optrel GBRmBH (thickness of SiO₂ = 1.8 ± 0.1 nm; $n_{\text{SiO}_2} = 1.4598$; $n_{\text{Si}} = (3.858 - i 0.018)$; $n_{\text{air}} = 1.0$).

4. RESULTS AND DISCUSSIONS

4.1 EVALUATION OF PARAMETERS OF INVERSE SWITCHING

Change of the size of core-shell particles due to the swelling of the core in water leading to increase of surface fraction covered with hydrophobically covered particles is a basic premise for inverse switching effect. In order to evaluate the feasibility of switching, various parameters of desired system should be optimized. For example, swelling ratio of the core-shell particles and the number of the particles per square unit of the surface (surface density) will determine the range of the surface coverage in a dry and wet states. This, together with a nature of the particles shell and substrate chemistry, will govern the contact angle of a composite surface according to the Cassie equation (Eq.2-8). On the other hand, the ability of hydrophilic core to stretch the elastic shell will depend on the intrinsic properties of the hydrogel (swelling ability, swelling pressure) as well as on the nature, thickness and permeability of the shell.

Hence, all of the aforementioned parameters of the designed system including swelling ability of microgels and their behavior upon deposition, shell material requirements and possible restrictions coming from the materials combination were evaluated.

PARTICLES SURFACE DENSITY AND SWELLING RATIO

For the best performance of “contraphilic” switching, the particles on the substrate should form densely packed layer in a swollen state, in

order to guarantee the complete shielding of the underlying surface, and opening of a wide surface space in-between particles upon drying.

In two-dimensional space the regular arrangement of circles with the highest density is achieved via hexagonal packing, in which the centres of the circles form a hexagonal lattice and each circle is

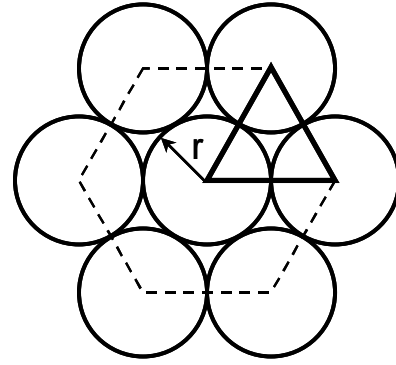


Figure 4-1 Hexagonal arrangement of circles as the densest plane lattice packing.

surrounded by 6 other circles (Fig.4-1). In case of spherical particles arranged on the surface, area of surface covered with particles is defined by the packing density. The term “packing density” is applied to a monolayer of spheres and it refers to a fraction of total volume occupied by given solid material^[156]. The projection of such spheres on a flat surface, which is an array of circles, is called “surface coverage” or “surface occupation”.

Numerical value of the maximum packing density as well as surface occupation by the array of uniform spherical objects can be calculated geometrically. Since the centres of three circles of their hexagonal packing in contact form an equilateral triangle, the maximal occupation of surface by one layer of hard spheres (F_{max}) can be found from the ratio of occupied area ($3 \times A_{circle}$) to the total area of surface ($6 \times A_{triangle}$):

$$F_{max} = \frac{3A_{circle}}{6A_{triangle}} = \frac{3\pi R^2}{6(2R)^2 \frac{\sqrt{3}}{4}} = \frac{3\pi R^2}{6R^2 \sqrt{3}} = \frac{\pi}{2\sqrt{3}} \approx 0.9069 \quad [4-1]$$

Thus by covering of a surface with one layer of hard spheres maximal packing density and correspondent surface coverage could not be more than ~ 0.9069 .

Since hydrogel is a soft material, this fraction can increase up to 1 due to possibility of deformation of flexible particles in swollen state.

The changing of a surface coverage is defined by the swelling ratio of a hydrogel (S_v). Volume swelling ratio for hydrogel particles could be determined as a ratio of particle's volume in swollen state (V_s) to a volume of the same particles in dry (collapsed) state (V_c) (Eq.4-2).

Required value of volume swelling ratio for particles, which partially cover the surface in dry

$$S_v = \frac{V_s}{V_c} \quad [4-2]$$

state, can be calculated assuming that in a swollen state fraction of surface occupied with particles should be at least 0.9069. This value will depend on an arrangement of dry particles on the surface, namely on their packing density. For correlation of these characteristics it is useful to introduce a function which relates particle's volume swelling ratio, needed for complete occupation of the surface by swollen particles, with a fraction of surface occupied with the same particles in a dry state (Eq.4-3).

$$S_v = \left(\frac{R}{r}\right)^3 = \left(\frac{\sqrt{S} \sqrt{\pi}}{\sqrt{\pi} \sqrt{s}}\right)^3 = \left(\frac{\sqrt{S}}{\sqrt{s}}\right)^3 = \left(\frac{1}{\sqrt{f}}\right)^3 \quad [4-3]$$

R - the particles radius in swollen state; *r* - the particles radius in dry state; *S* - the surface occupation by swollen particles; *s* - the surface occupation by dry particles, *f* - fraction of occupied surface.

Equation 4-3 defines the volume swelling ratio necessary to reach the complete (100%) coverage of substrate by particles in a swollen state assuming that in a dry state particles were deposited on the surface with density *f*. In the case of more rigid particles the Eq.4-3 adopts the following form:

$$S_v = \left(\frac{0.9069}{\sqrt{f}}\right)^3 \quad [4-4]$$

Graphically this function is shown on the Fig.4-2. From this dependence it is easy to find a suitable regime of swelling for any type of particles with any deposited surface density in their dry state for fulfilment of the conditions of full coverage of a surface with swollen ones.

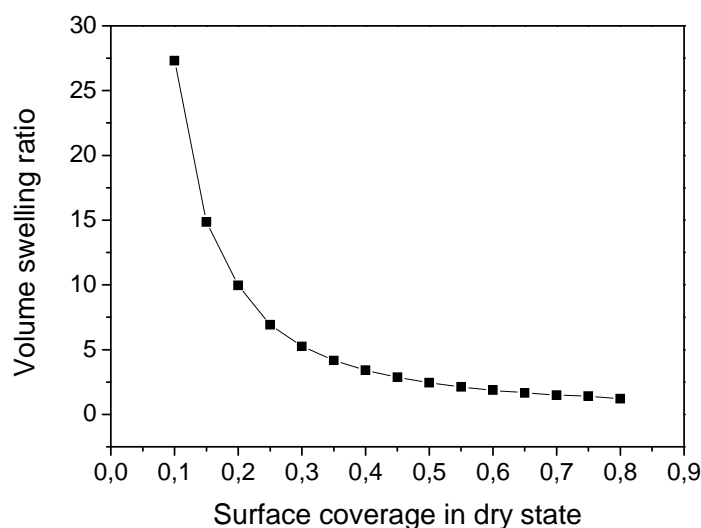


Figure 4-2 Particles volume swelling ratio required for complete surface coverage as a function of surface fraction covered with particles in their dry state.

MATERIAL OF THE SHELL

The hydrophobicity of the surface of microgels has to be provided by hydrophobic shell, formed on the surface of the hydrophilic microgels. Since the size of the resulted core-shell particles will be changing during the swelling-drying cycles, the shell should be elastic enough to be able to adapt variable geometrical sizes. Thus, elastic modulus of shell material is a critical parameter for swelling ability of the potential core-shell system. To this end utilization of polyisoprene as the shell material has at least two advantages. Firstly, polyisoprene posses high hydrophobisty (water contact angle of about 109°)^[157], and secondly, polyisoprene layer can be cross-linked, that can help the particles to enhance rigidity and prevent reformation (self-adaptation) of the particle upon the

changing of the surrounding conditions. The variation of cross-linking density gives the means to control the elastic modulus of polyisoprene, which has to be taken into account during the evaluation of a model system.

Linear dependence of force of retraction of stretched polyisoprene rubber from the cross-linking density was confirmed already by Flory, Rabjohn and Shaffer^[158]. They showed that increase of the cross-linking degree from 0.1% to 3.0% leads to gradual increase of Young modulus from 0.093 MPa to 1.227 MPa. It can be expected that good elastic properties of cross-linked polyisoprene will allow the shell to reversibly stretch and contract in a broad range of the core's swelling states. Relative stretching of the elastic shell of the core-shell particle could be expressed as increase of particle surface area upon swelling. The correlation between relative strain of the shell and volume swelling ratio (S_V) was calculated for S_V ranging from 1 to 100 (Fig.4-3).

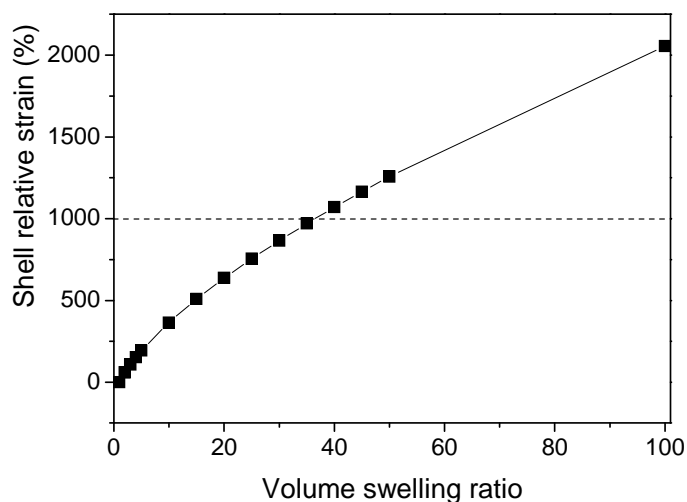


Figure 4-3 Relative stretching of the particle shell as a function of its volume swelling ratio. Dash line limits the region of stretching of polyisoprene rubber close to the limit of elongation at break [Ref.159-162].

From this graph it is evident that the limit of elongation at break, which for rubbers is typically around 1000% (the value have been taken

from the comparison of references data for polyisoprene rubber with different cross-linking degrees and molecular weights^[159-162]) defines the range of volume swelling ratio of desired core-shell system from zero to almost 40. In this range hydrogels covered with polyisoprene shell can swell and stretch the rubber on their surface without the risk of its breaking.

PERMEABILITY OF THE SHELL

Since hydrophobic cross-linked polyisoprene film provides sufficient barrier for water, it was assumed that the swelling of core-shell microgels covered with polyisoprene shell would only be possible, if some channels for water penetration will be introduced into shell body. In such a way, the swelling degree could be controlled by the number and size of holes introduced into the shell. However, some complications can arise if the fraction of the holes would be significant. According to Cassie equation, this would reduce the hydrophobicity of the shell, assuming the hydrophilic nature of the holes. Also, the holes can serve as the crack nucleation sites upon stretching of the shell, especially in the case of their irregular shape. Finally, in the case of very large channels, the hydrogel could be extruded from the core upon swelling. This would lead to destruction of the particles and failure of the whole system.

Taking into account all these suggestions, it's obvious that for proper functioning of the system the number and size of pervious to water channels in the shell should be optimized.

RESTRICTIONS OF SWELLING OF SURFACE-IMMOBILIZED MICROGELS DUE TO THE SUBSTRATE

Improper deposition of the particles on the surface and/or their deformation during the contact of soft particles with the solid substrate

could drastically reduce expected switching effect. Therefore it is important to achieve the deposition of particles onto the surface with minimum deformation of their spherical form, in order to minimize the contact of particles with surface and hence, to lower the swelling restriction due to the substrate.

RESTRICTIONS OF CORE'S SWELLING OF CORE-SHELL PARTICLES DUE TO THE SHELL

It is believed that swelling ability of the core-shell particles is mostly determined by the chemical composition of the hydrophilic core, but also it is significantly influenced by the nature and thickness of the shell. It was shown that even the presence of a hydrophilic shell such as polyvinylamine on hydrophilic core, like poly(acrylic acid) can restrict its normal swelling^[163]. Similarly, the PNIPAM shell on P(NIPAM-AA) cores restricts their total swelling so that resulting core-shell microgels were found to be smaller than the parent ones^[164].

The restriction could be even stronger in the case when the shell is composed from the material with properties, opposite to the core. Such shell could restrict, and even completely arrest the swelling. Therefore, evaluation of some critical parameters for microgels covered with hydrophobic elastic shell (supposing that such shell is no hinders in water access into the core) has to be done in order to determine limits of the expected swelling properties.

As it was mentioned before, the swelling ability of the gel is caused by extent of water uptake. Quantitatively swelling can be characterized by the swelling ratio S_v , i.e. by the volume ratio of the swollen microgels and the same ones in water-free state. A gel, which has not reached its maximum degree of swelling, will swell if it is submitted to an osmotic pressure. The equilibrium pressure difference between the hydrostatic pressure P_{gel} in the isotropic gel phase and the pressure in the solvent

$P_{solvent}$ is called swelling pressure $P_{swelling}$ ^[165]. Therefore, the osmotic pressure is the driving force of the swelling process.

The swelling pressure of nonionic gels, is typically described as a result of two contributions: contribution of the polymer/solvent mixing and contribution of the elasticity^[166]. Swelling process distends the network and is opposed by the elastic contractility ($P_{elastic}$) of the stretched polymer chains^[167]. In this case the swelling pressure ($P_{swelling}$) of a non-ionic hydrogel can be defined as:

$$P_{swelling} = P_{osm} - P_{elastic} \quad [4-5]$$

At equilibrium conditions, when:

$$P_{osm} = P_{elastic} \quad [4-6]$$

the swelling pressure ($P_{swelling}$) will be equal to zero.

For different microgels, the swelling pressure varies with the chemical composition and concentration of the polymer network (cross-linking degree).

In the case of PNIPAM-based gels, it is possible to measure the change in swelling pressure upon swelling-collapse transition as a function of temperature, or the temperature sensitivity of the polymer. Inomata et al^[168] determined that the swelling pressure of the PNIPAM network correlates with the amount of a cross-linker and lying in a range of 5-10 kPa. For some types of gels, including biological cross-linked systems, swelling pressure can reach the values up to tenth of MPa^[165]. Gels consisted of copolymer of methylmethacrylates and N-vinyl-2-pyrrolidone were also investigated in terms of swelling pressure and it was found that they are able to produce the maximal $P_{swelling}$ of ~ 30 kPa^[169]. The same authors evaluated the possibility of use of the

osmotically driven hydrogel systems for fabrication of expandable tissues. The range of possible volume expansions from 3 to 30 times for hydrogel-based tissues was determined.

Pressure arising from the swelling of the microgels was a next important parameter that was investigated in this work. It was done by measuring swelling pressure produced by the parent macroscopic gel having the same composition as the microgels used. The maximum value of the swelling pressure found was then taken into account for the shell design of the desired core-shell microgels.

Unlike shell-free microgels, core-shell particles, would experience additional forces, such as contraction of the elastic shell, which would restrict the swellability. These forces will be the greater the higher thickness and lower elasticity of shell will be.

Due to the tunable elastic properties of the cross-linked polyisoprene, it is logical to suppose that the shell will be able to undergo the reversible stretching and contraction in a broad range of swelling degree of the core. Nevertheless, some critical values, namely the maximum permissible thickness and tolerable elastic modulus of the shell, have to be determined in order to ensure the unhindered microgels swelling.

These limiting factors, which would enable microgels cores enclosed in the shells to swell up to a certain value could be calculated using an equation of pressure loaded thin-walled vessel (sphere)^[170]. In a thin-walled vessel by definition the thickness of the wall is no greater than one-tenth of its radius. Let us consider such a vessel (in our case microgels) subjected to an internal pressure above atmospheric pressure (in our case it will be the swelling pressure of the correspondent hydrogel). Knowing the initial geometrical parameters of microgels one can predict their expansion when the internal pressure (i.e., the swelling pressure) exceeds the atmospheric pressure, as follows:

$$\sigma_{sph} = \frac{P_{swelling} \cdot r}{2 \cdot t} \quad [4-7]$$

σ_{sph} - the stress of the shell, $P_{swelling}$ - internal pressure equal to swelling pressure of hydrogel, r - the radius of microgel before swelling, t - the thickness of the shell;

$$R = \frac{P_{swelling} \cdot r^2 \cdot (1 - \nu)}{2 \cdot E \cdot t} \quad [4-8]$$

R - an increased radius of the microgel during swelling, ν - Poisson's ratio, which is 0.5 for elastomers, E - the modulus of elasticity (or Young's modulus) of the shell material.

For polyisoprene rubbers modulus of elasticity depending on the cross-linking density can vary in the range from ~100 KPa to tenth MPa^[158]. Therefore, the range of pressures necessary to increase the core-shell particles size can also be variable. From the other side the critical value of permissible shell thickness will depend on cross-linking density of polyisoprene used.

In this work Eq.4-7 and Eq.4-8 were used for calculation of shell thickness limits and allowable elastic modulus at given microgels size and swelling pressure.

SWITCHING OF SYSTEM'S WETTING PROPERTIES

The last prediction, necessary for establishing the feasibility of the inverse switching effect, is a range of surface energy changes upon swelling-deswelling of core-shell particles.

As it was already mentioned in Chapter 2.1, the resulting contact angle θ of any heterogenic surface can be evaluated using phenomenological Cassie equation (Eq.2-8).

Dependence of the water contact angle of the system composed of highly hydrophilic substrate (WCA $<5^\circ$) and the particles with PI shell (WCA $\sim 109^\circ$)^[157] on the surface coverage is presented on Figure 4-4.

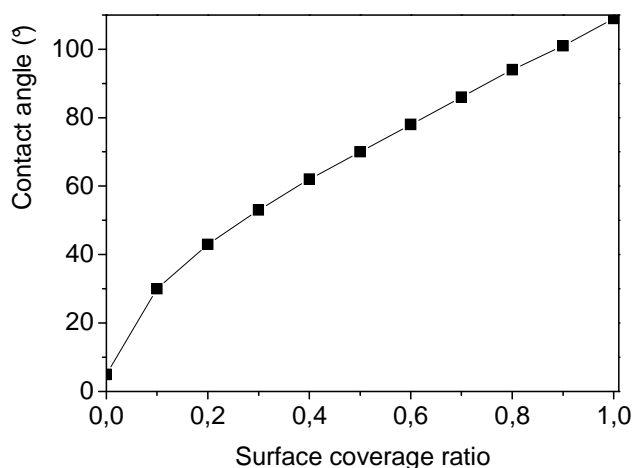


Figure 4-4 WCA of heterogenic (A+B) surface as a function of surface coverage ratio calculated by Cassie equation for the values of $\Theta_A = 109^\circ$ and $\Theta_B = 5^\circ$

As one can easily see, the water contact angle (WCA) of such surface should not exceed $30\text{-}40^\circ$ when the ratio of hydrophobic to hydrophilic material on the surface of about $0.1\text{-}0.2$ and it should be close to 100° when the surface coverage is approaching 100% .

Using this simple relationship it is possible to calculate the limits of WCA changes, knowing the initial fractions of the materials covering the surface and their own contact angles.

4.2 SYNTHETIC APPROACHES TO OBTAIN THE CORE-SHELL STRUCTURES HAVING HYDROGEL CORE AND HYDROPHOBIC SHELL

Synthetic challenges during preparation of the core-shell particles with hydrophilic core and hydrophobic shell arise from high incompatibility of the two components, which must be combined in one object. Two different approaches have been explored in this work for realization of this task.

The first method, which was chosen, is the polymerization of core-forming monomer in the droplets of inverse emulsion, using the block copolymer surfactant containing shell-forming block as stabilizer. Schematically the approach named as “one-pot method” is shown on Fig.4-5.

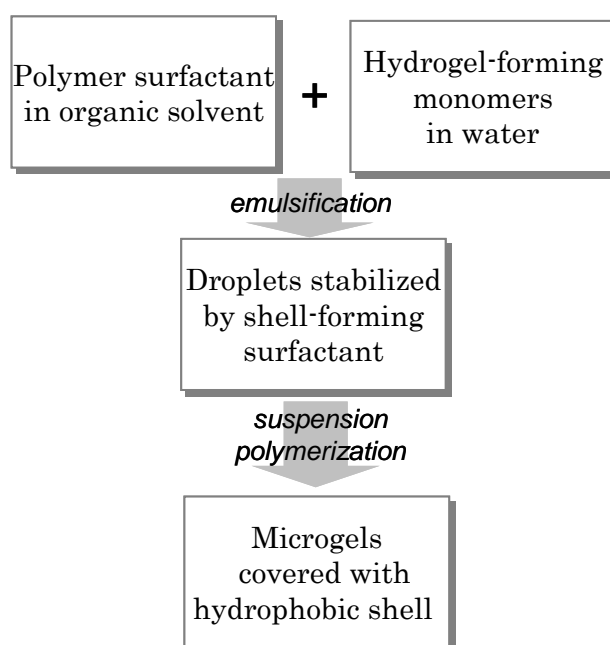


Figure 4-5 Schematic representation of “one-pot” approach used for preparation of core-shell particles.

This approach, however, is limited in terms of monomers, which can be used in the core synthesis. In order to provide homogeneous polymerization in the whole volume of the droplet the obtained polymer should remain soluble in reaction media upon the polymerization process. Oppositely, if precipitation is taken place during polymerization in droplets volume, network is formed inhomogeneously that leads to formation of hollow structures [171].

The shell on the microgels prepared by “one-pot” approach is produced simultaneously during the polymerization reaction. To form stable core-shell particles, it must be firmly bonded to the microgels core. Such bonding can be achieved either by covalent attachment of the shell-forming polymer to the core or, as an alternative, could be physically bonded to the core’s body forming the entanglements between the hydrogel network and hydrophilic part of block copolymer surfactant.

Thereafter, core-shell particles, synthesized by “one-pot” approach were deposited in a loosely packed manner and chemically bonded to the functionalized hydrophilic substrate with an aim to provide a sufficient fixation of particles during dynamic changes of the resulting “contraphilic” system.

Alternatively suggested in this work “bottom up” approach implies synthesis of the suitable microgels followed by covering of them with elastic hydrophobic porous shell (Fig.4-6).

Fabrication of the shell within this synthetic strategy was done by two different methods. The first method involves the modification of the microgel’s surface with initiator of radical polymerization followed by surface initiated polymerization of isoprene. In order to prevent coagulation and precipitation of the microgels upon the shell formation, pre-synthesized particles were immobilized on the solid support. Additional advantage of deposition of free-of-shell particles comes from the ability of some microgels to form long-range ordered 2D periodic arrays at certain conditions that simplifies the investigation of switching

behaviour of surfaces on micro – and macroscopic scales. The microgels parameters and deposition conditions influencing on the particles order and periodicity were analyzed in this work and used thereafter for the achievement of optimal surface coverage density of microgels.

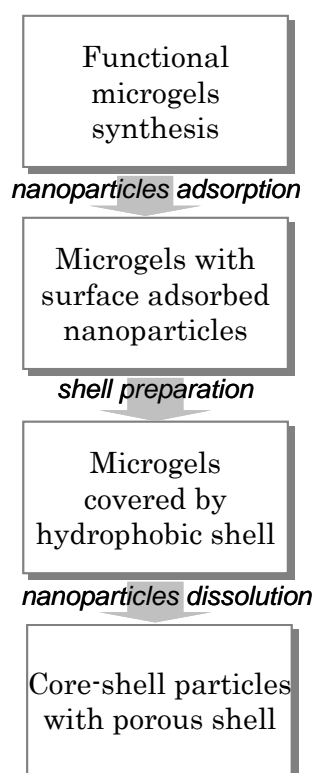


Figure 4-6 Schematic representation of “bottom up” approach used for preparation of core-shell particles.

Another “bottom up” technique of preparation of the shell is based on so-called “colloidosome” method. The shell-forming polyisoprene latex, bearing the charge opposite to the microgel network, was adsorbed onto the surface of pre-synthesized microgels, followed by latex coagulation. In this case the conflict of immiscible components of the core and the shell was overcome.

In order to create porous shell, the surface of the cores was decorated with sacrificial nanoparticles, e.g. silicon oxide or polystyrene

latex before formation of the shell. The particles were washed out after shell formation in order to provide water-permeable channels within hydrophobic shell.

5. SUBSTRATE SELECTION AND CHARACTERIZATION

As it was mentioned before, the major components of inversely switchable system should possess opposite properties. In contrast to the hydrophobized microgels, the second component, substrate, has to be hydrophilic. Covalent binding of the microgels to the substrate is necessary in order to provide stability of the system during swelling-deswelling cycles. Thus the substrate's top layer has to possess a certain functionality, complementary to the particles reactive groups. Si substrate modified with covalently grafted poly(acrylic acid) (PAA) brush was considered as a suitable substrate due to a high hydrophilicity of PAA coating and sufficient chemical activity of carboxylic groups.

Carboxy-functionalized surface was prepared using previously developed procedure^[172]. Highly polished single-crystal silicon wafers with ~1.5 nm thick native silicon oxide layer were used as a supports. They were cleaned with dichloromethane in ultrasonic bath and treated with aqueous solution of ammonium hydroxide and hydrogen peroxide (volume ratio $\text{NH}_4\text{OH}:\text{H}_2\text{O}_2:\text{H}_2\text{O}$ 1:1:1) in order to oxidize the upper layer and activate the hydroxyl groups of the surface. Then, poly(glycidyl methacrylate) (PGMA, $M_w=12700$, $M_w/M_n=1.15$) was spin-coated on the surface from 0.05% solution in chloroform and annealed at $T=130^\circ\text{C}$ for 2 hours to covalently bond PGMA layer to the substrate. The thickness of resulted PGMA film was measured by ellipsometry and found to be of ~7-8 nm. Next, polytertbutylacrylate (PtBA) film was deposited by spin-coating from chloroform solution. After annealing ($T=150^\circ\text{C}$ for 2 hours) the thickness of PtBA layer measured by ellipsometry was of ~4-5 nm.

Finally, the conversion of PtBA to PAA was done by acidic hydrolysis of tert-butyl ester groups to carboxylic ones by treatment of substrate with 1 wt% of methanesulfonic acid in dichloromethane for 1 hour. The thickness of obtained PAA layer measured by ellipsometry decreased for about 1 nm compared to the thickness of PtBA layer.

AFM imaging of the samples was done after each preparation step. Formation of smooth and homogeneous surfaces was confirmed. From the topography AFM images the roughness for PAA brush was measured for 10x10 μm area. The value of RMS roughness was found to be of about 1.2 nm (Fig.4-7). Taking into account the Wenzel equation (Eq.2-6), the influence of the topology on the contact angle could be considered as negligible. Stability of the surface with respect to all possible chemical and physical treatments, which were applied during further surface modification steps was also monitored by AFM. It was found that the modification procedures affect insignificantly the surface topology and homogeneity.

Water contact angle of the PAA surface measured using DSA technique was found to be dependent on protonation of carboxylic groups. In a protonated state PAA-covered surface demonstrated the value of water contact angle of 60-63°, while immersion of sample into ammonia solution (pH ~9) led to dissociation of carboxylic groups and decrease of WCA down to 22-23°.

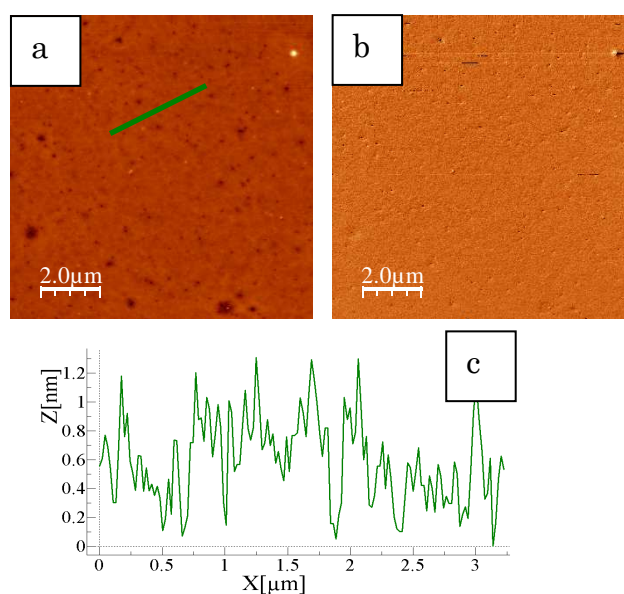


Figure 4-7 AFM topography (a) and phase (b) images and cross-sectional profile (c) of a substrate covered with PGMA/PAA layer.

To exclude the influence of the substrate charge, additional measurements of water contact angle were performed using ammonia solution instead of pure water.

5.1.1 “ONE-POT” SYNTHETIC ROUTE TO CORE-SHELL PARTICLES VIA INVERSE SUSPENSION POLYMERIZATION

The method of suspension polymerization was developed by Hoffman and Delbruch in 1909^[173] and first suspension polymerization of acrylic monomers leading to the formation of beads was performed by Bauer and Lauth in 1931^[174].

In suspension polymerization, an initiator is soluble in the monomer phase, which is dispersed in a medium (usually water) to form droplets (i.e. an emulsion is formed). Solubility of the dispersed monomer (droplet) phase, as well as resultant polymer in the dispersion medium is usually low. The volume fraction of the monomer phase in reaction mixture is typically within the range of 0.1–0.5. At higher monomer volume fraction, the concentration of continuous phase may be insufficient to fill the space between droplets what lead to coalescence^[175].

In contrary to classical oil-in-water suspension polymerization, the inverse suspension polymerization (water-in-oil) is suitable in cases when monomers and produced polymers are relatively water-soluble. For preparation of emulsion either pure monomers or their aqueous solution are dispersed within an immiscible organic solvent.

The size distribution of the initial emulsion droplets and, hence, the size of the formed polymer beads, is dependent on the balance between droplets break-up and droplets coalescence processes. Therefore, suspension polymerization usually requires an addition of small amounts of stabiliser to hinder coalescence and breaking-up of droplets during

polymerization. The majority of droplets stabilisers used in suspension polymerization are either soluble in continuous phase amphiphilic polymers, or small, usually inorganic particles, adsorbed at the oil/water interface.

Polymeric surfactants, mainly block or graft copolymers, but also functionalized oligomers and polysoaps, have aroused increasing interest over the last decades in connection with a variety of applications as emulsifiers, dispersion stabilizers, wetting agents, and compatibilizers. The interest in these polymeric amphiphiles and, especially, in block copolymers with well-defined structure, molecular weight and composition, arises mainly from their unique solution and associative properties. Block copolymers, consisting in the simplest case of hydrophilic and hydrophobic blocks, behave similarly to low-molecular-weight surfactants. However, polymeric surfactants have much lower diffusion coefficients and critical micelle concentrations than “classic” surfactants in general.

The research on block copolymers as polymeric surfactants and their colloidal behaviour was developed from the pioneering work of Molau^[176] in the mid 1960s.

Amphiphilic copolymers were exploited as emulsifiers in works of Perrin^[177], Richter^[178].

An ability of block copolymers to stabilize either droplets of oil in continuous water phase or vice versa water droplets in oil phase depends mainly on its composition and ratio between hydrophobic and hydrophilic parts of amphiphil and is determined by so called hydrophilic-lipophilic balance (HLB) of the particular surfactant.

The HLB concept was first introduced by Griffin^[179] as an empirical scale to describe the balance of the size and strength of the hydrophilic and lipophilic groups in the emulsifier molecule. In proposed by Griffin HLB system both surfactants and oil phases could be classified. The latter are described in terms of a “required HLB” value for their

emulsification. In this sense, every oil phase has two required HLB values, one of them for water-in-oil (w/o) and other for oil-in-water (o/w) emulsification. Usually HLB system classification is used for description of nonionic surfactants and typically ranges from 1 (most hydrophobic) to 20 (most hydrophilic). Therefore HLB value of 1 indicates oil solubility, while the value of 20 indicates a high degree of water solubility.

Ionic surfactants generally have a much higher HLB value than nonionics due to the higher hydrophilicity of the charged groups.

Generally, the applications of nonionic surfactants within the following HLB ranges are as follows:

<u>HLB range</u>	<u>Application</u>
3 - 6	w/o emulsifiers
7 - 9	wetting agents
8 - 18	o/w emulsifiers
13 - 15	detergents
> 15	solubilizers

Therefore, for creation of stable water-in-oil emulsion surfactants having HLB in the range 3-6 are required.

Rough estimation for the HLB of nonionic block copolymer surfactant could be done by calculating weight fraction of the hydrophilic part of the molecule and positioning this figure in scale from 1 to 20, assuming that 1 corresponds to 0% and 20 to 100%, respectively (Eq.4-9).

$$HLB = \frac{M_{hydrophilic}}{M_{sum}} \times 20 \quad [4-9]$$

Using the concept of HLB criteria it is easy to select a proper block copolymer calling to act as surfactant for stable emulsions by calculation of required molecular weight and a proper ratio between blocks with

opposite philicity. In such way series of polymeric surfactants with varied molecular weight while maintaining a constant hydrophilic–lipophilic balance (HLB)^[180] can be predicted and synthesized.

In this work, inverse suspension polymerization of hydrogel-forming monomers stabilized in droplets with polymeric, polyisoprene-based surfactant was applied for one step creation of microgels having hydrophobic shell.

5.1.1.1 Synthesis and characterization of shell-forming polymeric surfactant

As it was mentioned before, surfactants with low HLB are required for the dispersion of polar monomers in nonpolar dispersion media (i.e. w/o emulsion). To this end, two different block copolymers consisting of polyisoprene block and poly(ethylene oxide) block with different molecular weights and blocks ratios were synthesised by anionic polymerization (Fig.4-8).

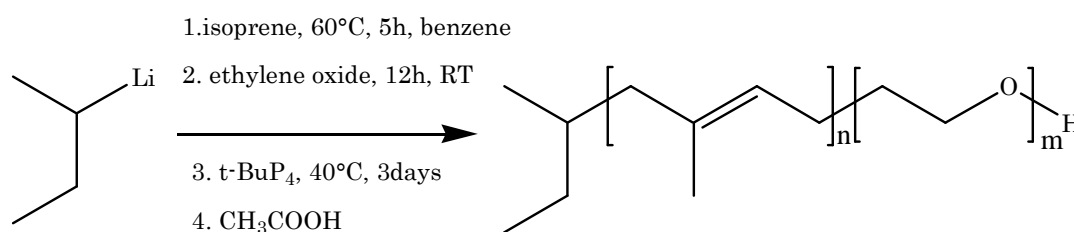


Figure 4-8 Scheme of synthesis of PI-b-PEO block copolymers

The molecular weights and distributions of the polymers, as well as block ratios have been determined using a combination of *Size Exclusion Chromatography* (SEC or GPS) and *Nuclear Magnetic Resonance* (NMR)

analysis. The results of GPC measurements are presented in the Table 4-1.

Suitability of both polymers for emulsion stabilization was proved in several different organic media (trimethylpentane, cyclohexane, toluene). It was found, that either of two synthesized block copolymers was suitable for preparation of water-in-oil emulsions due to proper HLBs values. Stability of emulsions was studied by *Dynamic Light Scattering* (DLS) measurements. It was found that the droplets size and size distribution remained almost unchanged for 20 hours after emulsifying.

Table 4-1 Molecular weights, polydispersity indexes and HLB factors of block copolymers used as surfactants in suspension polymerization of core-shell particles.

Polymer composition	M_n PI-block*	M_n PEO block**	PDI	HLB
PI ₃₅₇ -b-PEO ₁₃₂	24300	5830	1.30	3.97
PI ₅₇₃ -b-PEO ₁₇₂	51800	9768	1.05	3.25

* *Molecular weights of polyisoprene blocks determined by GPC.*

** *Molecular weights of poly(ethylene oxide) blocks calculated from GPC data of block copolymers, by subtraction of correspondent M_n of PI-block.*

Optimal ratio of oil/emulsifier has been found from DLS measurements of w/o emulsions. The results of measurements of freshly prepared emulsions and the same emulsions after equilibration showed that the 3-5 wt% of surfactant is appropriate amount to obtain droplets with average diameter in the range of ~1300-2000 nm and polydispersity index of 0.2-0.3. Such emulsions were also found to be stable in the temperatures range needed for polymerization reaction (60-80°C) with negligible coalescence effect in a time scale required for completing polymerization process. Regardless of surfactant concentration in all

studied emulsions, a certain amount of larger (~3-5 μm) and smaller (~0.5-1 μm) droplets was found, however their fraction in overall numbers varied from ~2% to ~10% (DLS data).

After investigation of surfactants, inverse water-in-oil emulsions were prepared and core-shell microgels stable in hydrophobic media were synthesized. Synthetic conditions, materials used for particles preparation and characteristics of obtained structures are described in detail below.

5.1.1.2 Selection of the monomer for the formation of inner part of core-shell particles

Among of various possible materials suitable for fabrication of water-swallowable hydrogel cores our attention was focused on poly(N-isopropylacrylamide) (PNIPAM) and polyacrylamide (PAAm) mainly due to their well-studied water swelling behavior^[97, 104, 105, 181-183]. However, when inverse w/o suspension polymerization using polyisoprene-based macromolecular surfactant was performed, the morphology of resulting core-shell microparticles was found to be strongly dependant on the monomer nature^[171]. As could be seen from the SEM images (Fig.4.9), in case of NIPAM polymerization hollow capsules (Fig.4-9, a) are formed, while the application of AAm results in non-hollow microspheres (Fig.4-9,b). The possible reasons of such different morphologies and mechanisms behind are discussed below.

It was previously reported that the formation of hollow PNIPAM structures could be achieved via selective generation of radicals at oil-water interface^[184, 185]. But, according to the observations, when the inverse suspension polymerization of NIPAM is carried out at temperatures above the LCST of PNIPAM, the selective generation of radicals is unnecessary for achieving of hollow structures, since the phase

separation of the formed cross-linked PNIPAM above the LCST is sufficient factor to induce the formation of the microcapsules.

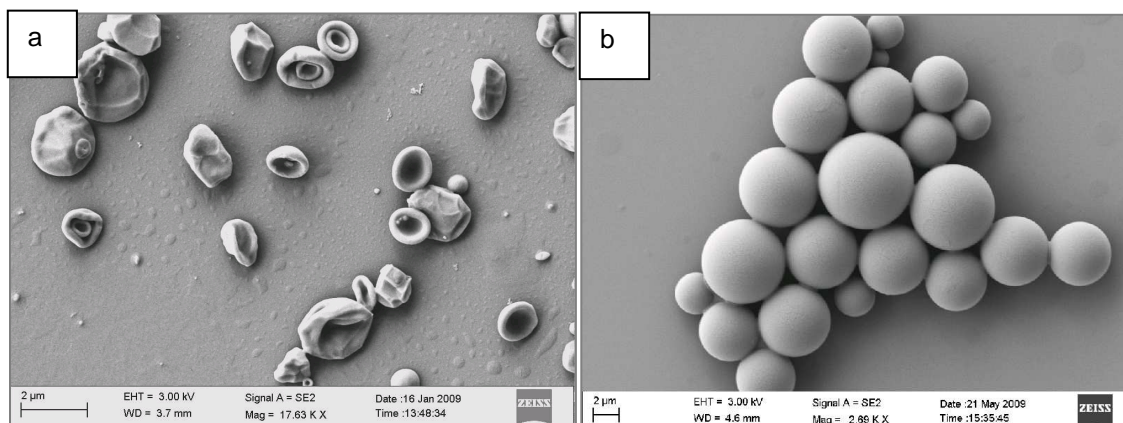


Figure 4-9 SEM images of (a) hollow PNIPAM capsules and (b) non-hollow PAAm spheres prepared via inverse w/o suspension polymerization using PI-b-PEO polymeric surfactant.

A most important condition for the formation of the capsules in this method is that polymerization is conducted at temperature above the LCST of polymer that, it is believed, induced precipitation of the formed PNIPAM phase at the w/o interface.

In aqueous solutions at temperatures above LCST polymerization of NIPAM follows so-called precipitation-polymerization mechanism. At such conditions hydrophobic NIPAM oligomers are formed at early stages of the polymerization and precipitate from the aqueous medium with further aggregation to form nuclei that grow finally resulting into well-defined PNIPAM microspheres^[106, 171]. However, if the polymerization of NIPAM is performed in the presence of template particles with an appropriate surface functionality, then the precipitation of the growing PNIPAM chains occurs selectively on the seeds (precipitation on convex surfaces)^[186]. It was suggested that similar “templated” mechanism takes place in our experiments with the only difference that the concave surfaces of the droplets act as “seeds” for selective precipitation of the phase-separated PNIPAM leading to the hollow microcapsules. It is likely

that formed hydrophobic NIPAM oligomers accumulate preferentially at the w/o interface rather than homogeneously nucleate in water due to a higher hydrophobicity of the continuous phase and of the block copolymer surfactant.

Fabrication of hollow microcapsules is of big interest for many applications, in particular, for drug-release systems, cosmetic industry etc., and, it is believed, this method of fabrication of hollow PNIPAM capsules could find its particular application due to facility of performance. However, such hollow microcapsules are not suitable for fabrication of coatings since they could not be properly assembled on the substrate. Therefore, our attention was switched to AAm as an alternative core-forming monomer.

As was already mentioned, in contrast to NIPAM, polymerization of AAm in inverse w/o suspension polymerization leads to formation of particles with non-hollow morphology. Such difference is most likely caused by more hydrophilic nature of PAAm.

Conventional inverse suspension polymerization requires that all of the components, including monomers, cross-linker, initiator and resulted polymer have to be soluble in water and non soluble or poorly soluble in the oil phase. In this case, during polymerization major portion of the reaction components will be located in the water phase and, thus, formation of the cross-linked polymer is expected to occur in the whole volume of the droplets, and not only at the w/o interface. If so, non-hollow spheres could be expected for polymerizations performed at the temperature 80°C if the formed polymer (e.g. polyacrylamide) is miscible with the dispersed phase (i.e. water). Indeed, it was demonstrated that when more polar acrylamide was used instead of NIPAM under otherwise identical polymerization conditions, solid polyacrylamide microspheres are formed (Fig.4-9, b). Schematic representation of inverse suspension polymerization and resulting morphologies for NIPAM and AAm monomers is presented on Fig.4-10.

To summarize, homogeneous polymerization of acrylamide within the droplets (microreactors) yields solid microgel beads (Fig.4-9, b), while if NIPAM is used as the monomer, the reaction inside droplets follows precipitation-polymerization mechanism, resulting in hollow microcapsules^[171] (Fig. 4-9 (a)).

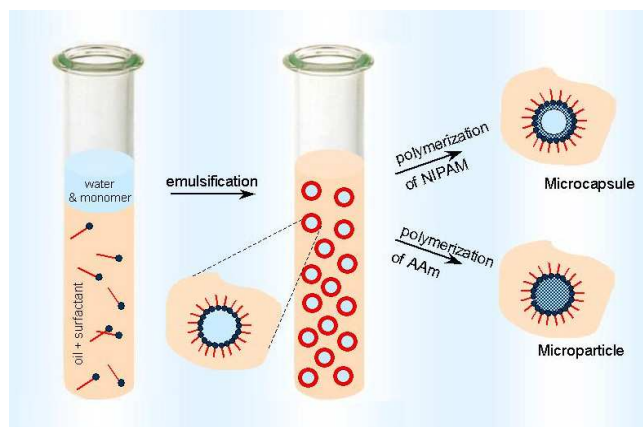


Figure 4-10 Scheme of formation of hollow capsules or non-hollow spheres in w/o suspension polymerization of different monomers.

With this in mind, core-shell particles having PAAm core and PI shell prepared via “one pot” approach were used further for preparation of surfaces with inversely switchable wettability.

5.1.1.3 Synthesis of core-shell particles via inverse suspension polymerization and their characterization

Using the “one-pot” synthetic approach, core-shell PAAm-PI particles were prepared by w/o suspension polymerization of hydrogel-forming acrylamide water solution using the polyisoprene-*b*-poly(ethylene oxide) (PI-*b*-PEO) block copolymers (for details see Table 4-1) as surfactants and, at the same time, as a shell-forming material.

Preparation of core-shell particles by suspension polymerization

0.15 g of polymeric surfactant was dissolved in 3 mL of trimethylpentane (TMP), forming the oil phase. Separately, 0.225 g of acrylamide (AAm), 3 mol% of cross-linker N,N-methylenbisacrylamide (MBA) and 1 mol% of initiator

potassium persulfate (KPS) were dissolved in 0.225 mL of deionized water. Water and oil phases were mixed with Ultra-Turax mixer (IKA, Germany) at 13500 rpm for 2 min. Obtained emulsion was transferred using a syringe into the closed glass tube equipped with magnetic stirrer. Temperature of reaction mixture was rapidly risen to 80°C and the polymerization was carried out for 1 hour. Afterwards reaction was stopped by cooling to room temperature and particles were washed by repeating centrifugation/redispersion cycles in pure TMP and THF in order to remove unreacted components and excess of surfactant.

After purification resulted particles remained able to form a stable dispersion in organic solvents, such as hexane, cyclohexane, isooctane, anhydrous THF. At the same time, addition of water to dispersion led to flocculation of the particles. Therefore, it was suggested that macromolecular emulsifier remained attached to the microgel's core forming the hydrophobic shell.

Size and polydispersity of core-shell PAAm-PI particles synthesized by “one-pot” approach were measured in dispersed state using DLS technique. Before measurements, particles were fractionated using centrifugation with a stepwise increase of rotation speed. Finally, particles with the diameter close to 1-2 μm and polydispersity index in a 0.2-0.3 range were isolated (Table 4-2).

For comparison, particles size and size distribution before and after fractionation were also evaluated from analysis of corresponding SEM images (Fig.4-11).

As could be seen from SEM images (Fig.4-11, a) as-synthesized particles are of well-defined spherical shape but display a broad size distribution. Here it should be mentioned, that all attempts to avoid polydispersity of as-prepared particles were not successful, resulting in a formation of a particles with a typical size range of 0.2-3.0 μm .

4 Results and Discussion

Table 4-2 Size and size distribution of PAAm-PI core-shell particles synthesized by the “one-pot” approach.

No	Fraction	DLS measurements*			SEM measurements
		Average diameter, nm	Mean peak value, nm	PDI	Average diameter, nm (SD**)
1	Fraction 1	2837	1931	0.344	1996 (397)
2	Fraction 2	1439	1423	0.180	1395 (302)
3	Fraction 3	1446	1280	0.247	1082 (212)

* - particles dispersions for measurements were prepared in anhydrous THF, all measurements have been performed in a closed glass cuvette to avoid the contamination with water from air. The partial swelling of particles in pure THF was not taken into account.

** - standard deviation

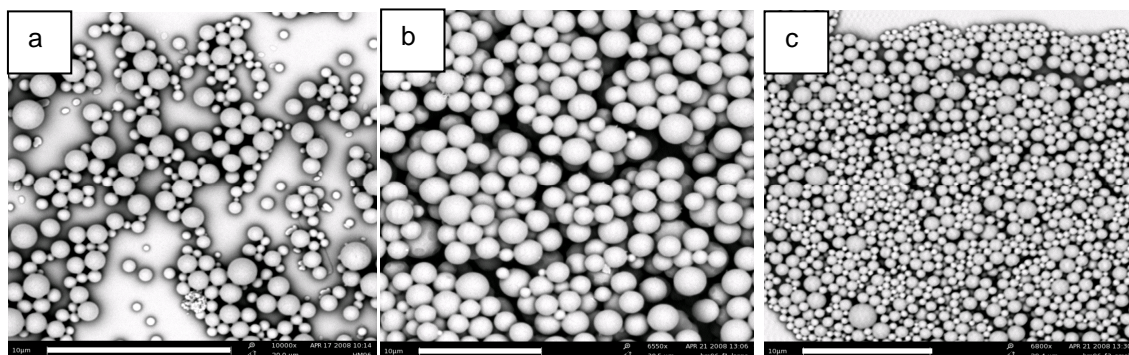


Figure 4-11 SEM images of PAAm-PI core-shell particles prepared via w/o suspension polymerization (a) before and (b, c) after fractionation (fractions 1 and 3 shown in the Table 4-2, respectively). Scale bars – 10 µm.

In some cases the local formation of ordered arrays of the particles of similar size was observed when deposited on a substrate (Fig.4-12), but generally it was not possible to avoid polydispersity of particles and separate them into monodisperse fractions. Nevertheless, taking into account softness of hydrogels in a swollen state, it was supposed that

particles with polydispersity close to 0.2 should be suitable for preparation of packed arrays of swollen particles.

For precise investigation of geometry and possible surface-induced conformation changes of PAAm-PI particles after deposition onto a solid substrate, SEM imaging was performed at different tilt angles (Figure 4-13). For this

reason samples were dried from water in vacuum oven at 100°C overnight in order to ensure their fully deswollen state. Then dry particles were redispersed in water-free organic solvent (hexane or cyclohexane). For measurements, a drop of prepared dispersion was placed onto silicon oxide support allowing solvent to evaporate at ambient conditions.

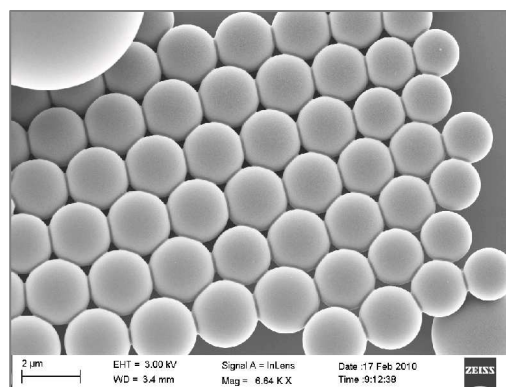


Figure 4-12 SEM image of spontaneous self-assembly of PAAm-PI core-shell particles after fractionation.

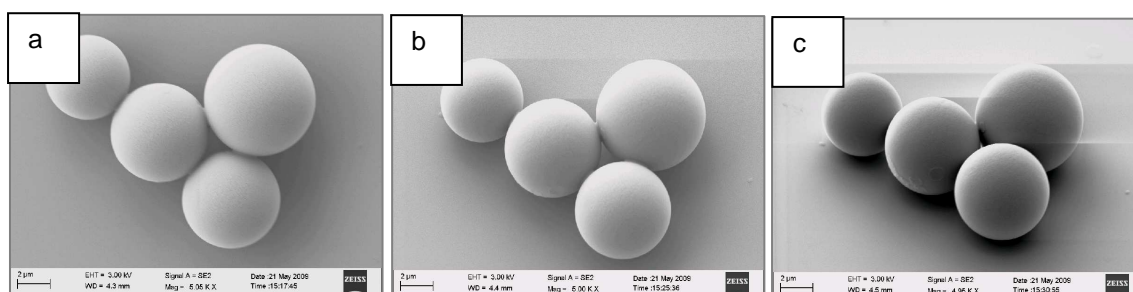


Figure 4-13 SEM images taken at different tilt angles, confirming the spherical shape of PAAm-PI core-shell microspheres deposited on the hydrophilic substrate. (a) – tilt angle 0°, (b) – tilt angle 25° and (c) – tilt angle 50°.

An important feature of obtained PAAm-PI core-shell particles was their ability to be deposited on the surfaces almost without deformation (See Fig.4-13) in contrast to shell-free PNIPAM-based microgels that usually adopt strongly squashed conformation on hydrophilic surfaces due to interplay of surface tensions and capillary forces.

In order to characterize the swelling ability of PAAm-PI core-shell particles obtained by “one-pot” suspension polymerization, DLS measurements were performed. As it was mentioned before, core-shell particles having the hydrophobic shell formed from PI-containing polymeric surfactant can be easily dispersed in organic solvents ranging from THF to hexane. However, they were not dispersible in polar media such as water or ethanol. This introduced certain difficulties in investigation of their water swelling behaviour. To circumvent the problem, dried microgels were dispersed in anhydrous THF and changes of their size upon dropwise addition of water were monitored by DLS. Reasonably, THF was chosen because of its miscibility with water. It was found that hydrodynamic radius increased when water was added to the THF dispersion (Fig.4-14, a) and reached its maximum when water content was approximately 10 vol% (relative to THF). Further increase of water content led to flocculation and precipitation of the particles. Determination of time required for complete swelling of PAAm-PI core-shell particles was made by kinetic measurements (Fig.4-14, b) and equilibrium volume swelling ratio of particles was calculated.

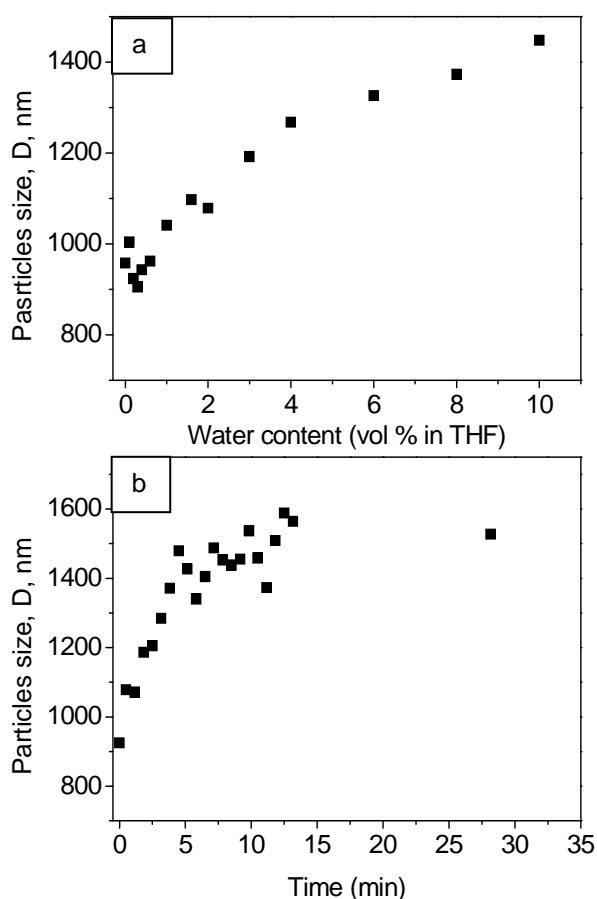


Figure 4-14 DLS measurements of swelling behavior of PAAm-PI core-shell particles in THF/water mixture: (a) - dependence of particles size on water content and (b) – swelling kinetic of particles upon addition of 20 vol% of water (relative to THF) in a one step.

The maximum water-swelling ratio detected for the particles dispersed in THF/water mixture of about ~6 was found to be insufficient compare to the value of ~11 required to provide the change of the surface coverage from 20% to 100%. Nevertheless, the particles were rated as suitable for fabrication of “contraphilic” switchable surfaces due to the following reasons.

Firstly, polyacrylamide particles are partially swellable in THF that was demonstrated by Winnik et al.^[187] and also confirmed in this work by optical microscopy of particles on surface in dry state and swollen with different solvents. Consequently, the “dry” diameter of particles in THF is overestimated. Secondly, because of flocculation of the particles it was not possible to measure maximal degree of water swelling of particles in dispersion. It might be true that the swellability of PAAm-PI particles in pure water should be higher than in THF/water mixture. Therefore, it could be expected that volume swelling ratio of particles from their dry to fully water-swollen state should be larger compare to obtained DLS data.

5.1.1.4 “Contraphilic” surfaces prepared using core-shell particles synthesized by “one-pot” approach

Appropriate deposition properties of PAAm-PI core-shell particles and their ability to swell upon contact with water make them promising candidates for interface-supporting organization processes. These advantages were used in this work to obtain the monolayer of loosely packed core-shell particles on the substrate.

First, the particles were deposited onto a substrate modified with PAA brush by spraying their TMP dispersion over the surface followed by drying of organic solvent. The swelling ability of particles and the change of the surface coverage during exposure to water were investigated using optical light microscopy (Fig.4-15).

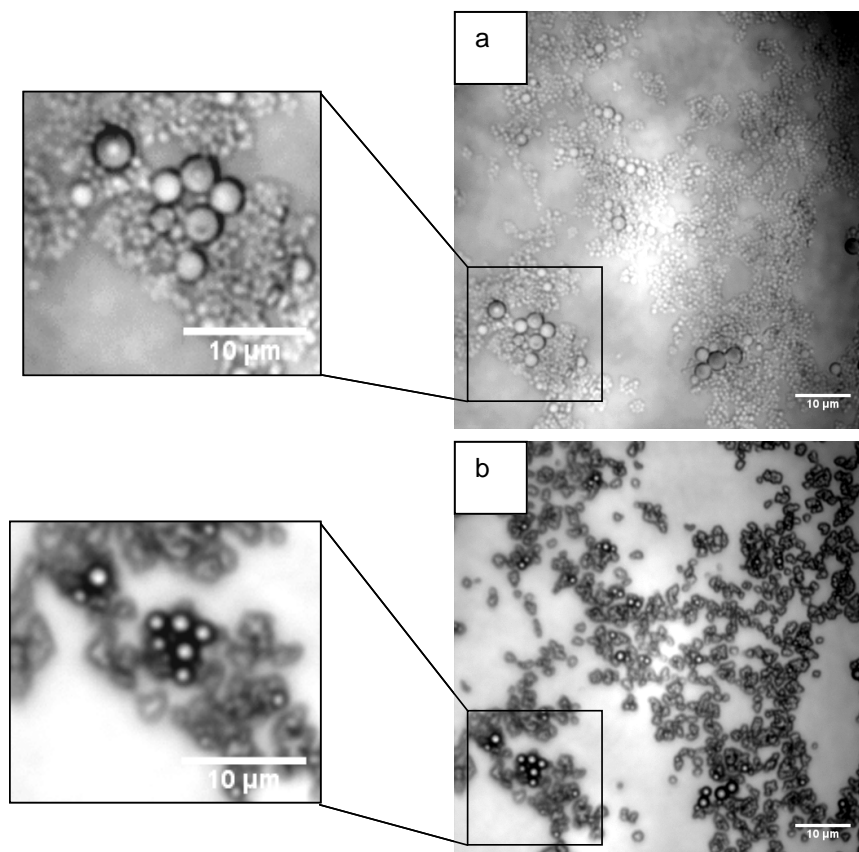


Figure 4-15 Optical microscopy images of the PAAm-PI core-shell particles (a) swollen with water and (b) after drying.

1D-swelling ratio was calculated from the optical images taken before and after particles swelling upon their contact with water and was found to be in a range of 2.0-2.5. Changes in a surface coverage were determined using ImageJ image processing software. For loosely arranged core-shell particles change in a surface coverage from ~30% to ~70% upon swelling in water was observed. Swelling-deswelling cycles have been monitored both after contact with water and in water-saturated air. In both cases the core-shell particles reversibly changed the surface coverage.

In order to obtain maximum coverage of substrate with swollen particles, a kind of interface-supporting deposition process was used (Fig.4-16). The dispersion of core-shell particles in hexane was spread on a substrate over the water surface (Fig.4-16, a). Upon the contact with

water particles swelled and assembled at the water/hexane interface (Fig.4-16, b). The amount of particles introduced onto the substrate was experimentally adjusted varying the concentration and the volume of the dispersion to form a monolayer after evaporation of organic solvent (Fig.4-16, c). After the drying of water the monolayer of particles remained on the substrate (Fig.4-16, d). In such a way, the array of swollen core-shell particles arranged in a closely packed fashion was deposited on the substrate. Upon drying, the particles underwent 3D collapse while retaining their spherical shape which is a desirable collapse scenario. This was proved by SEM-imaging at varied tilt angles after particles drying on the surface. Such behaviour of core-shell particles could be compared with droplets of a liquid with high surface tension, preventing the spreading on a low energy surface.

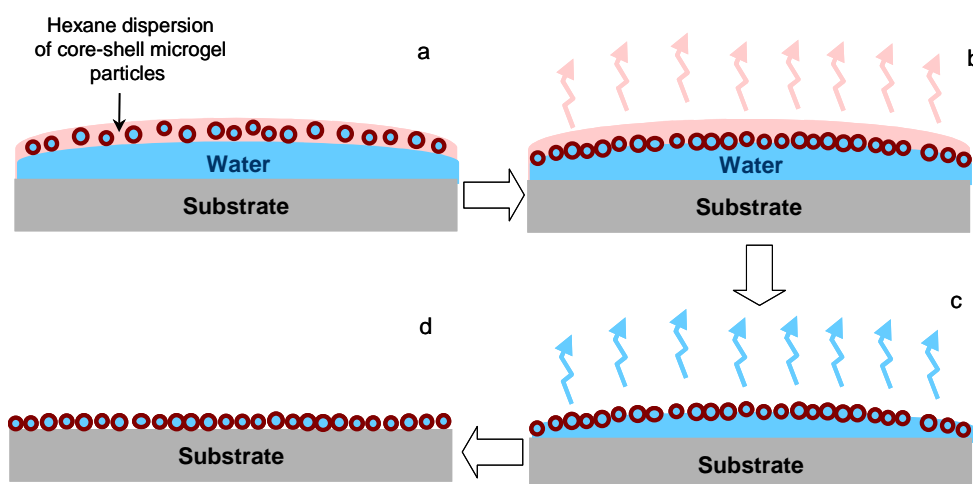


Figure 4-16 Scheme of interface-supporting deposition of PAAm-PI core-shell particles onto the hydrophilic substrate.

Upon drying of densely packed particles layer, obtained as described above, the coverage was reduced from about 100% to approximately 40% (Fig.4-17).

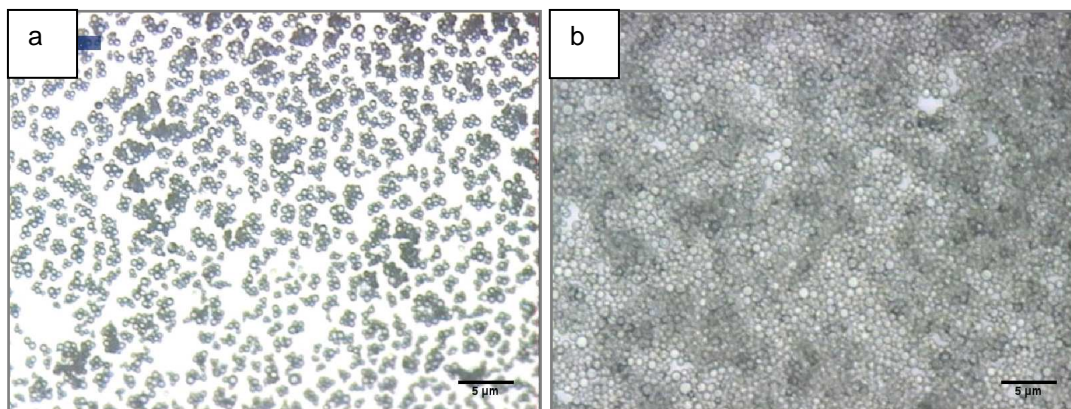


Figure 4-17 Optical microscopy images of monolayer of PAAm-PI core-shell particles deposited on the hydrophilic substrate. (a) – dry particles (b) – swollen particles. Scale bar 5 μm .

The values of expected WCAs for surface covered with PAAm-PI core-shell particles in dry and swollen states were calculated using Cassie equation (Eq.2-8). The calculated change of water contact angle was expected to be in a range from 58° to 108° , assuming the contact angle of PAA substrate as 25° and the surface contact angle of core-shell particles as 108° (WCA of PI). However the contact angle measurements were impossible until the particles were not chemically attached to the substrate due to washing out by the water droplet placed onto substrate during the measurement.

It was suggested that polyisoprene double bonds could be utilized for grafting of core-shell particles to the substrate. Here, it should be taken into account that besides the problem of attachment, the additional challenge was related to the necessity to obtain the loosely packed layer of particles after drying. In order to achieve the homogeneous distribution of the particles over the surface in the dry state, grafting of the particles should be accomplished when they are in the swollen state. Therefore, conventional straightforward chemical grafting methods requiring high temperatures are not applicable.

In order to circumvent this problem, photochemical grafting procedure, which could be performed in mild conditions, was applied. Subsequently, the substrate surface was modified with benzophenone moieties, able to generate radicals upon UV irradiation. The grafting of particles was achieved by trapping of the radicals generated on the surface upon UV exposure by the double bonds of the polyisoprene shell of particles.

The substrate preparation procedure was performed as described below. First, copolymer of tertbutyl acrylate and benzophenone acrylate (PtBA-co-PBPA) (Fig.4-18) was synthesised.

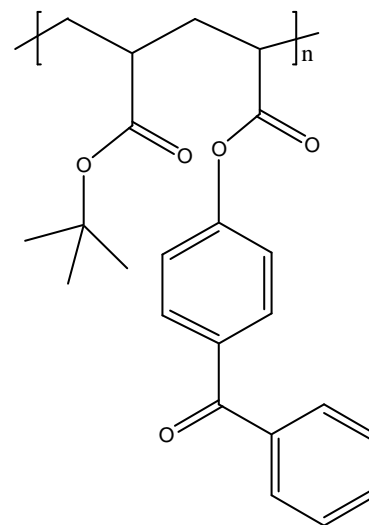


Figure 4-18 Structure of copolymer of tertbutyl acrylate with benzophenone acrylate (PtBA-co-PBPA) used for photochemical grafting of PAAm-PI core-shell particles to the substrate.

Synthesis of PtBA-PBPA.

Benzophenone acrylate (BPA) was obtained from 4-hydroxybenzophenone (BP) and acrylic acid (AA). To this end, 1 g of BP was dissolved in dichloromethane at 0°C followed by addition of equimolar amount of N,N'-dicyclohexylcarbodiimide (DCC) catalytic amount of 4-(dimethylamino)-pyridine (DMAP) and equimolar amount of acrylic acid dissolved in CH₂Cl₂. Temperature of reaction was raised to RT and the mixture was left at continuous stirring for 1 hour. Afterwards, precipitated dicyclohexylurea was filtered off, solvent was evaporated at reduced pressure and the residue was purified by column chromatography giving 0.8 g of pure BPA.

Afterwards, copolymer of tBA and BPA using the monomer molar ratio 10/1 was synthesized. Polymerization was performed in toluene, under argon atmosphere. Monomers were mixed in appropriate ratio, dissolved in oxygen-

free toluene and heated to 60°C. Initiator for radical polymerization, azobisisobutyronitrile (AIBN), was added to the mixture through a syringe and the reaction was carried out for 24 hours. Resulting polymer was precipitated into methanol and dried at 40°C overnight. The conversion of monomers of 77.9% was obtained. M_n of 35400-41600 g/mol and M_w of 95700-115000 g/mol with PDI of 2.67-2.76 for resulting PtBA-PBPA were determined by GPC.

Conversion of tBA units of copolymer into AA units was performed using acidic cleavage of tert-butyl groups. For analytic purpose this reaction was performed in solution. PtBA-PBPA copolymer, dissolved in dichloromethane was treated with 1.0 wt% of methanesulfonic acid in dichloromethane for 1 hour. Resulting PAA-PBPA was dissolved in THF, precipitated into diethylether and dried in vacuum at 40°C overnight. ^1H NMR analysis confirmed full cleavage of tert butyl ester groups, while benzophenoneacrylate units remained unchanged.

Preparation of PtBA-PBPA layer on the substrate surface requires heating up to 150°C for 2 hours, which is typical for grafting-from procedure. Accordingly, the bulk sample of PtBA-PBPA copolymer was studied by ^1H NMR before and after heating in order to check the thermostability of benzophenone groups. The spectrum of the sample after heating did not show changes compared to the non-heated one. However, the sensitivity of the method does not allow detection of minor changes. In contrast, a GPC analysis proved to be very sensitive to changes in macromolecules, since the formation of even a single link between two polymer molecules, in our case due to the possible decomposition of benzophenone, doubles the molecular weight. GPC measurements of the molecular weight of the obtained copolymer after heating gave only slightly higher value than its initial one ($M_n = 31400\text{-}31500$ g/mol, $M_w = 128100\text{-}130700$ g/mol, PDI 4.08-4.15) that could not be attributed to the polymer cross-linking. Therefore, both NMR and GPC studies confirmed the stability of PtBA-PBPA copolymer and its functional groups even after high temperature treatment, and the polymer was suggested as suitable for functionalization of the substrate.

Hydrophilic layer of PAA-PBPA was prepared directly on silica substrate using the similar procedure as was used for preparation of PAA-modified surface (Chapter 4.2.1). In short, Si-wafer was first covered with PGMA thin layer and then PtBA-PBPA copolymer was spin-coated from chloroform solution and grafted to PGMA by annealing at 150°C for 2 hours. Conversion of tBA residues of copolymer into AA moieties was performed by acid cleavage of tert-butyl groups to carboxylic ones by immersion of surface in 1 wt% dichloromethane solution of methanesulfonic acid for 1 hour.

Then, PAAm-PI core-shell particles were deposited on PAA-PBPA modified surface and chemically grafted using UV irradiation. In order to ensure loose packing of particles on the surface, they were kept in water-swollen state during the entire grafting process. Afterwards, particles were dried and their swelling ability and robustness against washing were checked. It was found that chemically grafted core-shell PAAm-PI particles retain their swelling properties and change the surface coverage from 40-50% in dry state to almost 100% in a swollen state. Moreover, particles remained firmly attached to the substrate even after extensive washing with water.

Nevertheless, all attempts to measure of WCA of the substrate covered with chemically attached core-shell particles were unsuccessful, most likely due to the insufficient thickness of the PI shell formed only by PI-b-PEO block copolymer. It was observed that when a water droplet was placed on the surface it was immediately absorbed by PAAm-PI particles, which indicated that the shell was obviously too thin to screen the hydrophilic interior of core-shell particles. Thus, just only water touching the surface, it was pulled by capillary forces and quickly spread over the whole substrate.

In order to achieve measurable hydrophobisation effect of substrate covered with core-shell particles, attempt to increase the shell thickness was made. For this, a new batch of PAAm-PI core-shell particles was

synthesized, using similar suspension polymerization method as the one described above, with the one difference that shell-forming monomers (namely, isoprene in a ratio 1/50 mol/mol regarding to AAm with an addition of 1.0 mol% of divinylbenzene cross-linker) were added to the oil phase of emulsion. Under the polymerization conditions (80°C), free radicals produced in water phase induced simultaneously polymerization of monomers on both sides of droplets: PAAm in water, forming the core, and PI on the outer side of droplets interface, forming an extra shell layer on obtained particles. The same technique was recently applied for creation of double-layer microcapsules, polymerized in emulsion^[188].

Prepared in such way core-shell particles showed the similar size and polydispersity as polymerized without addition of isoprene, but revealed thicker polyisoprene shell, which was clearly resolved by SEM (Fig.4-19).

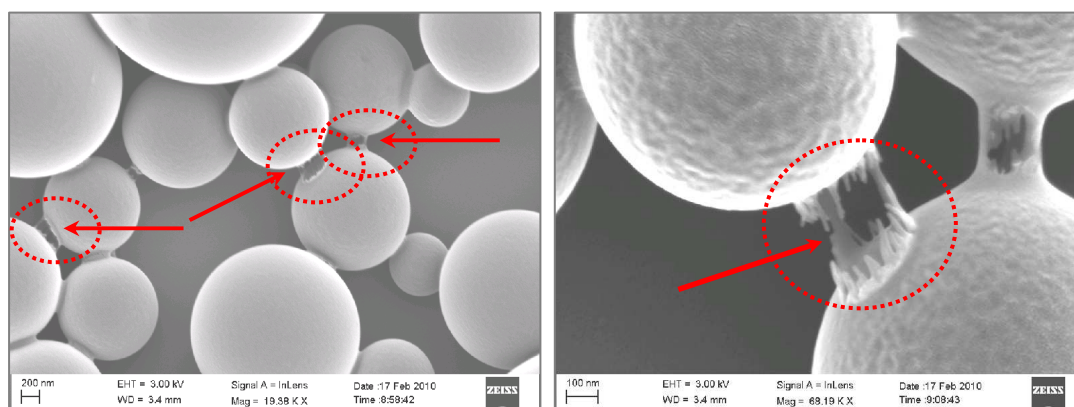


Figure 4-19 SEM images of PAAm-PI core-shell particles with PI shell formed by polymerization of isoprene from the oil phase. The presence of PI shell becomes evident upon its damages (marked with arrows). Scale bars are 200 nm (left) and 100 nm (right).

In order to study their swelling behaviour particles were deposited and chemically grafted onto the PAA-PBPA-coated substrate using UV irradiation. Then, additional cross-linking of polyisoprene was performed by hot vulcanization, namely by soaking of samples in 0.1% toluene solution of sulfur with further heating of samples at 150°C for 20h. The

particles were purposefully made poorly permeable for water in order to minimize capillary effects during the contact angles measurements and reduce the swelling rate in order to make attempt to monitor the changing of WCA in real time of measurement.

Water swelling behaviour of cross-linked PAAm-PI core-shell particles grafted to the substrate was observed using optical microscopy after immersion of sample in water. Comparing the size of the particles in dry and swollen states, minor 1D particles swelling ratio in the range of 1.19-1.24 and correspondently small change of surface covered area (from 17% to 26%) were found.

Thereafter, contact angle measurements of hydrophilic substrate covered with PAAm-PI core-shell particles were performed. The first measured equilibrium WCA (water droplet volume $\sim 10 \mu\text{l}$) was found to be ranging from $\sim 50^\circ$ up to $\sim 79^\circ$ depending on surface coverage in the specific area. In principal, the value of 58° calculated by Cassie equation for the surface with 40% coverage was in the range of measured values of WCA. Interestingly, there was some increase of advancing WCA within one measurement for all investigated samples after addition of water to the droplet (up to $\sim 25 \mu\text{l}$) and establishment of the new water contact line. The value of such increase ranged from several up to $\sim 19^\circ$ for all measured samples and was calculated of about $2\text{-}5^\circ$ in average (Fig.4-20). The difference in absolute values of measured WCA could be attributed to the inhomogeneous surface coverage and structures of particles coating (clustering etc), whereas the increase of the advancing contact angle within one measurement could be related to desirable switching effect. As soon as a droplet of water is applied onto the sample surface, neighbouring particles become be exposed to the saturated water vapours. This causes the swelling of the particles and, possibly, every next measurement detects WCA of the renewed surface with a higher surface coverage and thus, with a higher WCA value.

Although these results suggested that the described above system behaves as expected, the small changes of contact angles indicate that we are still far from the perfect switching effect.

For more pronounced hydrophobization effect the increase of core-shell particles swelling ratio is required. This could be achieved by tuning the cross-linking density of particles shell in order to optimize its elastic properties, or, by incorporation of some defects into the shell structure to ensure the maximum water access to the core. On the other side, presence of very small amount of such defects, which would not affect the hydrophobic nature of particles surface, is needed, because otherwise the particles surface will tend to remain hydrophilic because of influence of capillary forces, which, as it was shown, play an important role in case of direct contact of water with hydrophilic cores of the particles.

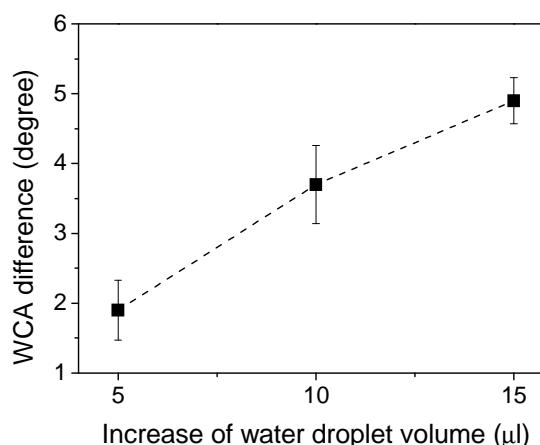


Figure 4-20 Increase of advancing WCA of PAA surface covered with PAAm-PI core-shell particles with increase of volume of water droplet within the DSA measurement.

5.1.2 PREPARATION OF THE CORE-SHELL PARTICLES VIA “BOTTOM-UP” APPROACH

As it was mentioned previously, “bottom-up” approach of synthesis of core-shell particles having hydrogels core and hydrophobic shell entails the initial step of preparation of the suitable microgels followed by second step of covering them with a shell. The composition of the microgel cores of such particles is the most important factor determining the extent of swelling ability of the composite core-shell particles. Therefore, the choice of the material for microgels preparation is the question, which ought to be examined very carefully.

Among all hydrogel-forming polymers thermoresponsive poly(*N*isopropylacrylamide) (PNIPAM) or related polymers used for preparation of microgels are studied most intensively^[189]. Possibility of obtaining monodisperse particles in a wide range of sizes^[190] and tunable polymeric composition makes this material effective in various applications, including surface modifications^[134].

Another advantage of PNIPAM as the core-forming material is that PNIPAM microgels can be prepared by a simple radical polymerization technique^[164, 191-193]. Furthermore, various functional groups can be incorporated by copolymerization during the synthesis or via post-polymerization modification procedures. Functional groups at the surface of microgels can assist in the process of creation of the core-shell structures with various types of shells^[164] or they can provide a starting points for different chemical reactions on the surface of microgels.

In addition to facile synthesis and functionalizations, PNIPAM microgels have good colloid stability in a wide range of dimensions, which make them ideal subjects not only for fundamental studies on soft matter but also for product-oriented research.

Thermoresponsive behavior of PNIPAM particles gives an opportunity to investigate their properties both in swollen and in collapsed state simply by changing the temperature in a narrow, easily controllable range. Copolymerization of NIPAM with other monomers with either hydrophilic or hydrophobic properties doesn't vanish this ability but shifts the LCST of the resulting polymer toward higher or lower temperatures^[194]. Introduction of additional hydrophilicity to the hydrogel copolymer leads to higher transition temperatures shift, and on the contrary incorporation of more hydrophobic moieties causes shift of LCST to lower temperatures. The volume phase transition range for copolymer microgels appeared to be broader and less defined.

Swelling ability of microgels could be tuned by changing the amount of cross-linking agent in a hydrogel network.

Taking into account all advantages of PNIPAM-based microgels, it was decided to prepare the cores for the future core-shell particles produced by the "bottom up" approach, using PNIPAM as the main component, methylenbisacrylamide (MBA) as the cross-linker and acrylamide (AAm) as the functional additive. AAm has been chosen for several reasons:

(1) PAAm is much more hydrophilic if compared to PNIPAM^[182, 195], that should lead to higher swelling ratio of microgels. Copolymerization of these monomers results in copolymer with LCST slightly shifted toward the higher temperatures, which varies depending on the amount of additive monomer.

(2) AAm can be easily copolymerized with NIPAM in the same conditions in a wide range of ratios because of the chemical similarity of both monomers (the copolymerization constants of $r_{\text{NIPAM}} = 0.50$ and $r_{\text{AAm}} = 1$ were reported by Chiklis et al^[196] for the copolymerization of NIPAM with acrylamide (AAm) in water).

(3) The serious limitation of PNIPAM hydrogels in many applications arises mainly from their low mechanical strength in a highly

swollen state. In this aspect, an addition of acrylamide in the PNIPAM network significantly improves its mechanical properties even in a fully swollen state^[197].

(4) Possibility for transformation of primary amide groups into the amines has been studied by different scientists on various types of organic compounds^[198-200]. The reaction of amide-to-amine conversion could be utilized for preparing the amino-functionalized microgels as an alternative to copolymerization technique.

Similarly to pure PNIPAM particles, one can exploit properties of copolymer particles for fabrication of ordered assemblies using various techniques. Some of them have been reported earlier by many researches and used for creation of colloidal crystals using thermal annealing procedures^[201, 202], or for preparation the microgel monolayers on oppositely charged surfaces with controlled packing density ^[135]. Even simple drying the thin film of water dispersed microgels^[134] allows to obtain an arrays of sufficiently well ordered microparticles on the surface with different surface coverage. The ability of microgels to form loosely packed colloidal arrays has been investigated in the present work and utilized for surface modifications.

5.1.2.1 Synthesis, characterization and tuning the composition of core-forming microgels with suitable swelling effect

Free-radical precipitation polymerization of NIPAM was chosen for synthesis of hydrogel cores,^[203] which were further utilized for preparation of core-shell particles by “bottom-up” approach.

This method takes advantage of the temperature response of PNIPAM in aqueous solution and yields stable colloidal dispersion of particles. Polymerization is typically carried out at ~70 °C, which is well

above the entropically favored coil-globule phase transition of the PNIPAM (LCST). Oligoradicals, formed in solution during the synthesis, phase separate and form collapsed, insoluble polymer globules that act as nucleation sites for further polymer growth^[189, 204, 205].

The main advantage of the precipitation polymerization technique, compared to other methods,^[89, 206-209] lies in unsophisticated synthetic procedure. It allows obtaining of highly monodisperse microgels with different compositions with a size ranging from several hundred nanometers to several micrometers.

Since PNIPAM based microparticles have neither charge no reactive groups on their surface, introducing a particular functionality to the core has been suggested for simplification of particles post-modification procedure. In our case either amino- or (and) hydroxyl-functional particles were most suitable. Both amino- and hydroxyl- functionalities are complementary to the carboxyl-groups, which were selected to introduce reactive functionality to the substrate, in the same time preserving its hydrophilicity and, therefore can be used for chemical tethering of particles. In addition, amino groups could be used for further particles surface modification e.g. for grafting the initiator of polymerization and thus, for growing the shell by surface initiated polymerization.

Desired functionality of the microgels could be achieved by copolymerization of the main component with some functional additives. For example, aminofunctional microgels can be obtained using aminoethylmethacrylate (AEMA) as a co-monomer. However, it was reported that the addition of ionomers like AEMA into the reaction mixture fundamentally changes the course of the polymerization, in accordance with the results presented elsewhere^[210]. It was found that formation of significant amount of linear polymer or macrogel simultaneously with microgel particles rapidly increases when the amount of AEMA in the monomer mixture exceeds 5 mol%. AFM and

DLS investigation of amino-functional microgels synthesized via copolymerization showed increase of polydispersity and worsening of their self-assembling ability, which are important characteristics for application of particles in surface coatings.

Therefore, functionalization of microgels was achieved using postpolymerization treatment. For this purpose, acrylamide was copolymerized with NIPAM to form well defined microgel particles and then was converted into vinylamine (VA) using the reaction of amide rearrangement^[200].

The synthesis of microgels was done as follows.

Synthesis of microgels

The polymerization experiments were carried out in a reaction tube equipped with magnetic stirring bar. Monomers (NIPAM, AAm, MBA and HEMA) were dissolved in water and filtered to remove a particulate matter through 0.2 μm membrane filter. The concentration of NIPAM was kept 0.02 g/ml while the comonomers weight ratio was varied with respect to NIPAM. (see Table 4.3). pH of solution was adjusted to 3.5-4.0 by adding of 0.1M HCl aqueous solution. The mixture was transferred into reaction vessel, sealed with rubber septum and stirred at 200 rpm for 30 min under argon flow to remove oxygen. Then the temperature was raised to 70°C and initiator (0.1 ml of 0.0025M aqueous solution of 2,2'-azobis(2-methylpropionamidine) dihydrochloride) was added. After approximately one minute, the light opalescence appeared and stirring speed was reduced to about 100 rpm to prevent flocculation. The reaction was continued for 4 hours with maintaining of the inert atmosphere throughout the whole experiment.

Purification of microgel particles was done by dialysis against water for at least 3 days followed by several cycles of centrifugation/re-dispersion in distilled water.

The series of microgels with different weight ratios of NIPAM/AAm and fixed amount of cross-linker were synthesized.

The composition of resulted microgels was determined by analysis of residue after particles separation. Monomer conversion as well as composition of water-soluble fraction was determined by ^1H NMR. Total amount of the residue was determined gravimetrically by evaporation to the dryness of a certain amount of supernatant.

Monomer mixture composition, resulting polymer particles composition and polymerization conditions are summarized in the Table 4-3.

Table 4-3 Composition of monomer mixture and resulted microgels.

Entry	Initial wt. ratio of NIPAM/AAm (in a monomers mixture)	Resulted wt. ratio of NIPAM/AAm (in polymer particles*)	Acrylamide content in a microgels, wt%
HGP 400	100 / 0	100 / 0	0
HGP 402	100 / 2.0	100 / 2.7	3.6
HGP 403	100 / 3.0	100 / 4.1	5.4
HGP 404	100 / 4.0	100 / 5.6	7.2
HGP 405	100 / 5.0	100 / 6.9	8.7
HGP 406	100 / 6.0	100 / 8.4	10.4
HGP 408	100 / 8.0	100 / 11.1	13.2
HGP 410	100 / 10.0	100 / 14.1	16.3

** In all cases (2,2'-Azobis (2-methylpropionamide) dihydrochloride) was used as initiator. In every monomer mixture 3 mol% of MBA as a cross-linker and 5 wt% of hydroxyethylmethacrylate (HEMA) as an additional functionality carrier were added.*

Adequate swellability of microgels is crucial for realization of the aim of the work. Therefore, investigation of the swelling behavior and tuning of the microgels composition in order to achieve the desired swellability was performed.

Volume swelling ratio could be calculated using the Equation 4-2 based on correlation of the volume of particles in their swollen and

collapsed (or dry) states. For this reason, size of water-swollen particles was determined in suspensions by DLS technique and further used for calculation of corresponding volumes.

In principle, the ability of PNIPAM-based microgels to undergo the VPT can be exploited in DLS measurements to determine the particles size in swollen as well as in collapsed states by simple changing the temperature of media. The ratio between the measured particles volume in swollen (below LCST) and in collapsed state (above LCST) gives the microgel's volume swelling ratio in dispersion. However, even above LCST, the PNIPAM particles contain certain amount of water, therefore such method inevitably leads to a systematic error. A much more precise determination of the “dry” volume of microgels implies measurements of particles dimensions by AFM.

As judged from the cross-sections of AFM images, shape of the particles, deposited on the substrate does not remain spherical. The particle shape was assumed to be a segment of sphere with characteristic dimensions h (segmental height) and d (segmental base diameter) (Fig.4-21).

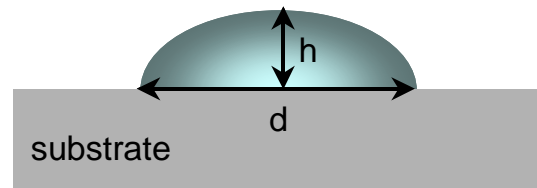


Figure 4-21 Schematic representation of a typical microgels shape adopted after their deposition onto a substrate. d and h denote characteristic dimensions of resulted hemisphere: base diameter and height respectively.

The volume of such spherical segment (V) was calculated using the Equation 4-10.

$$V = \frac{1}{6} \pi h \left(3 \left(\frac{d}{2} \right)^2 + h^2 \right) \quad [4-10]$$

Hence, the diameter of spherical particle (d_{rec}) with the same volume (V) has been recalculated (Eq.4-11). This value was suggested to be

identical to the particles diameter after complete dehydration of hydrogel network.

$$d_{rec} = 2 \sqrt[3]{\frac{3V}{4\pi}} \quad [4-11]$$

The characteristic dimensions of microgels with different composition and corresponding swelling ratios are presented in a Table 4-4.

Table 4-4 Characteristic dimensions of cross-linked PNIPAM-based microgels with different content of AAm in swollen and dry states and corresponding volume swelling ratios.

Entry	Acrylamide content in a microgels, wt%	Microgels diameter in a swollen state*	Microgels diameter in a dry state**	Volume swelling ratio
HGP 400	0	733.1	338.6	10.15
HGP 402	3.6	776.4	336.1	12.33
HGP 403	5.4	774.2	349.6	10.86
HGP 404	7.2	741.0	367.1	8.22
HGP 405	8.7	770.3	382.8	8.15
HGP 406	10.4	780.1	385.5	8.29
HGP 408	13.2	889.0	390.0	11.84
HGP 410	16.3	944.4	397.7	13.39

* as determined from DLS measurements at 25°C.

** as calculated from AFM images using Eq.2-10 and Eq.2-11.

It was found that up to 16 wt% of acrylamide as co-monomer could be incorporated without significant changing of microgels homogeneity. DLS measurements show variation of microgels polydispersity index from 0.013 to 0.025. The increase of particles diameter with the increase of AAm content was observed both in dry and swollen states, while the volume swelling ratio was found to be nearly independent on the

microgels composition. Estimated swelling ratios for all types of prepared particles varied in the range from 8 to 13 (Fig.4-22).

Further increase of the acrylamide content led to the formation of significant quantities of linear or cross-linked macrogel instead of particles during precipitation polymerization process.

For further experiments microgels with 16.3 wt% of acrylamide were used in order to obtain the highest possible content of amide-groups in microgels available for further transformation into amino-functionalities.

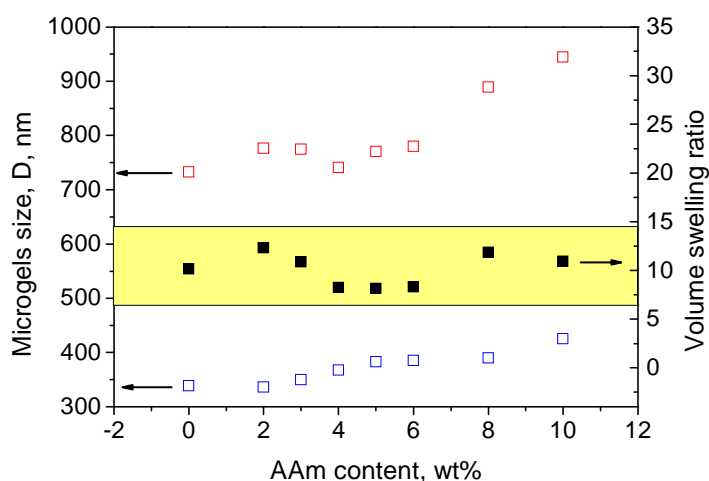


Figure 4-22 Dependence of diameter of swollen (red squares, DLS measurements) and dry (blue squares, AFM measurements) P(NIPAM-AAm) microgels on AAm content and calculated correspondent volume swelling ratios.

Variability of the swelling ratio of P(NIPAM-AAm) microgels as a function of cross-linker content was also studied. Microgels containing 16.3% of acrylamide and various amount of MBA were synthesized. As expected, with increasing of MBA content in the initial monomer mixture from 3 to 10 mol%, the swelling ability of resulting microgels gradually decreased from $S_V = 13.39$ to $S_V = 4.23$. Moreover, further increase of MBA content resulted in drastic decrease of particles yield. Therefore, for preparation of responsive surfaces, microgels with 16.3 wt% of acrylamide and 3 mol% of methylenebisacrylamide were suggested.

5.1.2.2 Formation of loose periodic arrays of microgels on the substrate

One of the important requirements for realization of the idea of contraphilic surfaces is covering of the substrate with hydrophobic particles in a non-close packed fashion in order to minimize their contribution into the total WCA of the surface.

Typically, the loosely packed arrays of colloidal assemblies are constructed by means of lithographic techniques, which are expensive, time consuming, and difficult to scale up. Self-assembly of temperature-sensitive PNIPAM microgels could be an attractive alternative for preparation of non-closed arrays in a single technological step. The formation of loosely-packed arrays from such particles was first demonstrated by Pelton and Chibante in 1986^[117]. Thereafter, this phenomenon was explored and used for different applications by several research groups^[133, 211]. In this work attention to this phenomenon as a critical step for the realization of the goal was also paid.

In general, the assembly of both hard spheres and soft gel particles into ordered periodic structures occurs as a result of minimization of the free energy when attractive and repulsive forces are simultaneously applied to the particles. Repulsion comes onto play if the particles are brought closely enough to each other so that they touch because of elastic restoring forces of particles deformation. If the particles are charged, they may “feel” each other even on some distance due to the long-range Coulomb interactions. The ordering may occur if particles are pulled by surface tension forces developing upon drying of the dispersion. Thermodynamically favoured arrays are always formed depending on particles density, particles physical properties (hard or soft) and whatever the final state (close or non-close packed). If the particles within the two-

dimensional close-packed ordered array are in the swollen state, for instance PNIPAM particles deposited from water, they may form non-closed and ordered arrays upon drying. This is possible if the swollen microgels undergo lateral collapse (not only in direction normal to the surface plane) and if the initially ordered state is preserved by a strong enough adhesion of the particles to the surface that prevents their displacement and aggregation.

As follows from the above mechanisms, the formation of non-close but ordered colloidal arrays is only possible if several counter-acting forces and parameters are properly balanced.

In order to investigate the deposition processes of synthesized microgels, Si-wafers were covered with particles and examined by AFM. The procedure of fabrication of ordered microgels arrays on the substrate was performed as follows.

Fabrication of ordered microgel arrays

Si wafers were rinsed in dichloromethane and cleaned in oxygen plasma for 30 seconds. Afterwards, a 100 μ l drop of the dispersion (5 mg/ml) of the respective microgels was deposited onto the freshly cleaned, slightly wetted Si wafer and spread homogeneously over the whole area. Finally, water was evaporated under hot air stream applied by a hot-air gun positioned appr. 10 cm over the sample. In such conditions, water typically, evaporated completely within 10 seconds.

The arrays with long-range periodicity up to several square centimetres were produced in such a way (Fig.4-23).

It was found that particular details of the deposition procedure, e.g., a distance from the heater to the sample and the angle at which the air flux was applied have little influence on the final result whatever the drying proceeds within 10-15 seconds. A free evaporation of water at ambient conditions (room temperature and without air flux) is also

applicable for obtaining of ordered microgels arrays, however requires much longer deposition time and gives rather less reproducible results.

Surface pre-treatment procedure has also little influence on the result until it provides highly hydrophilic surfaces, although cleaning with oxygen plasma was found a bit more efficient. It was also found that the ordered microgel arrays could be obtained in a broad range of initial microgels concentrations, in an agreement with Kawaguchi et al [134], although the best results were obtained at 5 mg/ml concentration. The only parameter affected by the initial microgels concentration is the area, which is uniformly covered by the ordered monolayer of the microgels. If the drop contains a larger amount of microgels than it is needed for the formation of the monolayer, excess of microgels forms multilayered structures in the middle of the sample.

It was found also that all types of synthesized microgels form well-ordered monolayer under such conditions. The longest centre-to-centre distance between neighboring particles was found in the case of highest content of acrylamide.

Evaluation of the microgels periodicity was made using 2D fast Fourier transformation (FFT) of AFM topography images. The 6-fold

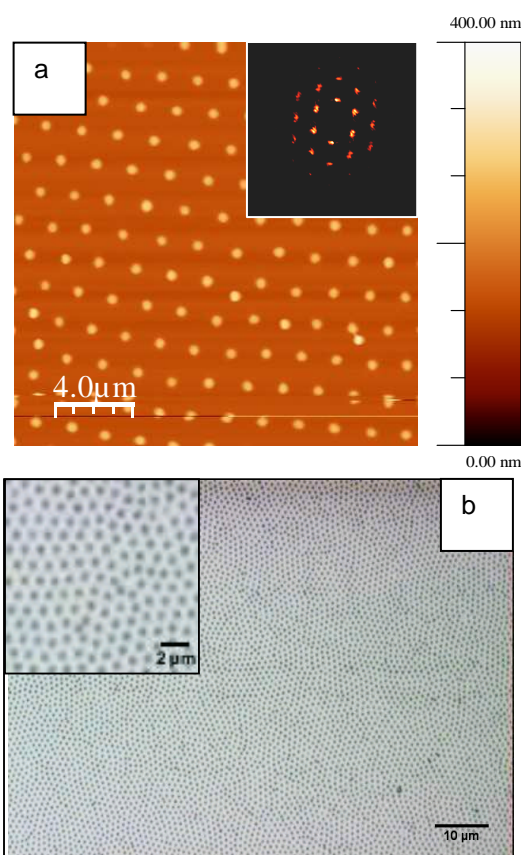


Figure 4-23 AFM (a) topography and (b) optical microscopy images of regularly packed P(NIPAM-AAm) microgels on the substrate. Inset – FFT of AFM topography image with multiply hexagonally arranged peaks.

symmetry of the FFT image (inset on the Fig.4-23, a) clearly shows that the particles form a hexagonal structure in plane of substrate surface.

Analysis of power spectrum density (PSD) of the FFT gives the periodicity in range ~ 1600 - 1700 nm. This value corresponds to an average distance between the centers of neighboring particles.

Taking into consideration AFM topography images, the obtained structures would be qualified as non-close packed arrays. However, at a closer look AFM phase images reveal “sombbrero”-like morphology of collapsed particles (Fig.4-24). This suggests the “hairy” structure of microparticles so that only cores of the microgels within the arrays are well separated, whereas the “hairy” coronas are packed closely to each other.

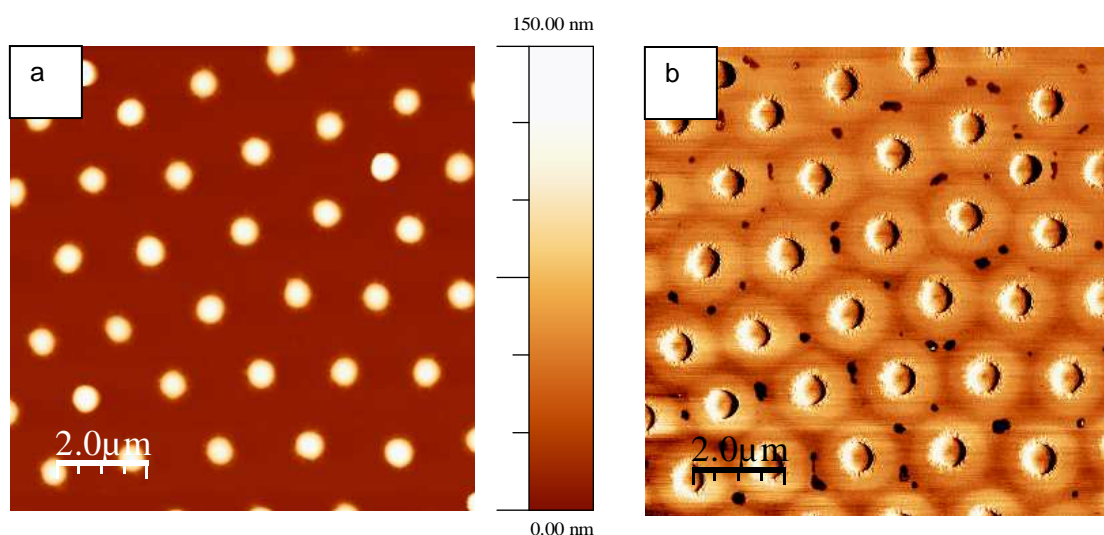


Figure 4-24 AFM (a) topography and (b) phase images of P(NIPAM-AAm) microgels arrays on the Si-substrate.

A cross-sectional analysis of AFM topography images performed with WSxM software^[212] reveals the height of the “hairy” part of the microgels below 1 nm, the height of the cores in a 100-150 nm range.

When comparing these values with DLS data, one can conclude that the dried microgels on surfaces are strongly collapsed flat on the surface, in accordance with previous observations^[213]. In a view of the revealed “hairy” structure of the microgels, the microgel arrays can be better

described as periodic close-packed microgel arrays with non-close-packed cores.

The “hairy” structures of microgels prepared via precipitation-copolymerization of NIPAM and MBA cross-linker was first suggested by Pelton et al^[204] and confirmed by other research groups on the basis of light and neutron scattering studies^[214, 215] as well as by SEM observations^[216]. It was reported that during the formation of PNIPAM particles MBA was consumed faster and therefore preferentially incorporated into the particles^[217]. As a result of a progressive depletion of the polymerization mixture by the cross-linker and because of a peculiarity of the precipitation-polymerization mechanism according to which the initially formed polymeric material appears in the centre of the resulting particles, the cross-linking density for the PNIPAM microgels decreases from the centre to a periphery. It can be proposed that at certain conditions a kind of “hairy” microgels are formed, in which more highly cross-linked core is decorated by branched or even linear dangling polymer chains. The inhomogeneity of the microgels structure can be even more pronounced upon the copolymerization of several monomers with different reactivity.

Taking into account “hairy” structure of microgels used for surface modification, the mechanism of well ordered arrays formation proposed by Kawaguchi et al^[134] could also be valid in our case.

In water, individual microgel particles are dispersed by inter-particle repulsion and move by Brownian motion. As water evaporates, the microgels become trapped inside the thin film of liquid on the substrate surface. In this state, the swollen microgels are forced together by capillary forces and they pack closely. They assemble as a result of increasing concentration but do not cluster because of the volume exclusion effect of the “hairy” layer. It is important that the swollen and packed microgels adhere to the surface so that the following evaporation of water causes shrinkage of the microgel. The fact that there is

practically no space between the adjacent “hairy” microgel particles within the dried arrays suggests they are mostly stuck to the surface plane upon the drying.

As for preparation of heterogenic surface of loosely packed arrays of microgels on the substrate are essential, the spaces between microgels have to be cleaned before development a hydrophobic shell on microgels.

Therefore, the microgels arrays deposited onto PAA brush surface were subjected to a brief (15-20 seconds) oxygen plasma treatment to remove the microgels “hairy” coronas. As it was revealed, this procedure is essential since otherwise the “hair” extend significantly beyond the cores diminishing the space between microgels. After the plasma etching, a surface coverage of about 15-20% was found for microgels in the dry state (measured by AFM) that is an optimal value for realization of the main concept.

5.1.2.3 Surface density as a function of swelling effect

Since the deposition density for microgels in their dry state was estimated from the analysis of AFM images, the required volume swelling ratio for complete covering the substrate with swollen particles was calculated using Eq.4-3 and Eq.4-4. For soft particles, the swelling ratio should be in a range of 11.2-17.2 in order to achieve the increase of the surface coverage from 15-20% in a dry state up to 100% in the swollen state (Eq.4-3). For more rigid particles, hardly changing their shape and not overlapping their spherical walls during swelling, this ratio should be in between 9.7 and 14.8 to cover 90.69% of the surface with the same particles after swelling (Eq.4-4).

From the calculations shown above it could be concluded that volume swelling ratio of 8-13, which is valid for all synthesized PNIPAM-based microgels with various content of acrylamide, is sufficient to reach

the utmost covering of surface with swollen particles if the initial particles fraction on the surface is close to 20%. Thus, all synthesized microgels including the ones with highest content of acrylamide in the structure seem to be suitable for achievement of the final goal of this work.

5.1.2.4 Measurements of the maximal pressure developing upon the swelling of the microgels

The swellability data presented above refer to the shell-free PNIPAM-based microgels freely dispersed in water. However, in applications such as “contraphilic” coatings, the changes in swelling ability of core-shell particles due to the presence of hydrophobic shell have to be considered. It is obvious, that core-shell microgels would experience effect of additional confinement, such as contraction induced by the shell, which would restrict swellability. Therefore, pressure developing upon the swelling of the microgels is the very important parameter and it was estimated for the parent macroscopic gel having the same composition as the microgeles used in this work.

The principle of the method proposed for these measurements can be described as follows. A dry gel with the same composition as used in the synthesis of the microgels was made in a shape of a cylinder and enclosed in a vessel of the same diameter. The bottom of the vessel was a porous membrane for the solvent (water) input, while the top of the cylinder was a piston, which held the volume of the gel constant. After addition of water to the system through the membrane, the pressure on the piston due to the swelling of the gel was measured. When osmotic swelling equilibrium has been established and the maximum force acting on the piston was measured, a small upward displacement of the piston has been fixed and a new equilibrium of the system was established. The

equilibration of each step took about 5 hours. Such stepwise force measurement of hydrogel swelling with equilibration of the system at every step gave the information about the swelling pressure of the hydrogel at every specified swelling ratio (Fig.4-25).

The maximum value of the swelling pressure at the very beginning of the gel swelling was found to be of ~143 kPa and calculations of critical shell parameters of core-shell system have been done in accordance to this value.

Using the model of thin-walled vessel described in Chapter 4.1 (Eq.4-7 and Eq.4-8) and knowing the initial parameters of investigated microgels, a critical value for polyisoprene shell thickness and its permissible limit of elastic coefficient were calculated.

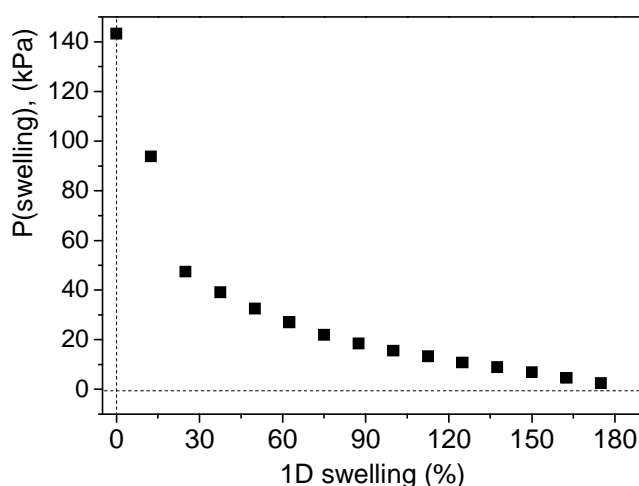


Figure 4-25 Dependence of maximal equilibrium swelling pressure of P(NIPAM-AAm) hydrogel with 3 mol% of cross-linker on the degree of swelling in water.

For the calculations several parameters were fixed as:

- radius of microgels in a dry state – 300-400 nm;
- maximum value of produced swelling pressure for given microgels - ~143 kPa;
- required volume swelling ratio of ~8-12 that corresponds to the value of ~2.00-2.35 for 1D swelling;
- Poisson ratio for polyisoprene of 0.5.

At such given data the variable parameters are thickness of shell and its elastic modulus. This gives us the certain degree of freedom in the determination of shell parameters.

From calculations it was found that if the shell made of PI with the cross-linking density of 0.1% (that corresponds to the Young modulus of ~90 kPa^[158]) the thickness up to 70 nm would not prevent the swelling of core-shell particles in required range. However, if the cross-linking density of the PI shell is increased up to 3.0% (characteristic Young modulus ~ 1300 kPa^[158]) the swelling degree of the microgel of 10 becomes achievable only if the shell thicknesses decreased down to ~6.0 nm.

5.1.2.5 Chemical modification of hydrogel microparticles

Preparation of a microgels with reactive amine groups is of particular interest itself for many applications ^[198, 218] due to high reactivity of primary amines. For such microgels attachment of various additional units (organic molecules, polymer chains etc.) with a chemistry complementary to amine becomes possible^[198]. It was also reported^[218, 219] that amino functionalized hydrogel surfaces are good substrates for adsorption and growth of some types of cells. Application of amine-containing microgels as sorbents for removal of dyes and metals ions from aqueous solutions is also described^[220]. Variety of bioactive molecules such as proteins, peptides, enzymes and drugs could be immobilized on amino-functionalized microgels via amidation reaction^[221].

To the best of my knowledge, there are no reports of successful direct copolymerization methods, producing amino-functional microgels with a high yield. It was possible, however, to introduce amino-groups by various types of reactions, starting from other functional groups. The conversion of amide groups into amino ones, namely by the reaction of Hoffmann degradation of primary amides, is one the most investigated methods. The

method of effective conversion of polyacrylamide to polyvinylamine via Hofmann reaction using a sodium hypochlorite as an oxidation agent was initially developed by Tanaka and co-workers^[222] (Fig.4-26).

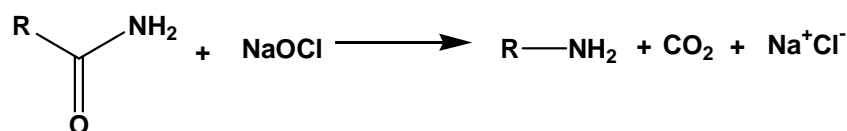


Figure 4-26 Scheme of Hofmann degradation (rearrangement) of primary amides

This method is suitable not only for homogeneous solutions of polymer, but also for the surface of latex particles^[223]. However, in a contrast to soluble polymers, application of sodium hypochlorite to styrene-acrylamide copolymer latexes led to the formation of appreciable amounts of carboxyl groups together with amines due to the competitive hydrolysis reaction. The yield of amino groups increased with decreasing of the reaction temperature and increasing of sodium hypochlorite concentration. Similar results were obtained in the Hofmann reaction of polyacrylamide grafted on magnetic PVA beads^[224]. It was also shown that the dominant side-reactions of polyacrylamide are hydrolysis of amide groups at low concentrations of NaOCl and formation of urea bridges at higher amount of hypochlorite^[200].

The reaction is conducted under softer conditions if iodobenzene diacetate (DAIB)^[225] or bis(trifluoroacetoxy) iodobenzene^[226] are used as oxidative agents (Fig.4-27). Using these reagents it was possible to achieve higher reaction rate, avoid side reaction of urea formation and isolate the clean product. Although both these reagents are suitable for quantitative amide degradation, an advantage of DAIB over bis(trifluoroacetoxy)iodobenzene are in the lower cost and a higher stability of the reagent.

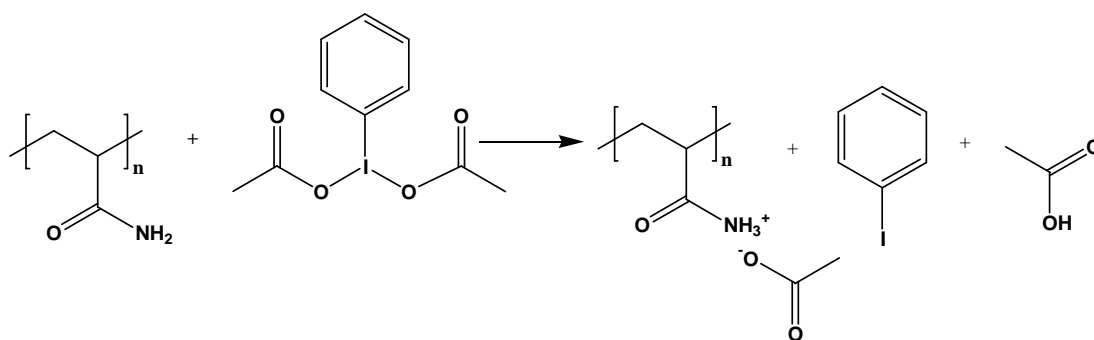


Figure 4-27 Scheme of conversion of primary amides into amines induced by iodobenzene diacetate (DAIB).

Therefore, in this work it was decided to use DAIB for conversion of amide-containing microgels into amino-functional ones. One more reason, which pushed us to use this reagent, is a fact that the reaction of degradation in this case should be carried out in acetonitrile, which is organic solvent, miscible with water. This condition was highly required because the microgels make a stable dispersion only in a water-containing phase. At the same time, solubility of all reagents in organic solvent facilitates a purification process after the reaction.

The general procedure of conversion of amide-containing microgels to amino-functional was the following:

Amide-into-amine degradation of microgels

DAIB in the molar ratio of 2:1 with respect to content of acrylamide groups in hydrogels was dissolved in acetonitrile and cooled to 0°C. Water dispersion of microgels was added and the reaction mixture was stirred at 0°C for 4 hours.

Afterwards, unreacted DAIB and organic by-products were extracted with chloroform and the water phase containing particles was separated. Organic solvent residues were removed from the water phase at reduced pressure; the particles were concentrated by centrifugation at 10000 rpm, and redispersed in distilled water.

The success of the reaction was proved by electrokinetic measurements (Fig.4-28).

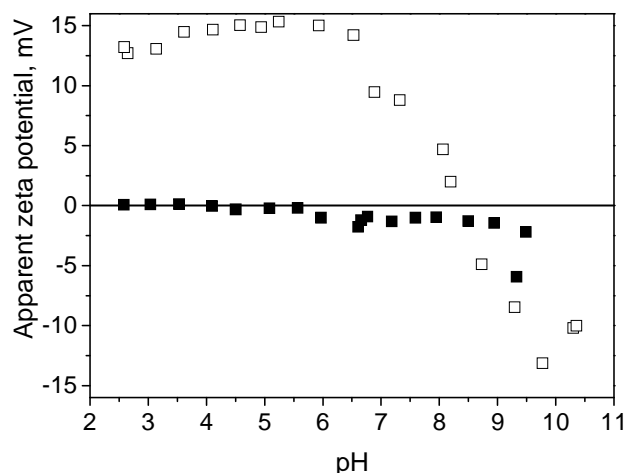


Figure 4-28 Z-potential measurements of P(NIPAM-AAm) microgels before (black squares) and after (open squares) amide-into-amine conversion.

The amide-containing microgels (black squares) showed zero surface charge within entire investigated pH range, while after reaction (open squares) strongly pronounced change of Z-potential, with an isoelectric point at pH of 8.47, which is typical value for amines was observed.

The yield of amination was estimated by UV-visible spectroscopy. For this amino-groups were converted into imines, having the characteristic adsorption band, using reaction with 4-nitrobenzaldehyde (NBA). This technique has been used previously to determine the density of primary, secondary, and tertiary amine groups on solid surfaces^[227, 228], but for the first time was applied in the present work for studying of amino-functionality of microgels.

Transformation of amino-groups into imino-groups was performed as follows:

Amine-into-imine conversion and hydrolysis

Water was removed from the dispersion of microgels (1 ml) by azeotropic distillation with THF. Dispersion was transferred into the flask with inert atmosphere containing solution of 4-nitrobenzaldehyde (14 mg) in THF (2 ml) and Linde 4-Å molecular sieve (ca. 1 g) for water elimination. The mixture was

refluxed for 4 hours. After that, the particles were separated by centrifugation and purified by several centrifugation/ redispersion cycles in THF.

For hydrolysis of imino-groups, particles were transferred in water (5 ml) containing acetic acid (0.05 ml), and heated at 30°C for 1 hour. Particles were washed with water several times by centrifugation/redispersion cycles.

The content of imino-residues (and therefore amino-groups in the microgels) was evaluated from measuring the absorption of resulting particles dispersed in water in the wave range from 200 to 600 nm. The concentration of reactive amino-groups was calculated using Beer-Lambert Law (Eq.4-12), which determines the absorbance (I) depending linearly on the concentration (or number density) of absorbers.

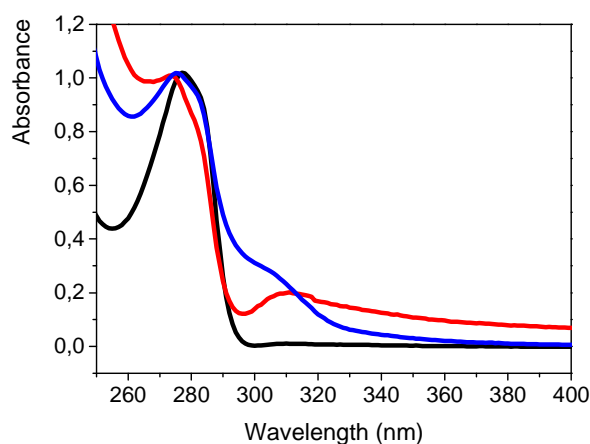


Figure 2-29 UV-vis spectra of the amino-functionalized microgels (black), the corresponding imine-containing microgels (red) and (4-Nitrobenzylidene) octylimine as a reference (blue).

$$I = \varepsilon \cdot l \cdot c$$

[4-12]

ε - molar extinction coefficient (the value of $1.55 \times 10^7 \text{ l/mol}^1 \text{ cm}^{-1}$ was used), l - path length of the sample, c - molar concentration of the compound in solution.

As a reference, (4-nitro-benzylidene)-octyl-imine, prepared from octylamine and 4-Nitrobenzaldehyde (NBA) was used. The imine-functionalized microgels showed a small peak around 310 nm, while primary amino-functionalized microgels were transparent there (Fig.2-29). The reference substance also showed adsorption in this region.

Concentration of amino-groups reactive in these conditions in microgels was calculated from this peak absorbance. The calculated value was of 4.6% (mol/mol microgels), which corresponds to the charge density of 0.44mmol/g. These data allow estimation of the conversion of amide-groups into amines in microgels close to 20%. After hydrolysis the peak of imines disappears, suggesting that amino groups recover after hydrolysis and microgels return into the initial state.

5.1.2.6 Confined swelling of the microgels

The realization of the “contraphilic” behaviour envisages the swellability of core-shell particles even under conditions of different restrictions, which was a subject of the investigations.

As it was mentioned before (see Chapter 4.4), polymeric gels swollen with a liquid can change their volume in response to external stimuli. In particular, PNIPAM macrogels can undergo a first-order volume phase transition as a function of temperature or solvent composition^[96]. In water, PNIPAM macrogels are swollen at temperatures below and deswollen above 32°C due to the hydrophobic interaction between polymer chains. The colloidal PNIPAM counterparts, however, do not exhibit such discontinuous size change despite identical chemical composition and qualitatively similar swelling behavior^[127, 189, 229]. This is due to the differences in preparation procedures for macro- and microgels: macrogels are usually made at room temperature while microgels are typically synthesized at 70°C, under bad solvent conditions. In addition, microgels typically have a certain charge on their surface as a result of the ionic character of the initiator used^[127, 189, 230, 231]. Perhaps, these facts affect the continuous or discontinuous character of the phase transition. These differences also affect the kinetics of swelling. The swelling kinetics of the particles is well described with a model by Tanaka considering a modified

Fick equation of motion for the polymer gel network^[95]. In other words, the flux of solvent inside of gel is equal to the negative diffusion coefficient times the change in concentration divided by the change in distance. The diffusion coefficient that controls the process includes both the network elastic modulus and the gel-solvent friction coefficient. This model was found to be valid regardless of particle size and synthesis procedure. The estimated value of diffusion coefficient (D) was $\sim 1.2 \times 10^{-10} \text{ m}^2/\text{s}$ ^[105], which is in between the water self-diffusion coefficient ($\sim 2.3 \times 10^{-9} \text{ m}^2/\text{s}$ at 25°C)^[232] and the values reported for PNIPAM macroscopic gels ($\sim 5 \times 10^{-11} \text{ m}^2/\text{s}$)^[233]. The presence of charge in the particles periphery, which is not present in macrogel systems, could perhaps affect the kinetic process. The cross-linker concentration would also allow D to be varied thus affecting the speed of the size change^[105].

For microgel particles with more complicated structure, namely for core-shell particles, which have attracted attention lately^[164, 234-237], the process of swelling-shrinkage is more complex. Swelling of microgels which is restricted by various factors was a subject of intense investigations during the last decade and remains the point of interest till the present time. For instance, Ballauff and co-workers investigated the volume transition in colloidal core-shell particles comprised of polystyrene core and a thermosensitive cross-linked PNIPAM shell by small-angle X-ray scattering^[238]. They found that core-shell microgels exhibit distinctively different solution behaviour compared to the PNIPAM homopolymer thermosensitive gels because of the presence of a solid boundary between the core and the shell of the particles, which decrease the maximum degree of swelling of the shell at low temperatures but also prevent the full collapse of the network above the volume transition temperature of PNIPAM.

Multiresponsive core-shell microgels consisting of a core that is responsive to a particular stimulus, whereas the shell is sensitive to another external stimulus, have been investigated also ^[239, 240]. Li et al.

showed that in the core-shell microgels comprising a temperature-responsive cross-linked PNIPAM core and a pH-sensitive poly(4-vinylpyridine) (P4VP) shell temperature-induced volume phase transition of the PNIPAM core is not significantly affected by the P4VP shell, whereas the deswelling of the latter upon deprotonation of the pyridine moieties is influenced by the core-shell topology^[240].

Other type of structures, namely P(NIPAM-AA) based core-shell microgels display complex pH-dependent swelling behaviour and a multistep volume phase transition at high pH when the acrylic acid units are highly charged^[164].

All above-mentioned studies were focused on either entirely hydrophilic microgel particles or on the particles having hydrophobic core and hydrophilic shell. In a recently published report Christodoulakis and Vamvakaki^[241] attempt to examine the swelling ability of hydrophilic core in a presence of hydrophobic shell and vice versa using an core-shell amphoteric particles comprised a cross-linked poly(2-(diethylamino)ethyl methacrylate) (PDEA) or poly(methacrylic acid) (PMAA) network surrounded by a cross-linked PMAA or PDEA shell, respectively. It was shown that whereas the marginally hydrophilic PMAA gel does not affect the swelling behaviour of the PDEA network when located in either the core or the shell of the particles the presence of the hydrophobic PDEA network reduces the swelling of the cross-linked PMAA in the particle shell and strongly suppresses its expansion when the latter is restricted in the core of the particles.

Since core-shell particles having hydrophilic core and hydrophobic shell are subject of our interest and they are poorly studied in terms of their swelling properties, investigation of swelling ability of the acrylamide-based microgels having polyisoprene shell was an important task. In particular, it was interesting to analyze the influence of substrate and the presence of non-swellaable material on the overall swelling effect of the core-shell particles. An ultimate goal of such investigation was to

evaluate the possible applicability of the core-shell particles for preparation of “contraphilic” switchable surfaces.

Swelling ability of microgels freely dispersed in solvent can be measured by DLS technique. In the case of PNIPAM-containing particles, VPT behavior of polymer allows to make measurements upon swelling-deswelling within one experiment simply by heating and cooling the dispersion above and below LCST of PNIPAM. From these data, volume swelling ratio can be calculated by dividing the volume of particles in swollen by the volume in collapsed state.

In this work, in addition to DLS measurements, determination of microgels size in dry state was performed by AFM.

It is well known that the gels, based on copolymers of NIPAM with more hydrophilic monomers show different properties (swellability, LCST, etc.), as compared with purely PNIPAM-based gel. This effect is more pronounced in the case of ionic comonomers^[242].

Thus, for amide-containing PNIPAM-based microgels, having more hydrophilic nature than PNIPAM microgels, the region of VPT is broader, but still can be determined. LCST of about $\sim 35^{\circ}\text{C}$ was found as of midpoint between temperatures of the beginning and the end of the particles collapse (Fig.4-30). As expected, it was shifted to higher temperatures compared to the pure PNIPAM.

After conversion of acrylamide in microgels into charged vinylamine (VA) VPT region become too broad for proper determination of its limits (Fig.4-30). Nevertheless, volume swelling ratio of P(NIPAM-AAm-VA)

microgels could be calculated from these data. For microgels used in this work volume swelling ratio was in the range of ~20 if

measured in dispersion. Definitely larger swellability of P(NIPAM-AAm-VA) microgels as compared to P(NIPAM-AAm) is due to the introduction of amino-groups which are protonated at $\text{pH} < 8$. Hydrodynamic diameters of amine-containing particles in both swollen and collapsed states were found to be larger than that for uncharged microgels presumably, due to the electrostatic repulsion between charged moieties.

Determination of true volume swelling ratio of positively charged amino-functional microgels, taking into account the particles dry dimensions was measured with AFM, and was estimated close to 50. It was at least four times higher compared to the same value for parent non-ionic P(NIPAM-AAm) microgels. The increase of the swelling ability of microgels due to their charge could be considered as a favorable feature for the main goal of the present works.

To investigate the effect of supporting substrate on the swelling behaviour of microgels, immobilized amino-functionalized microgels were studied by in-situ AFM measurements using a liquid cell. To this end, the microgels were first imaged in the dry state and afterwards, the

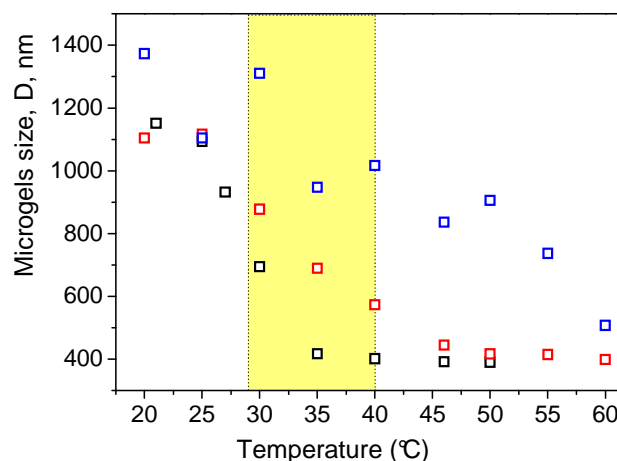


Figure 4-30 DLS measurements of hydrodynamic diameter of PNIPAM (black squares), P(NIPAM-AAm) (red squares) and P(NIPAM-AAm-VA) (blue squares) microgels as a function of temperature. The region of VPT marked with yellow.

measurements of the same particles were performed in water environment. The P(NIPAM-AAm-VA) microgels deposited on surfaces showed reversible swelling, however their shape was significantly affected by interactions with the surface. In fact, the immobilized microgels are no longer spherical and their height is much smaller than their diameter. After the drying, microgels adopt the conformation of spherical cap (segment of sphere), and a direct comparison of AFM and DLS results becomes difficult. Therefore, the average volume of the particles was estimated from AFM images for each sample (Eq.4-10) and then used for calculation of the diameter of the corresponding spherical particles (Eq.4-11). Obtained values of volume swelling ratio of deposited microgels were compared with results of DLS measurements of swelling ratios calculated for dispersed microgels. The results are summarized in Table 4-5.

Table 4-5 Characterization of swelling ability of freely dispersed microgels compared to the restricted swelling of surface-immobilized microgels.

No	Description	D_{dry} , AFM, nm	$D_{swollen}$ AFM, nm	$D_{collapsed}$ DLS, nm	$D_{swollen}$ DLS, nm	S_v deposited	S_v dispersed
1	P(NIPAM-AAm) microgels cross-linked with 3 %wt MBA	~392	~687	~398	~944	~5.4	~13.39
2	P(NIPAM-AAm) microgels cross-linked with 10 %wt MBA	~498	~627	~465	~752	~2.0	~4.23
3	P(NIPAM-Aam-VA) microgels cross-linked with 3 %wt MBA	~365	~787	~508	~1373	~9.99	~19.77

D_{dry} AFM, $D_{swollen}$ AFM – diameter of spherical microgels, calculated from AFM cross-sectional profiles using Eq.4-10 and Eq.4-11.

$D_{collapsed}$ DLS, $D_{swollen}$ DLS – average hydrodynamic diameter of microgels dispersed in water at 60°C and at 25°C, respectively.

S_v – volume swelling ratio calculated by Eq.4-2

It was found, that effect of restriction of microgels swelling by the substrate is significant. Whereas the equivalent diameter of the dry particles calculated from AFM images was found to be comparable to hydrodynamic diameter of collapsed particles determined by DLS, the volume of the adsorbed particles in the swollen state was substantially smaller than that in the solution. In all cases decrease of the swelling ability roughly by a factor of 2 was found. Decrease of the volume swelling ratio of microgels was also observed by Hellweg et al^[213] and it was explained as a result of attraction forces between the substrate and microgels leading to substantial deformation of microgels and restriction of the flexibility of a network.

It was shown that swellability of the PNIPAM-AAm microgels decreases significantly upon their immobilization onto the surface from the swelling ratio of ~13 for freely dispersed particles down to ~5.5 for the surface-immobilized ones.

However, the amino-containing microgels further used in this work for fabrication of the switchable surfaces exhibited reasonably high volume swelling ratio approaching to ~10 even after immobilization on the surface.

As it was already shown in *Chapter 4.2.3.2*, microgels due to their “hairy” morphology form “sombbrero-like” structures after deposition on the substrate. In order to obtain loosely packed microgels on the surface their footprint was reduced by plasma etching. In a view of this, it was interesting to investigate the influence of such treatment on the swelling behaviour of the microgels in water by in-situ AFM measurements.

Figure 4-31 shows images of the as-deposited P(NIPAM-AAm-VA) microgels in the dry and the swollen states measured by AFM using a liquid cell. It can be seen that immersion of the sample in water leads to increase of the height of the microgels from ~140 nm to ~300 nm due to the water uptake. A more important observation is that the swelling of the microgels also occurred in lateral direction increasing the footprint

diameters from less than 900 nm for dry microgels up to more than 1200 nm for the swollen ones.

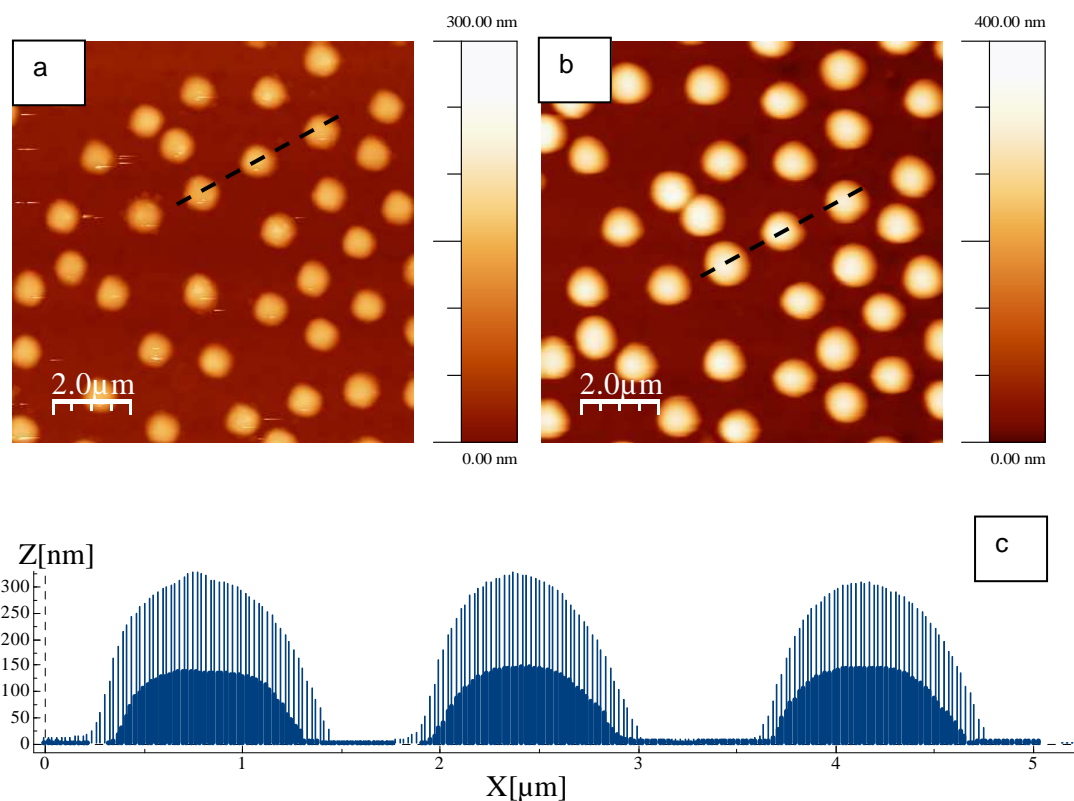


Figure 4-31 AFM topography images of non-etched P(NIPAM-AAm-VA) microgels (a) in a dry and (b) in a swollen states and (c) corresponding cross-section profiles of dry (blue) and swollen (blue shaded) microgels.

As seen from AFM images (Fig.4-32), the mild etching did not affect much the microgels height in the dry and swollen states (their heights decreased after etching only slightly from ~ 140 nm and ~ 300 nm for the dry and the swollen non-etched microgels, respectively, down to ~ 130 nm and ~ 280 nm for the dry and the swollen etched microgels, respectively). At the same time, the performed plasma treatment affected significantly the lateral swelling of the microgels so that the swelling occurred preferably normal to the surface plane.

The increasing of surface coverage in case of etched microgels during swelling was measured and it was found to be of 5-10%. According to Cassie equation, it corresponds to expected increasing of WCA of about 5-10°.

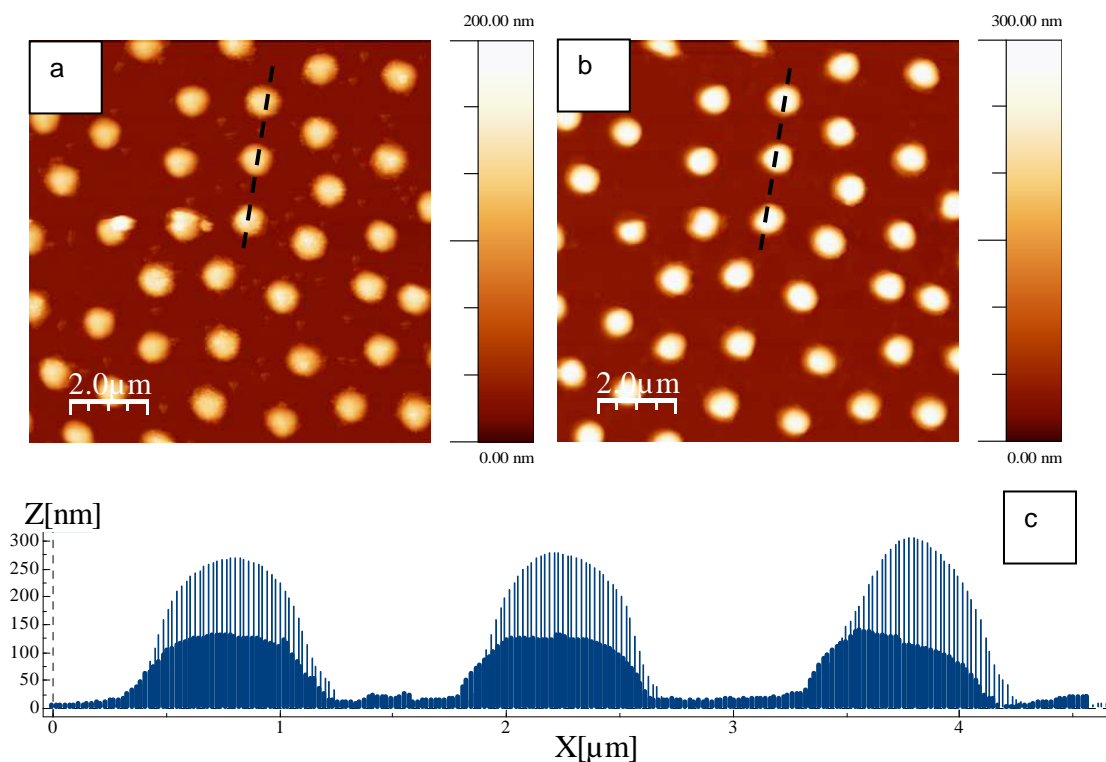


Figure 4-32 AFM topography images of etched P(NIPAM-AAm-VA) microgels (a) in dry and (b) in swollen states and (c) corresponding cross-sectional profile of dry (blue) and swollen (blue shaded) microgels.

It becomes obvious that deposition of the microgels onto surface leads to their significant deformations due to the surface attraction that affects their surface swelling behaviour. The major problem is that the deformed surface-immobilized microgels undergo swelling-deswelling predominantly in the direction normal to the substrate that is strongly undesirable for “contraphilic” coatings for which in-plane (lateral) swelling is needed. With this regard, the core-shell microgels obtained in a one-pot suspension polymerization seem to be more suitable as building blocks for the preparation of the “contraphilic” coatings. As it was shown

before, the polyacrylamide microspheres synthesized in water-in-oil emulsion stabilized by PEO-b-PI macromolecular surfactant retain their spherical shape even after immobilization onto surface in contrast to the shell-free microgels (compare Fig.4-31, c) and Fig.4-13).

5.1.2.7 Adsorption of oppositely charged nanoparticles on the surface of microgels

One of the important prerequisite of the swellability of the core-shell particles is water permeability of the hydrophobic shell. To achieve such permeability, the surface of microgels can be decorated with smaller “sacrificial” particles before formation of the shell. Later on, these particles have to be removed from the shell creating pores to provide access to water into the core.

Since so far, positively charged microgels were obtained, adsorption of oppositely charged nanoparticles on the surface of microgels has been investigated. Negatively charged polystyrene (PS) latex, used for this purpose, was synthesised by emulsion polymerization:

Synthesis of polystyrene latex

0.844 g of sodium dodecylsulfate (SDS) and 0.242 g of NaHCO₃ were dissolved in 31.5 g of water and the solution was purged by argon for 30 min. After addition of freshly distilled styrene (9 ml) purging with argon was continued for the next 30 minutes. Then reaction mixture was heated to 90°C and solution of initiator (0.08 g of KPS in 1.5 ml of water) was added to start the polymerization. After 20 hours reaction was stopped by cooling, resulted latex suspension was dialyzed against water for 3 days in order to remove unreacted reagents and excess of surfactant.

Purified latex has been investigated with DLS, which detected monodispersed particles (PDI 0.05-0.07) with an average diameter 38.8-39.1 nm.

In order to find the proper concentration of PS latex for the close packed adsorption on the surface of microgels, the weight ratio of guest particles (PS latex) to host particles (microgels) has been determined by the following equation^[243] based on calculation of the highest packing density of smaller particles on the surface of larger ones^[244]:

$$W_g / W_h = 4(R + r)^2 r \rho_g / (R^3 \rho_h) \quad [4-13]$$

R, r, ρ_h , ρ_g - radius and density of individual host (subscript h) and guest (subscript g) particles, respectively. (In calculations values of densities of polymer particles have been taken as equal to 1).

Adsorption was carried out in water dispersion of microgels by dropwise addition of dispersion of latexes with different $W_{PS}/W_{microgels}$ ratio. In the case of the charged amino-functionalized microgels specific adsorption of negatively charged PS latex was observed (Fig.4-33, Fig.4-34).

The latex remains on the surface of hydrogels even after different types of treatment, such as washing with water, ethanol, DMF or short-time oxygen plasma treatment.

It was also found that variation of $W_{PS}/W_{microgels}$ ratio leads to controllable increasing or decreasing of the amount of adsorbed particles on the surface of microgels that allows regulating the amount of pores (and therefore swelling rate of resulted core-shell structures).

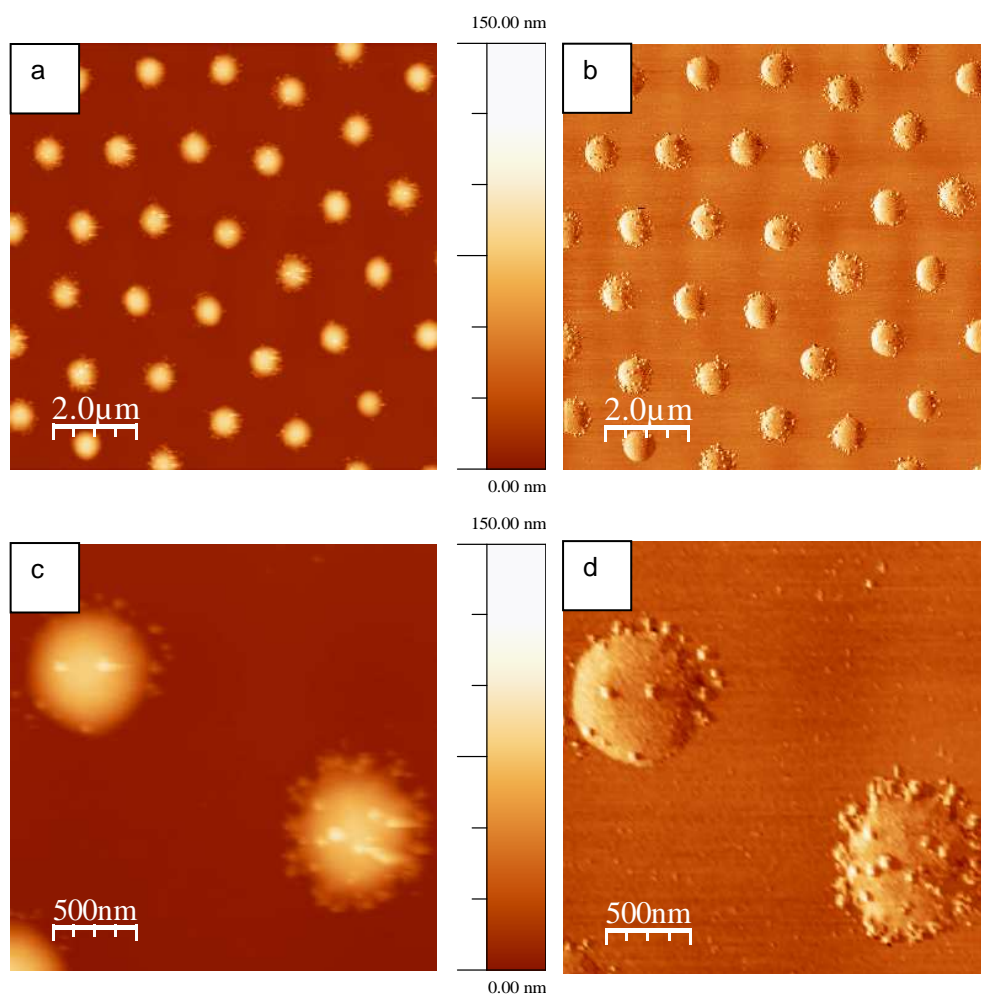


Figure 4-33 AFM (a, c) topography and (b, d) phase images of P(NIPAM-AAm-VA) microgels with adsorbed ~ 40 nm polystyrene (PS) latex, $W_{\text{PS}}/W_{\text{microgels}} = 0.02$.

Commercially available SiO_2 nanoparticles have been also successfully adsorbed onto the surface of amino-functional microgels. However, application of polystyrene latex was found to be more favourable due to simpler removal procedure. In contrast to SiO_2 particles, removal of which requires relatively harsh conditions (strong base or aqueous HF), dissolution of the PS latex particles could be done in very mild conditions (solvent extraction) without affecting of the substrate.

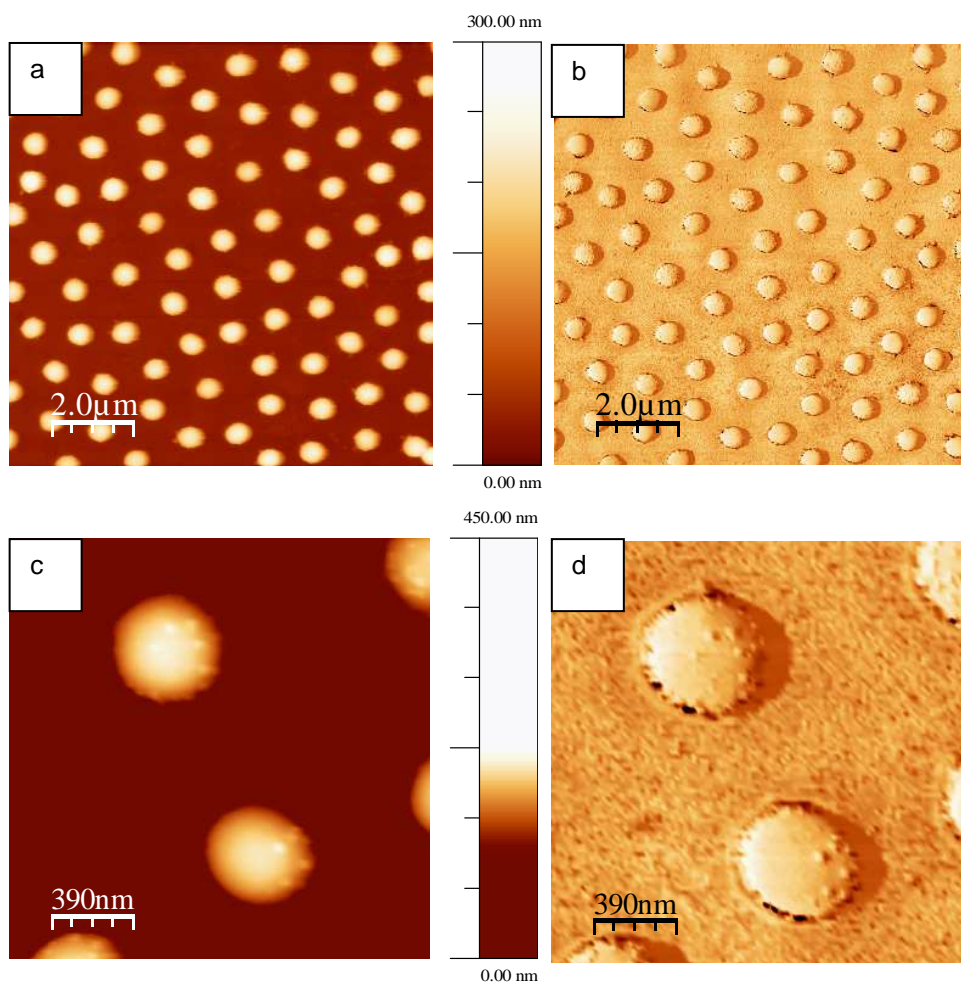


Figure 4-34 AFM (a, c) topography and (b, d) phase images of P(NIPAM-AAm-VA) microgels with adsorbed ~ 40 nm polystyrene (PS) latex, $W_{\text{PS}}/W_{\text{microgels}} = 0.01$.

Microgels with adsorbed latex showed the same deposition behaviour as native microgels, namely they formed “sombbrero-like” “hairy” structures on the substrate. The “hairy” coronas were eliminated by oxygen plasma treatment of samples after particles deposition. It was shown that this procedure reduces the particles footprint and did not destroy the PS latex on the microgels surface (Fig.4-35).

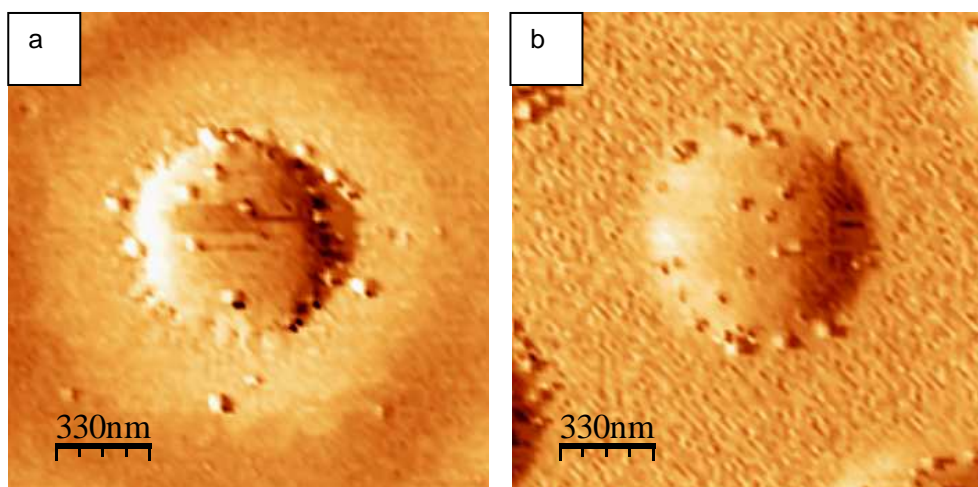


Figure 4-35 AFM phase images of P(NIPAM-AAm-VA) microgels with adsorbed ~ 40 nm PS-latex (a) before and (b) after plasma treatment; weight ratio $W_{\text{PS}}/W_{\text{microgels}} = 0.02$.

1.1.1.1 Grafting-from polymerization of shell on the microgels surface

As it was shown previously, diene monomers (butadiene and isoprene) can be polymerized under nitroxide-mediated radical polymerization (NMRP) conditions using surface-immobilized alkoxyamines as initiators^[245, 246]. In this work we used this approach to initiate the polymerization from the surface. NMRP initiator (NMRPI-1) was synthesized by trapping of radicals, generated by decomposition of the benzoyl peroxide in presence of vinylbenzylchloride, with 2,2,5-trimethyl-4-phenyl-3-azahexane-3-nitroxide (Fig.4-36).

In initial experiments, the efficiency of the initiating process was tested using flat surfaces, which allowed to easily follow the thickness changes with ellipsometry. To this end, thin poly(glycidyl methacrylate) layer was deposited onto Si-wafer surface by spin-casting technique and amino-functionality was introduced by ethylenediamine treatment.

Further modification of this layer with NMRPI-1 in acetone at 55°C for 24 hours followed by polymerization of isoprene at 125°C for 20 hours produced the 30 nm thick polyisoprene brush.

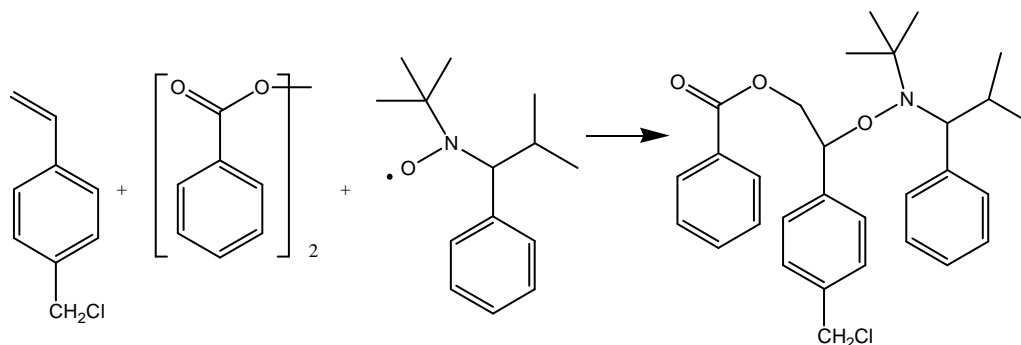


Figure 4-36 Scheme of synthesis of chlorobenzyl-functionalized NMRP-initiator (NMRPI-1)

An attempt to synthesize polyisoprene shell on microgels by NMRP was performed at first using freely dispersed microgels. For this purpose, NMRPI-1 was grafted to the surface of amino-functional microgels, dispersed in THF and isoprene was polymerized at 125°C. The resulting particles were covered with polyisoprene layer but, in the same time, bonded together (Fig.4-37) and were no longer dispersible in any solvents. It was suggested that this is due to intercross-linking of polyisoprene between particles during the polymerization.

In order to overcome this problem, microgels were attached to the solid substrate before polymerization of hydrophobic shell. The chemical attachment of microgels was done by reaction between carboxylic groups on substrate and amino-groups of microgels. 1-

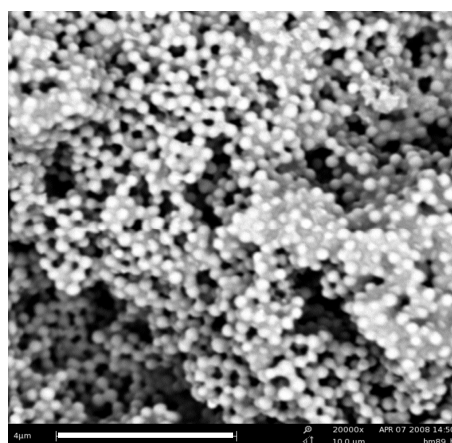


Fig. 4-37 SEM image of P(NIPAM-AAm-VA) microgels after surface-initiated polymerization of isoprene. Scale bar 4μm.

Ethyl-3-[3-dimethylaminopropyl] carbodiimide hydrochloride (EDC) (Fig.4-38) was used to promote reaction of carboxy-groups with primary amines. EDC reacts with carboxylic functions to form an amino-reactive intermediate. If this intermediate does not encounter the amine, it hydrolyzes and regenerates the carboxylic group. The addition of *N*-hydroxysulfosuccinimide (NaHSS) stabilizes the amine-reactive intermediate by converting it to an amine-reactive NaHSS ester, thus increasing the efficiency of EDC-mediated coupling reactions^[247].

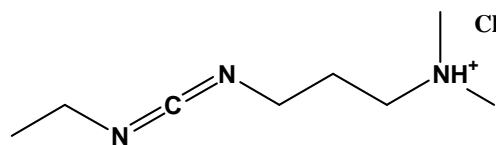


Figure 4-38 1-Ethyl-3-[3-dimethylaminopropyl] carbodiimide hydrochloride (EDC)

Thus, the treatment of surface before particles deposition with EDC/NaHSS solution allows grafting the particle to the substrate chemically (Fig.4-39).

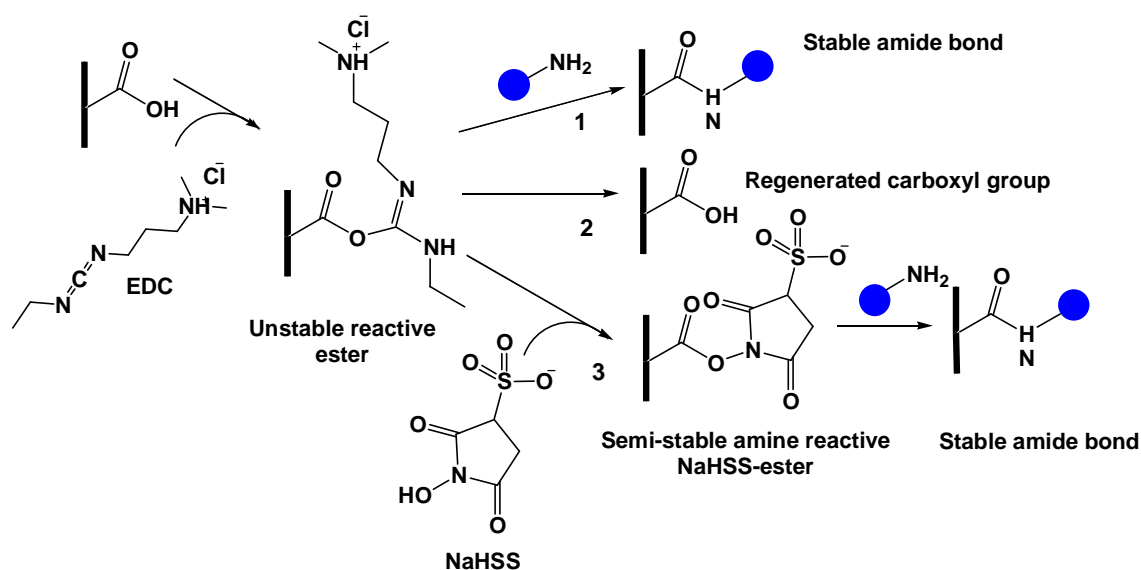


Figure 4-39 Schematic representation of EDC coupling reaction between surface-immobilized carboxyl groups and amino-functionalized microgels. Unstable intermediate ester formed by EDC can: 1) directly react with amines, 2) hydrolyze to carboxyl group or 3) form stable ester with NaHSS, which further react with amines forming amides.

After attachment of microgels to the PAA and grafting of the NMRPI-1 to the particles surface, polymerization of isoprene was carried out at 130°C, for different time (from 2 up to 24 hours). AFM investigations of resulted samples showed the increase of particles height in the range of ~50-170 nm depending on reaction time due to the grafting of polyisoprene layer. Since grafting of NMRPI-1 to the surface of microgels was done in water-free conditions, the microgels were in deswollen state during shell polymerization that decreased concentration of accessible amino-groups.

In order to achieve a higher initiator density on microgels surface, immobilization of the initiator and preparation of the shell on swollen microgels were attempted. Since solubility of PNIPAM in organic solvents is very low, *N,N*-dimethylformamide (DMF) was chosen as reaction media (thanks to its polarity PNIPAM is partially swellable in this solvent^[248]). Correspondingly, carboxy-functionalized NMRP-initiator (NMRPI-2) (Fig.4-40), soluble in polar organic solvents was synthesised and grafted to amine-functional particles in the presence of *N,N'*-dicyclohexylcarbodiimid / 4-dimethylaminopyridine (DCC/DMAP).

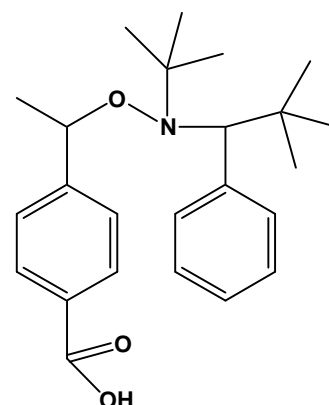


Figure 4-40 Carboxy-functionalized NMRP-initiator (NMRPI-2)

Polymerization of isoprene from NMRPI-2 modified microgels led to increase of the height of the particles by ~150-160 nm as measured by AFM (Fig.4-41).

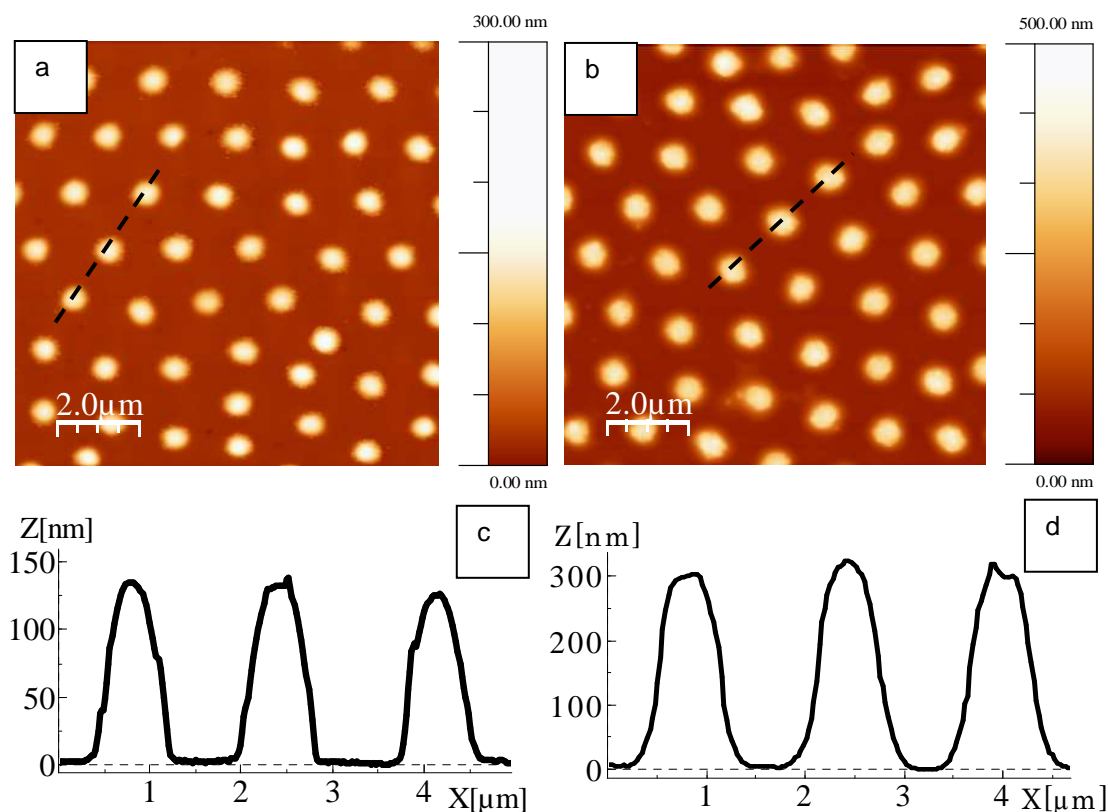


Figure 4-41 AFM topography images (top) and corresponding cross-sectional profiles (bottom) of surface-immobilized P(NIPAM-AAm-VA) microgels (a, c) before and (b, d) after surface-initiated radical polymerization of isoprene using NMRPI-2 as initiator.

In order to evaluate molecular weight of the grafted polyisoprene, the free polymer formed in the bulk simultaneously with the surface-grafted polymer was isolated, purified by dissolution-precipitation and analyzed with GPC. GPC measurements gave M_w value of 9500-10600 g/mol and PDI 2.50 against polystyrene standards.

In addition to NMRP-initiators, commercially available initiator for free-radical polymerization having two functional carboxyl

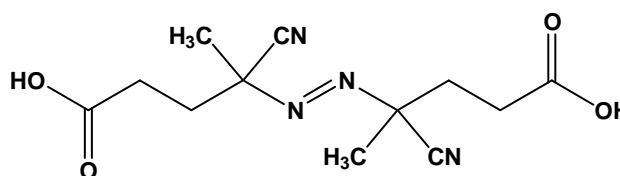


Figure 4-42 4,4'-azobis(4-cyanovaleric acid).

groups, namely, 4,4'-azobis(4-cyanovaleric acid) (Fig.4-42) was also used for preparation of the PI shell.

After treatment of the substrate-immobilized microgels with 4,4'-azobis(4-cyanovaleric acid) in the presence of DCC / DMAP, polymerization of isoprene was carried out at 70°C. AFM analysis of particles before and after polymerization showed the height increase in the range of ~ 50-60 nm, which corresponds to the thickness of polyisoprene on microgels (Fig.4-43).

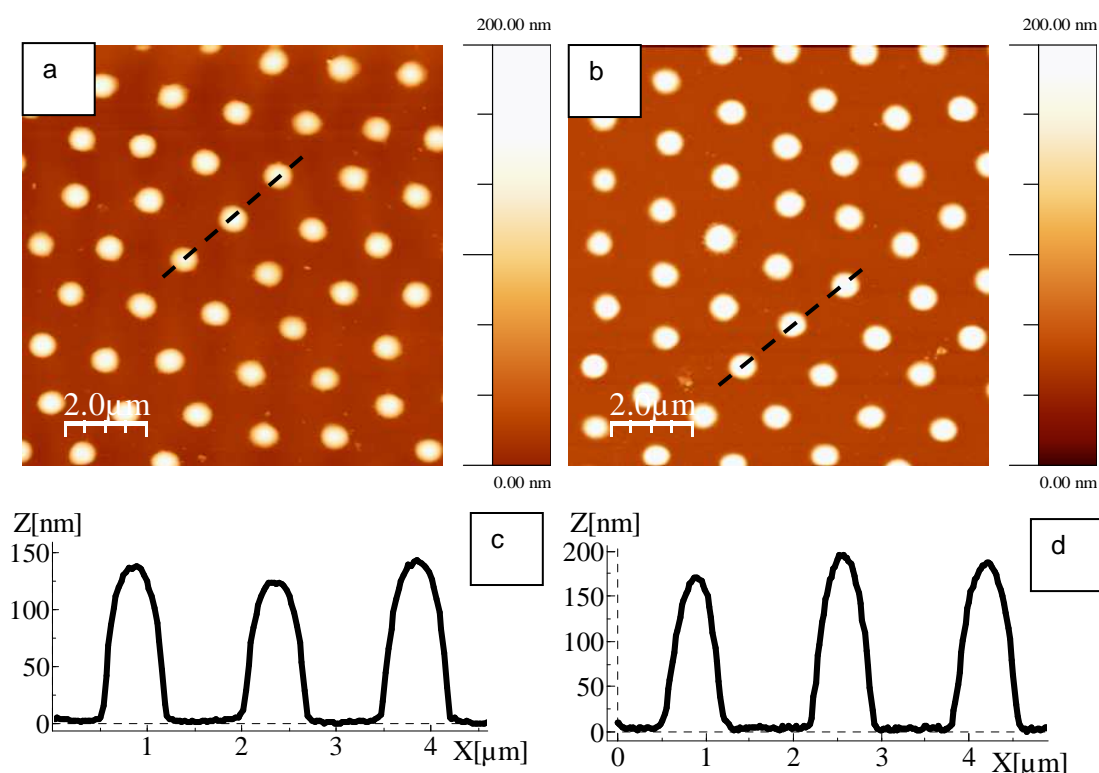


Fig. 4-43 AFM topography images (top) and corresponding cross-sectional profiles (bottom) of surface-immobilized P(NIPAM-AAm-VA) microgels (a, c) before and (b, d) after surface-initiated radical polymerization of isoprene using 4,4'-azobis (4-cyanovaleric acid) as initiator.

Non-grafted polyisoprene has been analyzed by GPC after isolation from the reaction media. As expected for uncontrollable polymerization process, PDI of resulted polymer was extremely large (in the range of 8),

molecular weight M_w of polymer was calculated with respect to the polystyrene standards and found to be ~ 52800 g/mol.

Comparison of these results with the calculations made before in *Chapter 4.1* and further discussed in *Chapter 4.2.3.4* leads to conclusion that presence of the shell with such thickness should not prevent the swelling of microgels by itself. So, if free access of water to the hydrophilic core is provided and shell elastic modulus is not exceeding the value of ~ 100 kPa, all requirements for the adequate core-shell particles swelling on the surface will be fulfilled.

5.1.2.8 Utilization of polyisoprene latex for PI shell formation

In principle, graft-polymerization is a universal method for formation of covalently bound coatings, and can be applied for various surfaces and different monomers^[62, 249, 250]. However, this method involves relatively complex procedure. In particular, if radical polymerization is the underlying grafting process, the reaction must be carried out under anaerobic conditions using pure monomers. Also, the process is hardly scaleable for preparation of large samples.

An alternative approach, suitable for preparation of the polyisoprene shell on the surface of microgels is adsorption of polyisoprene latex from water suspension onto oppositely charged surface followed by latex coalescence. This so called “colloidosome approach” have been used by many scientist for creation a various types of core-shell structures using different particles and structures as building blocks: “raspberry”-like particles^[251], hollow spheres^[252] etc. The organization is possible due to ability of solid particles to form self-assembled monolayer at liquid/liquid or liquid/gas interfaces. This enhances the stability of the interface and is often referred to as Pickering stabilization^[253]. Stabilization is achieved when nanometer to micrometer-sized particles diffuse to the interfacial

region and remain there in a stable mechanical equilibrium. Thus, particles residing at the interface between the dispersed and continuous phases usually form rigid structures stabilizing the surface of droplets which approach one another, by arresting rupture, and minimizing coalescence^[254].

On the other hand, method of formation of nanocomposites, based on regular coagulation between two kinds of pre-formed particles, so-called “heterocoagulation method” is widely used for creation of nanostructured organic/inorganic materials^[255]. It is induced by the mean of electrostatic or other interactions between two kinds of particles. A similar process, layer-by-layer (LbL) method based on the electrostatic action is often applied to fabricate the composite microspheres^[256]. Recently, a fabrication of novel structured colloidosome with shell of polymeric microparticles and microgel cores have been reported^[257].

All these achievements in nanostructuring obtained by “colloidosome method” constitute a backdrop for our approach according to which hydrophobic shell on the surface of pre-synthesized charged microgels could be created by means of adsorption of monodisperse polyisoprene latex bearing opposite charge.

Negatively charged polyisoprene latex was synthesized following the known procedure ^[258].

Synthesis of negatively charged polyisoprene latex

Batch emulsion polymerization of isoprene was carried out in the reaction flask using the following amounts of reagents with respect to isoprene: potassium persulfate (KPS) 1 wt%, sodium dodecyl sulphate (SDS) 10 wt%, sodium hydrocarbonate 3 wt% and dodecyl mercaptane 0.87 wt%. All ingredients except isoprene monomer were dissolved in 30 ml of water and charged into the reactor. The reactor was purged with nitrogen gas to remove dissolved oxygen for at least 1 hour at room temperature, before 8g of isoprene monomer was added to the reactor. Then the reactor temperature was ramped to 60°C in about 10 min and the nitrogen flow was stopped. The reaction was

then allowed to proceed under nitrogen atmosphere for 24 h with an agitation speed of 100 rpm. Unreacted isoprene monomer was removed from the resulting latex by bubbling with nitrogen gas at ambient temperature overnight followed by rotary evaporation under reduced pressure. For purification obtained latex was dialyzed against deionized water using the membrane with MWCO 3500 for 3 days.

The resulting latex was examined by DLS measurements and was found to be of 39.8 nm in diameter with PDI of 0.407.

A possibility for preparation of uniform shell using latex particles was verified using commercially available amino-functional 1 μm SiO_2 particles, as model “host” particles and synthesized negatively charged PI latex as “guest” particles. The guest/host particles weight ratio for close-packed surface coverage was determined by Equation 4-13. From these data, the feed ratio of PI latex to SiO_2 was calculated and was kept 1.5 times over the theoretical value. Silica hosts were blended with PI latex at room temperature and stirred to promote complete mixing. After 15 min of stirring, the heterocoagulates were separated out by four centrifugation/redispersion cycles to remove the residual latex that did not adhere to the silica surface. Finally the product was dried and investigated by SEM in order to look into the core-shell structure.

Polyisoprene shell formed on silica particles was clearly visualized on SEM images (Fig.4-44, a). Additional evidence of shell formation was obtained after etching of SiO_2 -core with hydrofluoric acid (Fig.4-44, b). Quantitatively the thickness of the shell on the particles was calculated from *Thermogravimetric Analysis* (TGA).

At first, the native amino-functional SiO_2 particles were investigated by TGA. The total weight lost of 9.8 wt% was detected in two different temperature regions. In particular, weight loss of 6.6 wt% at temperatures below 175°C could be attributed to release of strongly adsorbed water, while the rest of weight lost (3.2 wt%) could be due to adsorbed or immobilized organic compounds, which were in a contact with the particles during their synthesis. TGA analysis of SiO_2 particles modified with PI latex also showed the loss of bonded water of 5.9 wt% at $60\text{-}150^\circ\text{C}$, and the lost of 6.2 wt% around 368°C that is typical decomposition temperature of isoprene. Polyisoprene usually decomposes between $325\text{-}400^\circ\text{C}$ depending on the type and cross-linking density^[259]. Therefore, the difference in the weight loss at the higher-temperature range between the pristine and modified particles was attributed to the presence of polyisoprene shell. The amount of polyisoprene of about 3.0 wt% found corresponds to shell thickness of ~ 14.3 nm.

The same procedure was applied to arrange 40 nm PI latex onto amino-functional microgels. After separation of the prepared colloidosomes from excess of the latex, Z-potential measurements were performed and compared with the data for parent amino-functional microgels and negatively charged PI latex (Fig.4-45).

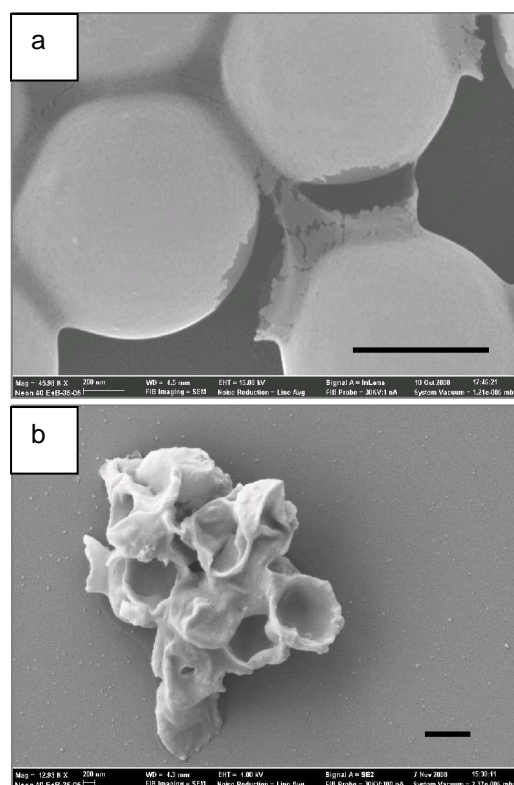


Figure 4-44 SEM-image of SiO_2 particles covered with polyisoprene latex (a) before and (b) after etching of silicon oxide. Scale bar 1 μm .

Electrokinetic

measurements demonstrated that adsorption of the latex shifts the isoelectric point of the microgels from pH 8.47 to pH 7.56. Polyisoprene latex used in this experiment, as expected, showed the negative values of Z-potential in the whole range of investigation (pH 2.5-10.5). The observed shift of the isoelectric point confirms adsorption of the

oppositely charged latex, however the fact that the resulting composite microgels particles neither reverse nor fully compensate their native positive charge suggests that the latex layer is not dense.

To visualize the core-shell structure, the microgel cores and latex shells were labelled with different fluorescent materials. To this end, amino-functionalized microgels were treated with Fluorescein Sodium salt (excitation at 493 nm and emission at 517 nm) and then mixed with negatively charged PI latex pre-treated with Ethidium Bromide (excitation at 524 nm, emission at 605 nm). The resulting labelled composite particles were visualized by fluorescent microscopy applying different filters. As expected, the resulting composite particles indeed display the core-shell morphology (Fig.4-46).

However, PI latex does not cover the microgels surface uniformly that could be clearly seen from AFM phase images (Fig.4-47).

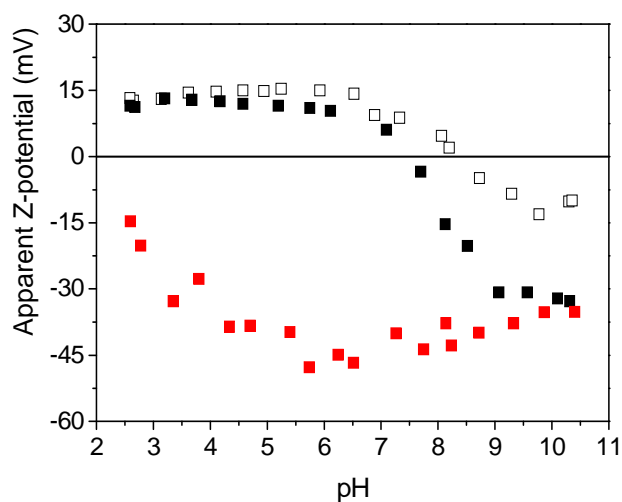


Figure 4-45 Electrokinetic measurements of P(NIPAM-AAm-VA) microgels (black squares), negatively-charged PI latex (red squares) and colloidosomes prepared by adsorption of PI latex on microgels surface (open squares).

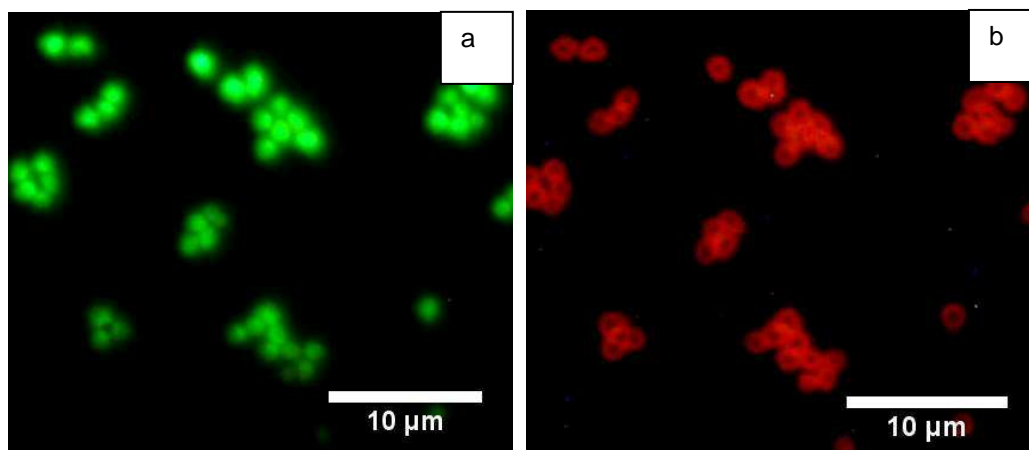


Figure 4-46 Fluorescent microscopy images of Fluorescein labeled P(NIPAM-AAm-VA) microgels covered with Ethidium Bromide labeled PI latex: (a) selective excitation of Fluorescein at 450-490 nm; (b) selective excitation of Ethidium Bromide at 510-560 nm.

Swelling ability of amino-containing microgels after adsorption of negatively charged polyisoprene latex was first investigated in dispersions. It was found that presence of hydrophobic material on the surface of microgels substantially decreases the swelling effect of composite particles (Fig.4-48).

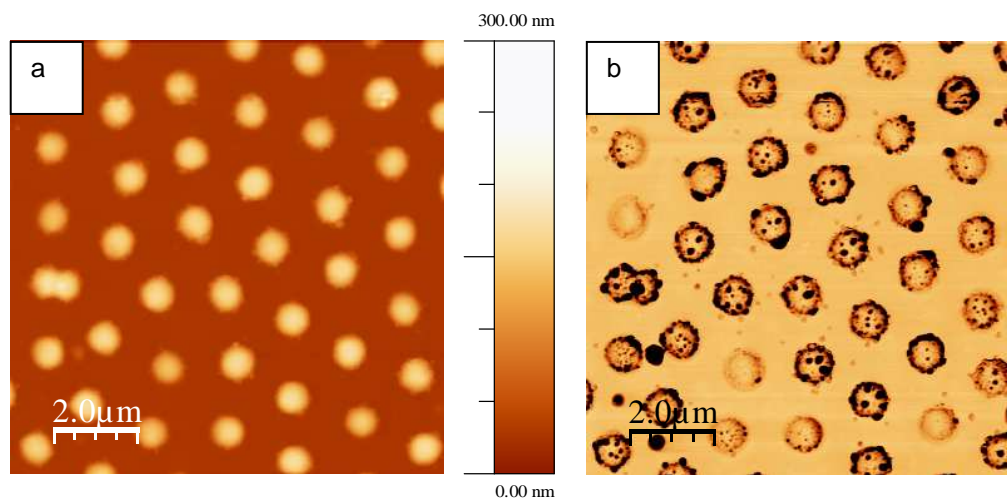


Figure 4-47 AFM (a) topography and (b) phase images of P(NIPAM-AAm-VA) microgels after adsorption of negatively charged PI latex.

Partial compensation of positive charges on the particles surface led to narrowing of VPT region and brought LCST to the value of $\sim 30^{\circ}\text{C}$. At

the same time, the size of collapsed colloidosomes became larger possibly due to the presence of the latex layer on the microgels surface. Volume swelling ratio of resulted colloidosomes was calculated using DLS data and gave a value of 2.38. Such swellability seemed to be insufficient for changing the water contact angle of surface via particles swelling

for more than 10° (See calculations in a Chapter 4.1). However, taking into account calculation of really “dry” dimensions of colloidosomes, obtained from AFM-measured, the swelling ratio was determined to be as high as 10.3, which is close to the target value.

The problem remained that PI latex did not form a continuous layer on the microgels. Besides that, it has other limitation for the final goal of this work. Thus, the presence of hydrophobic material on microgels affects the process of ordered deposition of particles on the surface. The worsening of self-assembly properties of particles after modification could be explained by changes in particles/surface interactions upon the deposition. Also hydrophobic latex could prevent microgels from proper attachment to the hydrophilic surface. For these reasons, preparation of colloidosomes directly on the surface using surface-immobilized microgels seems to be more promising route. Therefore, negatively charged PI latex was adsorbed on the top of pre-deposited and chemically attached amino-functionalized microgels. Reducing of microgels footprint on the surface after deposition has been performed using oxygen plasma treatment. For

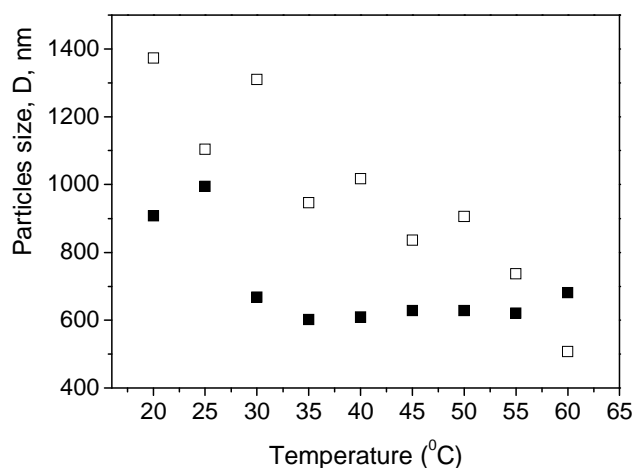


Figure 4-48 DLS measurements of hydrodynamic diameter of P(NIPAM-AAm-VA) microgels as a function of temperature before (open squares) and after (black squares) adsorption of negatively charged PI latex.

increasing of coagulation of latex, substrate with microgels was preliminary immersed in the solution containing 0.05M BaCl_2 . Afterwards, the substrate was dipped into diluted dispersion of latex for 1 hour, and then carefully washed with water and ethanol.

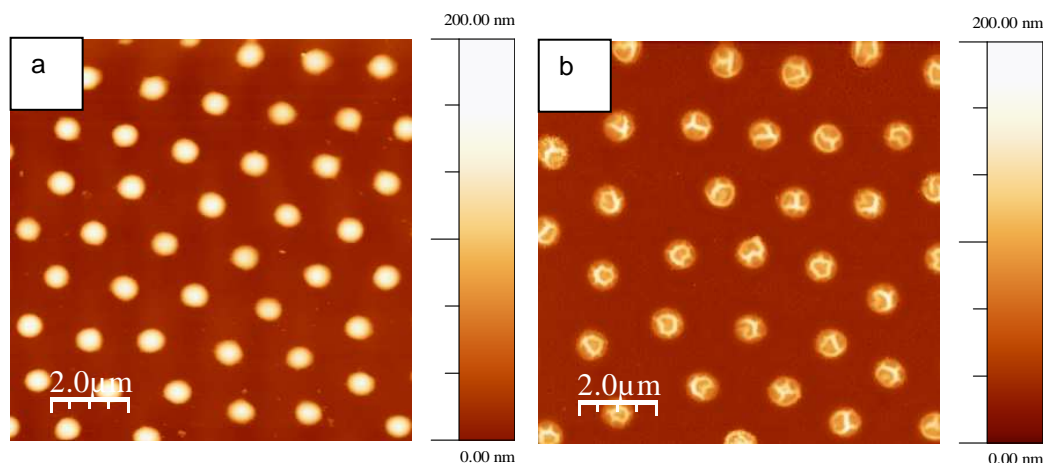


Figure 4-49 AFM topography images of P(NIPAM-AAm-VA) microgels (a) before and (b) after adsorption and coagulation of negatively charged PI-latex.

Resulted surfaces were studied with AFM (Fig.4-49) and the observed morphology of resulted composite particles was different from the initial seeing that folded structures were clearly visible atop of each particle. We suggest that these folded structures were formed upon the drying of swollen particles already covered with polyisoprene layer.

Another important observation is that the coverage degree of the oppositely charged latex was obviously much higher for surface-immobilized microgels than for freely dispersed ones. It could be due to the material used for adsorption always appears in large excess compared to the surface-immobilized microgels since absolute amounts of surface deposits are negligible compared to amounts of the material in the “bulk” solution. This factor is very important since the adsorption process is reversible. On the other hand, in the case of surface-immobilized microgels it is possible to apply a multiple deposition procedure, or

intensify the coagulation process via the treatment of the substrate with multivalent salts before and with ethanol after the latex adsorption.

5.1.2.9 Cross-linking of the shell

The ability of rubber or rubber-like materials to be stretched and then to return to the original conformation is known as “elasticity”. Polymers that exhibit rubber elastic properties named elastomers, i.e. these are materials that can be stretched to several times their original length without breaking and upon release of the stress, immediately return to the original length.

This unique characteristic of rubbers is determined by molecular conformation of material and by presence of network sustaining the stretching and its ability to recover.

Rubbers exhibit predominantly entropy-driven elasticity, this means that entropy of rubber decreases upon stretching. In an unstressed state rubber polymer chains adopt random-coil conformation but become oriented during extension. As conformational entropy decreases upon stretching, the long chain molecules try to return to statistically more favorable relaxed state.

Although individual polymer chains can be stretched or deformed, and restore their conformation after stretching force is eliminated, these phenomena alone are not sufficient to provide recoverability of a material as a macroscopic object. Even natural rubber itself does not have this ability because there are no cross-links of the macromolecules. Only when the cross-links are introduced between chains to form a three-dimensional network, recoverability becomes the intrinsic property of the material.

Sulfur was historically the first agent used for chemical cross-linking of rubber. The process of heating rubber with sulfur to form cross-linked network was called vulcanization^[260]. In general form it could be described as on Fig.4-50.

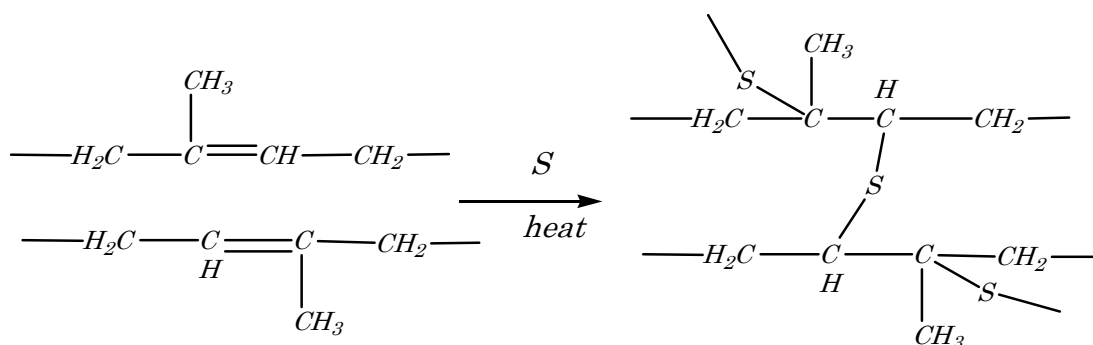


Figure 4-50 Schematic representation of sulfur vulcanization of polyisoprene.

Vulcanization often requires 5-8 wt% of sulfur, except the special hard rubbers, which require as much as 25-50 wt% of sulfur. Today the term vulcanization is used for all the reactions, which lead to the cross-linking of elastomers. Thus, one can vulcanize unsaturated elastomers (e.g. isoprene or butadiene), not only with sulfur, but also with peroxide, trinitrobenzene, dinitrobenzene, urea or phenol-formaldehyde precondensates.

Various methods of polyisoprene cross-linking have been already described in literature. Among them, UV irradiation in the presence of some photoinitiating agents^[261], heating^[262], action of ozone^[263], pressure^[264] in a combination with temperature or oxygen, peroxide cross-linking^[265] or reaction of double bonds with chemicals substances like sulfur monochloride,^[266] etc.

Thermal, UV-irradiation and chemical cross-linking procedures were used in this work for vulcanization of surface-immobilized core-shell particles. Thermo cross-linking was found to be only of limited suitability, because a large part of polyisoprene was melted and flowed down from the particles upon heating (Fig.4-51).

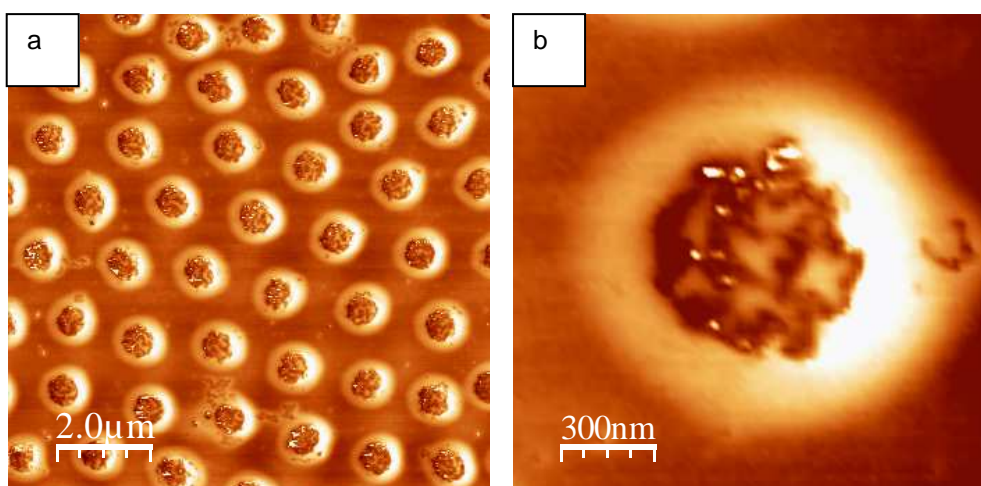


Figure 4-51 AFM phase images of an (a) array of microgels covered with “grafted-from” polyisoprene shell after thermal cross-linking and (b) magnified AFM image of individual particle.

Next, chemical cross-linking of polyisoprene with sulfur monochloride, so-called “cold vulcanization” process (Fig.4-52), based on linkage of adjacent isoprene units by means of carbon-sulfur bonds formation was tried.

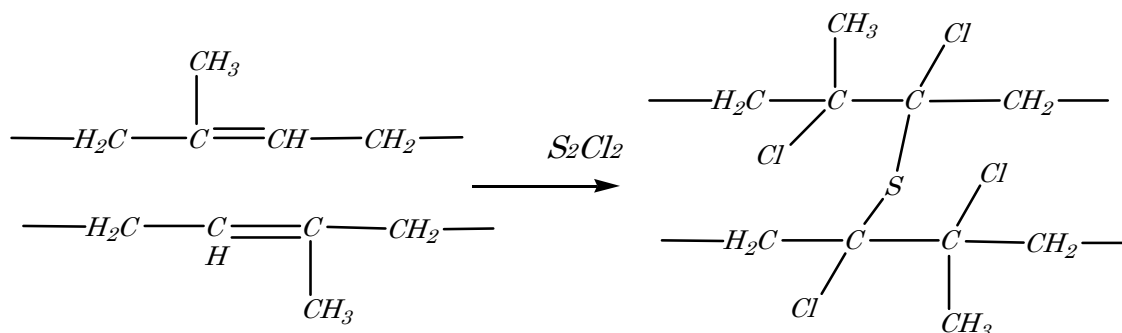


Figure 4-52 Schematic representation of vulcanization of polyisoprene with S_2Cl_2 .

This process contrasts with the hot (sulfur) vulcanization where the reaction does not involve the sulfurization of any appreciable number of olefin groups^[267]. An important advantage of this reaction is that cross-linking degree can be easily controlled by the amount of S_2Cl_2 added^[268].

In present work the cross-linking of polyisoprene by sulfur monochloride was performed as described in a literature^[268], namely by soaking of the substrate with attached core-shell particles in n-heptane/chloroform (8:2 v/v) solution of S_2Cl_2 of various concentration (0.001 - 0.1 %) at room temperature for 24 hours.

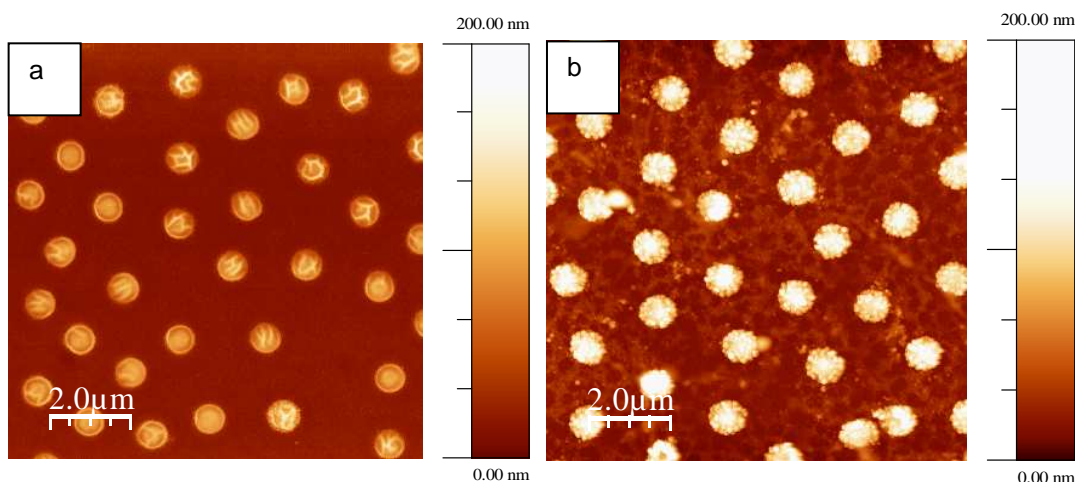


Figure 4-53 AFM topography images of P(NIPAM-AAm-VA) microgels (a) with adsorbed and coagulated PI latex on the surface and (b) with polyisoprene layer synthesized by “grafting-from” approach after cross-linking with sulfur monochloride.

Figure 4-53 shows AFM topography images of surface-immobilized microgels having S_2Cl_2 cross-linked PI shell prepared via (a) “colloidosomes approach” based on coagulation of PI latex on surface immobilized microgels and (b) surface-initiated polymerization of isoprene on the surface of pre-deposited microgels. As follows from the images, in the case of core-shell structures prepared by “colloidosome approach” cross-linking procedure did not affect the particles topography (compare Fig.4-53,a with Fig. 4-49,b) whereas in the case of shell formed by surface-initiated polymerization of isoprene cross-linking results in increase of roughness of the particles surface (compare Fig.4-53,b with Fig.4-43,b). The increased roughness is, most likely, due to inhomogeneity of polymer distribution on the microgels surface and high molecular weight distribution of the grafted polyisoprene.

5.1.3 SWITCHING PROPERTIES OF HYDROPHILIC SURFACES COVERED WITH HYDROPHOBIC CORE-SHELL MICROGELS SWELLABLE IN WATER

5.1.3.1 Responsive surfaces fabricated via “bottom-up” approach: in-situ AFM monitoring of the water-induced change of the surface coverage

Two most important parameters of responsive surfaces prepared via “bottom-up” approach have been studied: (1) changes of surface coverage ratio and (2) changes in wettability induced by particles swelling.

Direct observation of the change of the surface coverage upon swelling of the core-shell particles on the surface was performed by in-situ AFM measurements of samples in the air and under water. AFM measurements showed that the PI shell of hydrogel particles was impermeable to water if PS latex particles were not removed from the shell. No swelling of the particles was observed for at least 1 hour of the AFM measurements under water.

After removing of the PS latex and thus creating pores in the shell for water access, the particles became swellable in water (Fig.4-54). The process was confirmed to be fully reversible: after drying of the samples, the size of the core-shell particles was the same as their initial size before the swelling.

Analysis of the AFM images showed the increase of the surface coverage from 13.7% to 24.7% upon the swelling in water. According to Cassie equation, absolute values of WCA for such composite surface in a dry state were calculated as 67° and 36° supposing the PAA brushes between the hydrophobic particles. The calculations were performed assuming the contact angles of PAA substrate as 60° for protonated and 25° for deprotonated states, respectively, and the contact angle of core-

shell particles as 108° (WCA of PI). After exposure to water, the fraction of hydrophobic material on the surface were increased up to 24.7% and the expected WCA should be of about 72° for the substrate covered with protonated PAA and of about 46° for the deprotonated one.

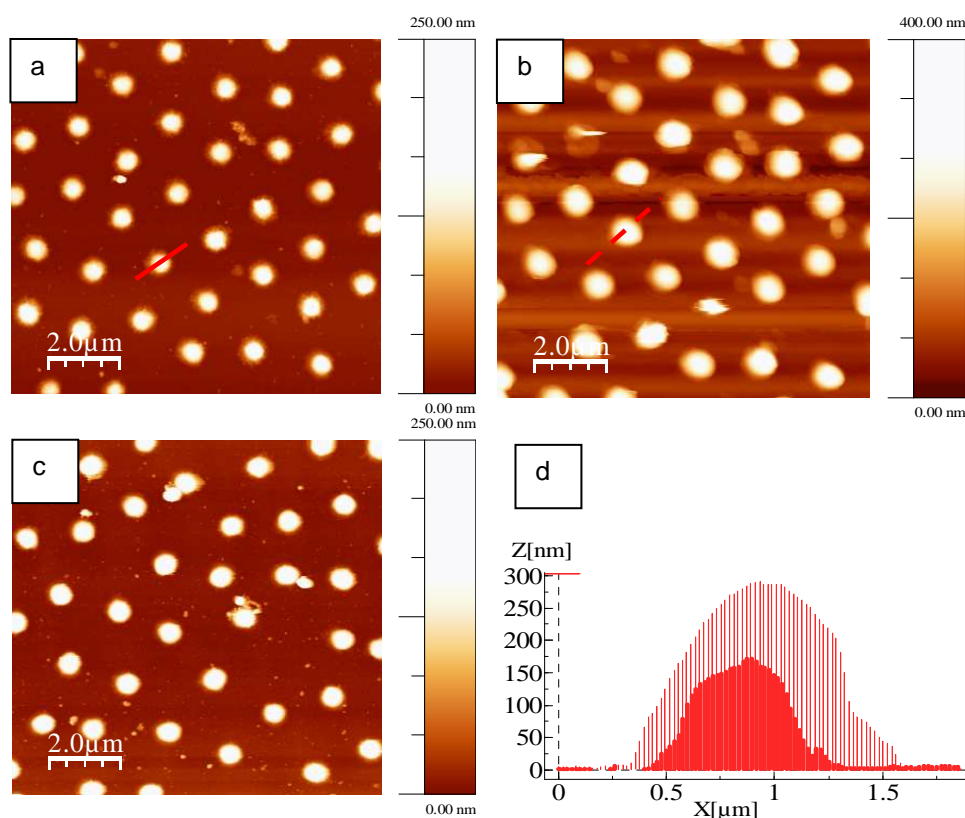


Figure 4-54 AFM topography images of deposited onto PAA-modified substrate P(NIPAM-AAm-VA) microgels with polyisoprene shell formed by surface-initiated polymerization after removal of PS latex: (a) in dry state, (b) swollen with water and (c) dried after contact with water. (d) corresponding cross-sectional profile of dry (red) and swollen (red shaded) microgel particle.

To verify if the surfaces indeed demonstrate the switching effect, the measurements of WCA were performed for the same sample in two states: 1) in the “dry” state, when the sample was dried for prolonged time at elevated temperature under vacuum and 2) in the “wet” state, after the exposure of the sample to water for about 2 hours followed by short drying with nitrogen.

It is noteworthy that the WCAs in both cases reflected rather hydrophobic behavior (76.5° and 77.4° for the “dry” and the “wet” states, respectively) with virtually no difference in WCA between the protonated and deprotonated PAA and only a minor hydrophobization effect was observed with the difference between the WCA in the “dry” and the “wet” states of about 1° . Such a deviation from the predicted values could be explained either by the fact that PAA brush could be contaminated by hydrophobic material during the multistep modification procedure, or alternatively, by the very fast swelling of the particles on the surface. In this case the swelling and, hence, the switching of the surface to the hydrophobic state occurs immediately after the water droplet is deposited onto the surface for the WCA measurements.

To verify the latter hypothesis the swelling kinetics was studied by environmental AFM (Fig.4-55). Due to technical reasons, the first topography image of the swollen particle array was recorded about 10 minutes after the addition of water to the environmental cell. It was found that during this time the surface coverage increases to about 50% of its plateau value; the latter was reached at about one hour. Thus, the swelling of the particles during the initial stage was proved to be a quite fast process, and therefore the water contact angle measurement of the “dry” state does not provide reliable result. Hence, further optimization of

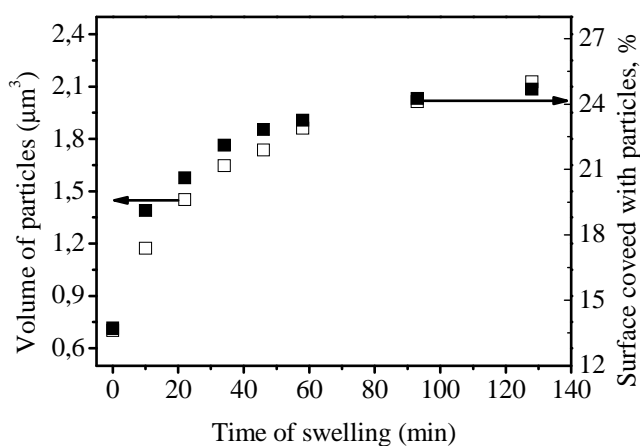


Figure 4-55 Time dependence of swelling behavior of surface-immobilized p(NIPAM-AAm-VA) microgels with PI shell formed by surface initiated polymerization and cross-linked with S_2Cl_2 .

the system, such as decrease of the swelling rate, is necessary to record the inverse-switching behavior of surface by WCA measurements.

Similar results were obtained during investigation of the surfaces prepared by “bottom-up” method using “colloidosome approach” for fabrication of polyisoprene shell. Exposure of the samples to water caused swelling of hydrophobically covered microgels (Fig.4-56) with returning to the same dry state topology of particles upon dehydration of the samples.

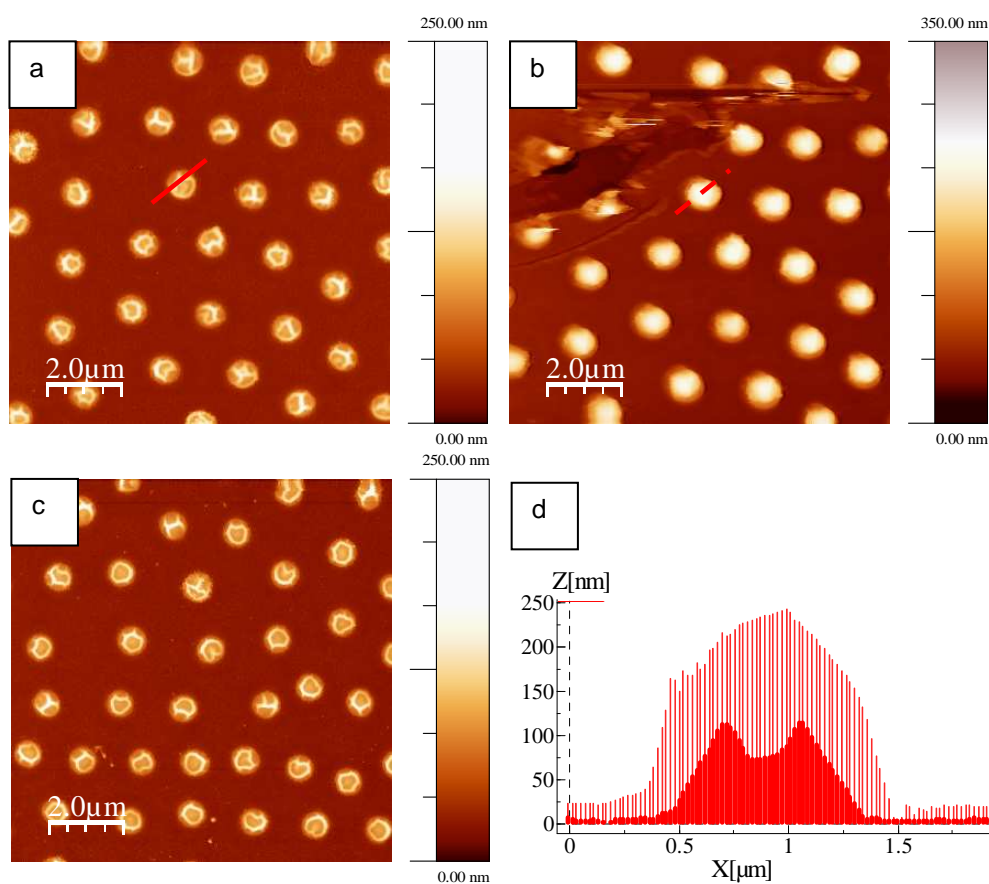


Figure 4-56 AFM topography images of deposited onto PAA-modified substrate P(NIPAM-AAm-VA) microgels with polyisoprene shell formed from PI latex: (a) in dry state, (b) swollen with water and (c) dried after contact with water. (d) corresponding cross-sectional profile of dry (red) and swollen (red shaded) microgel particle.

Kinetics of swelling showed the same tendencies, with fast increase of the particles' sizes and respectively the surface coverage with achieving of maximum values after 2 hours. Increase of surface coverage from 12.9% to 29.2% was detected upon swelling in water (Fig.4-57).

The switching of the water contact angle from 72.1° to 73.7° for such surfaces has been measured which was close to the expected values for swollen particles (calculated from Cassie equation). As in the previous case, the high contact angle values obtained can be explained by high probability of surfaces being contaminated during latex deposition process. Although the surfaces were carefully washed after preparation, some hydrophobic latex could remain and reduce the hydrophilicity of substrate.

Cross-linking procedure had no significant effect on switching properties of surfaces. Thus, after the photo cross-linking of the shell with an aid of benzophenone, change of WCA between 73° and 74° for samples in “dry” and “wet” state were measured, whereas after cold vulcanization procedure using sulfur monochloride surface WCA was found of about $75\text{--}76^\circ$ with the difference between “dry” and “wet” state of 1° .

As it was mentioned above, the observed insignificant switching of wettability could be explained by a contamination of the hydrophilic substrate (PAA brush) by the hydrophobic components. To check this hypothesis, AFM force volume measurements were performed. The particular aim of this study was to understand whether there is a contrast of properties, such as adhesion, indeed exists between the core-shell microgels and the substrate. To compare the adhesion properties of PAA and PI, additionally two reference surfaces were prepared. One of sample, was PAA brush prepared by the grafting-to approach similar to

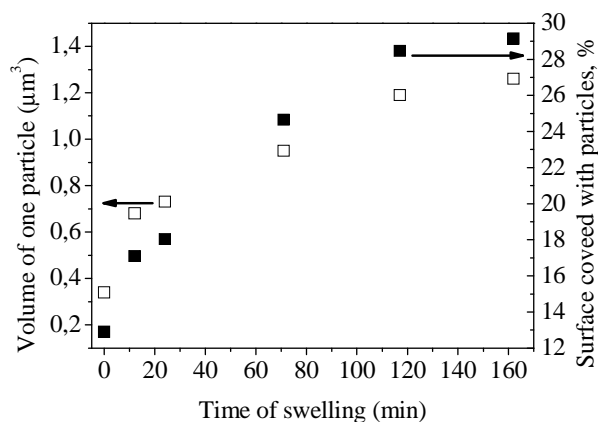


Figure 4-57 Time dependence of swelling behavior of surface-immobilized p(NIPAM-AAm-VA) microgels with PI shell formed from PI latex and cross-linked with S_2Cl_2 .

the procedure used for surface prepared for microgels deposition, whereas the second sample was a layer of PI on a Si wafer obtained by spin-coating of PI (Mw ~21000, Polymer Source Inc) from chloroform solution. In all cases preliminary calibrated cantilevers with determined spring constant value of 0.35 N/m were used. At first, the force-distance curves were measured in dry state for both reference surfaces and for the samples with the arranged hydrophobized microgels.

As can be seen from Figure 4-58, the two reference samples show clearly distinct force-distance curves. At the same time similar force-distance curves have been recorded on both PAA brush and on the surface between particles. The difference was more pronounced when measurements were performed under water (Fig.4-59). The areas with higher adhesion corresponded to the regions with a higher topography, i.e., to the hydrophobized microgels. It is noteworthy that force-distance curves obtained in-between the

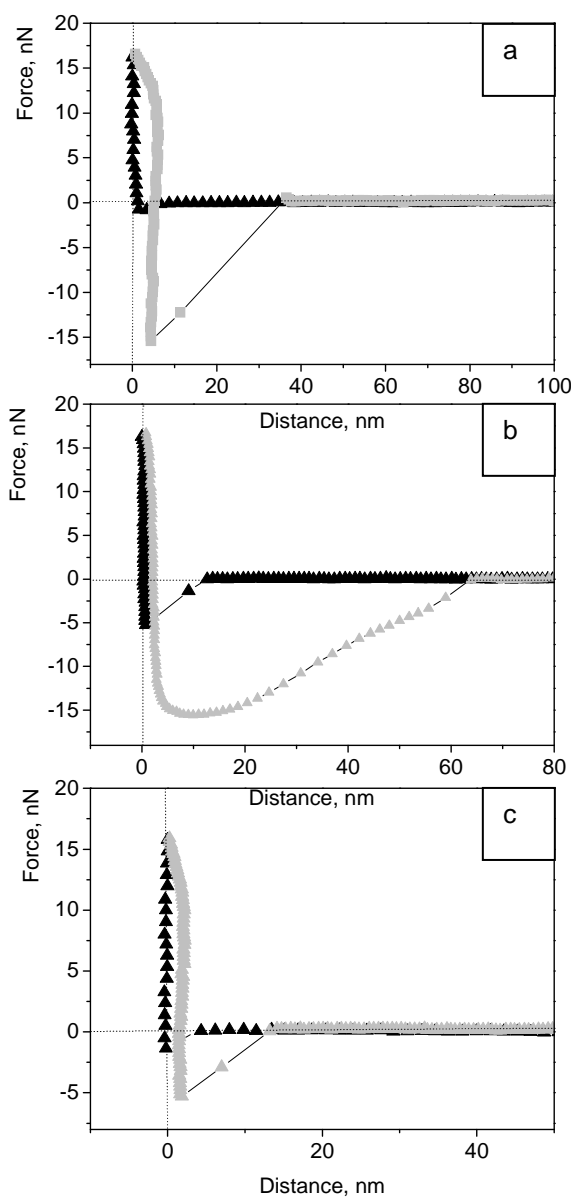


Figure 4-58 Typical force-distance curves measured on (a) PAA brush, (b) PI layer and (c) area between hydrophobized microgels. Black triangles - approaching cycle, gray triangles - retracting cycle.

hydrophobized microgels under water and values of the adhesion force extracted from those curves (0.79 nN) were rather similar to those for the PAA brush on reference sample (adhesion force 0.70 nN) and were far from measured adhesion force 1.34 nN for PI layer on reference sample. This confirmed selective grafting of PI at the microgels.

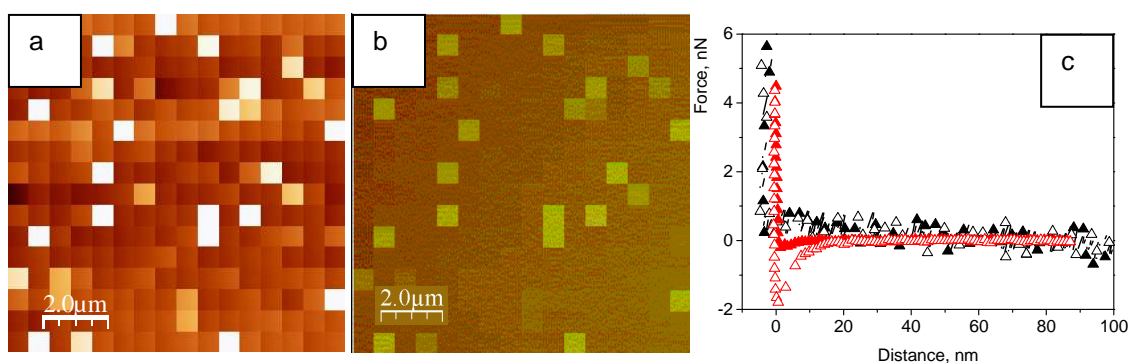


Figure 4-59 AFM (a) topography and (b) force-volume images obtained on the surface covered with core-shell microgels in water. Scan area - $10 \times 10 \mu\text{m}$, scan resolution - 16×16 . Bright regions correspond to higher topography and adhesion. (c) force-distance curves measured atop of core-shell particles (red triangles) and on the surface between the particles (black triangles). Approached and retracted curves are presented as closed and opened triangles, respectively.

The obtained results disproved our suggestion of a strong contamination of the surface with hydrophobic components during the polymerization procedure. It nevertheless did not exclude the possibility that PAA brush is not the perfect hydrophilic component for desired “contraphilicity” of the system. In other words, it becomes obvious that the “contraphilic” switching effect is strongly suppressed by deformation (low height-to-diameter aspect ratio) of the core-shell microgels upon deposition on the surface. This causes particles swelling and deswelling occur predominantly vertically and to far lesser extent laterally. Therefore, additional studies are necessary to improve mechanical properties of the core-shell microgels in order to achieve the lateral swelling-deswelling behavior.

6. SUMMARY

Nowadays the idea of application of hydrogel microparticles as coatings is being thought by many researchers as a promising way to modify the material's surface properties or prepare switchable and responsive surfaces. Facile, inexpensive synthetic methods, variability of structure and composition together with tunable responsive behaviour make microgels a promising material for a numerous practical applications. Environmentally friendly compounds used for microgels synthesis and, in many cases, compatibility with biological substances are additional advantages for their wide application.

In this work, an attempt to create responsive surfaces, able to inversely switch the wettability was made. It has been suggested that core-shell particles having water-swelling hydrogel core and hydrophobic, but water permeable shell regularly arranged on the hydrophilic substrate should increase the total amount of hydrophobic component on the surface upon swelling of the composite particles.

Different approaches of preparation of such core-shell particles have been developed and several types of the particles were successfully prepared and extensively characterized.

In the "one-pot" approach, acrylamide-based core-shell microgels were prepared by inverse suspension polymerization using block copolymer surfactant containing shell-forming block. The shell on the microgels was produced simultaneously during the polymerization reaction. Thereafter, the core-shell particles were deposited and chemically bound to the functional hydrophilic substrate. Using this approach, the inverse-switching effect up to 19° was detected, as revealed by the water contact angle measurements.

In the alternative "bottom-up" approach, structured two-component surfaces were prepared in the following way. PNIPAM-based microgels were first self-organized into quasiperiodic loosely packed arrays and

were chemically grafted to the functionalized hydrophilic substrate. Afterwards, a surface-initiated polymerization of isoprene was performed selectively atop of the microgels making them hydrophobic. The resulted surface has been found to be water-sensitive and showed an increase of the fraction of the hydrophobic component from 13% in the dry state up to 25% in water environment due to the particles swelling, as observed by in-situ AFM measurements. However, rather small switching effect of about 1° was recorded by water contact angle measurements because of a moderate lateral swelling of the core-shell microgels and due to a fast swelling of the microgel particles upon the contact angle measurements.

Thus, it was demonstrated that correctly designed and properly prepared core-shell hydrogel particles could be successfully applied for preparation of smart coatings and have the potential to change surface properties of the substrate making it adaptive to the environment. However, to get more pronounced inverse switching effect further optimizations of the system would be necessary.

During investigations in the frame of this work a number of useful applications of hydrogel microparticles were developed.

Self-assembly of microgels prepared via precipitation polymerization of N-isopropylacrylamide (NIPAM) with N,N'-methylenebisacrylamide (MBA) and acrylamide as comonomers was investigated on surfaces with the aim to establish factors that govern the formation of periodic loosely packed surface arrays, necessary for realization of the main task of the thesis. A "sombbrero-like" structure was revealed for all microgels. It was suggested that the major factor driving the formation of loosely packed arrays and regulating the interparticle distance is the presence of low-density "hairy shell" around the microgel cores formed due to gradually decrease of cross-linking density of microgels from the centre to periphery. The obtained results contribute to a better understanding of the structures of the PNIPAM-based microgels deposited on the substrate

and their self-assembly into periodic arrays which turns out to be a useful tool for microparticles lithography.

Periodic microgel arrays were used as masks for preparation of patterns of reactive silanes with controllable spacing between the patterned features and their applicability to the selective modification of surface was demonstrated (Fig.5-1).

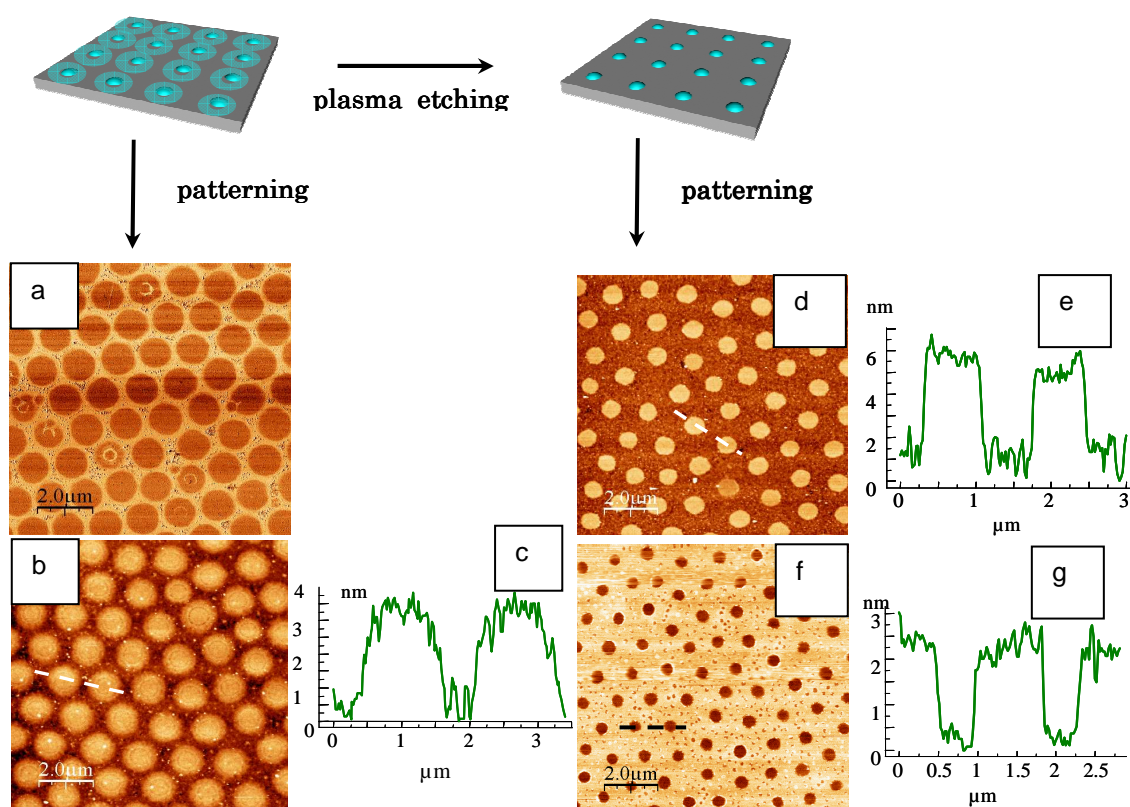


Figure 5-1 AFM phase (a) and topography (b, d, f) images of patterned surfaces prepared using P(NIPAM-AAm) microgels arrays as masks; (c, e, g) cross-sectional profiles obtained as shown on (b, d, f), respectively; (a) octadecyltrichlorosilane (ODS) monolayer surrounds circles of bare substrate; (b, c) P4VP₂₅-*b*-PS(*l*)₃₅₀ grafted to the areas where P(NIPAM-AAm) microgels were initially located; (d, e) the same as shown in (b, c) after plasma etching of P(NIPAM-AAm) microgels mask for 20 s before the patterning; (f, g) patterned ODS monolayer prepared using P(NIPAM-AAm) microgels mask etched by plasma for 150 s.

Patterned structures with different size and periodicity were prepared (Fig.5-2). For this microgels were deposited on the substrate

and size of microgels footprint was reduced via plasma etching applied for different time ranging from 15 to 120 seconds. It was shown that the use of the plasma-etched microgels mask leads to loosely packed arrays with controllable spacing between spots. The etching led to progressive reducing of the microgels size and, therefore, patterned features. Reduction of the size of the patterned circular structures from 1330 to nearly 500 nm was already observed after 20 seconds of the etching. Longer etching times led to further reduction of the features down to 417 nm. This corresponds to loosely packed particle arrays with the center-to-center and the particle-to-particle distances up to 1500 and 1100 nm respectively. Obtained results suggest that complete removal of the “hair” occurs during a brief etching, whereas etching of the much thicker core is more time-consuming and less efficient in terms of reduction of the features size.

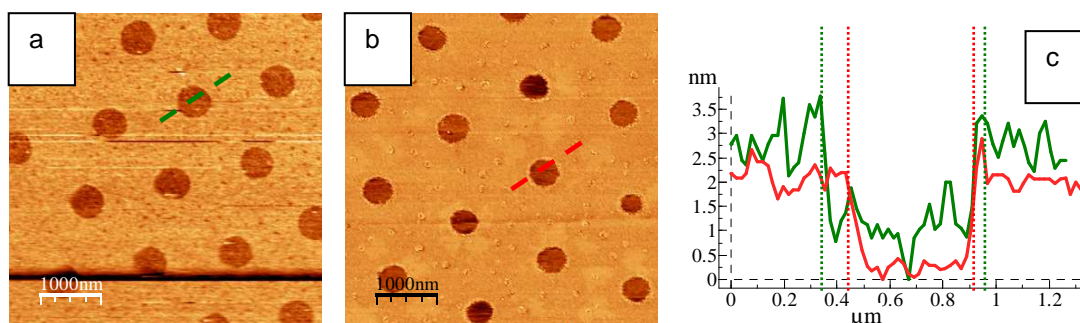


Figure 5-2 AFM topography images (a, b) of patterned surfaces prepared by microparticles lithography. Structures correction made by (a) 30 s and (b) 120 s of plasma etching. (c) cross-sectional profiles obtained as shown on (a, b).

Preparation of porous multilayer membranes from loosely packed arrays of hydrogel particles was also demonstrated (Fig.5-3). They were prepared by vacuum deposition of nickel and gold onto the ordered arrays of hydrogel microparticles. No additional treatments, like plasma etching or other, were needed in this case for preparation of Ni/Au perforated films. Closer inspection of the SEM images (Fig.5-3, c) allowed

differentiating the nickel and gold layer located one over another. The metal films prepared this way are promising materials for extraordinary optical transmission devices^[269, 270] or, alternatively they could be found application in optoelectronics as electrically conductive transparent coatings.

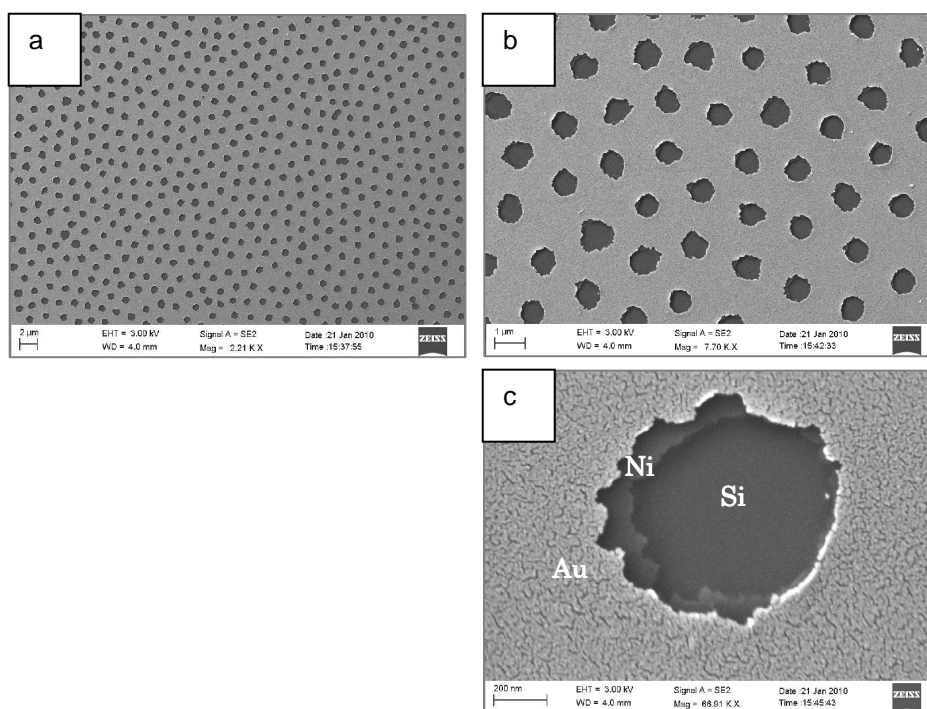


Figure 5-3 (a, b) SEM images of different magnifications of the perforated Ni/Au film formed upon nickel/gold sputtering over the P(NIPAM-AAm) microgels array followed by removal of the microgels by ultrasonication; (c) magnified image of a single hole reveals the area of bare Si wafer as well as gold and nickel layers.

As a responsive material, microgels are promising candidates for preparation of multilayered structured films. Layer-by-layer technique was applied in order to obtain dense microgel film with up to 250 nm thickness. Oppositely charged microgels allowed to use electrostatic forces in the process of deposition. Negatively charged microgels were widely used in such type of structuring in the past, but since positively charged hydrogel particles are rather rare, cationic polyelectrolytes are usually

used in LBL assemblies as a second component. In this work a simple synthetic route to amino-functionalized, positively charged (at certain pH), PNIPAM-based microgels was developed, so that microgel-microgel LBL assembly is now possible, as demonstrated in the preliminary results (Fig.5-4).

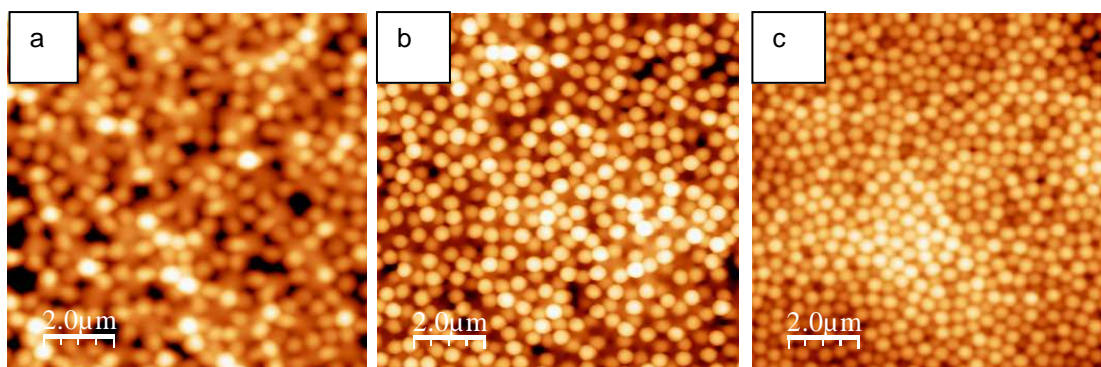


Figure 5-4 AFM topography images of films prepared via electrostatic layer-by-layer assembly of oppositely charged (a) two (b) three and (c) four layers of microgels.

Another field of research where smart hydrogel materials were involved is microencapsulation. Simple synthetic method allowing to fabricate PNIPAM-based microcapsules dispersible in organic solvents was developed in this work^[171]. Water uptake and release of small molecules by such capsules have been shown on the example of Rhodamine dye.

7. REFERENCES

- [1] Q. Y. Wang, Q. H. Zhang, X. L. Zhan, F. Q. Chen, *Progress in Chemistry* **2009**, *21*, 2183.
- [2] I. Topala, N. Dumitrascu, *Journal of Adhesion Science and Technology* **2007**, *21*, 1089.
- [3] A. Sekine, N. Seko, M. Tamada, Y. Suzuki, *Radiation Physics and Chemistry* **2010**, *79*, 16.
- [4] D. Quere, *Reports on Progress in Physics* **2005**, *68*, 2495.
- [5] X. Li, J. F. Tian, G. Garnier, W. Shen, *Colloids and Surfaces B-Biointerfaces* **2010**, *76*, 564.
- [6] S. M. Li, S. Z. Zhou, J. H. Liu, *Acta Physico-Chimica Sinica* **2009**, *25*, 2581.
- [7] S. L. Peterson, A. McDonald, P. L. Gourley, D. Y. Sasaki, *Journal of Biomedical Materials Research Part A* **2005**, *72A*, 10.
- [8] F. Xia, H. Ge, Y. Hou, T. L. Sun, L. Chen, G. Z. Zhang, L. Jiang, *Advanced Materials* **2007**, *19*, 2520.
- [9] J. Q. Jiang, X. Tong, D. Morris, Y. Zhao, *Macromolecules* **2006**, *39*, 4633.
- [10] M. L. Kovarik, S. C. Jacobson, *Analytical Chemistry* **2009**, *81*, 7133.
- [11] A. A. Brown, O. Azzaroni, W. T. S. Huck, *Langmuir* **2009**, *25*, 1744.
- [12] X. J. Feng, L. Feng, M. H. Jin, J. Zhai, L. Jiang, D. B. Zhu, *Journal of the American Chemical Society* **2004**, *126*, 62.
- [13] G. B. Crevoisier, P. Fabre, J. M. Corpart, L. Leibler, *Science* **1999**, *285*, 1246.
- [14] T. N. Krupenkin, J. A. Taylor, T. M. Schneider, S. Yang, *Langmuir* **2004**, *20*, 3824.
- [15] J. Lahann, S. Mitragotri, T. N. Tran, H. Kaido, J. Sundaram, I. S. Choi, S. Hoffer, G. A. Somorjai, R. Langer, *Science* **2003**, *299*, 371.
- [16] J. Hemmerle, V. Roucoules, G. Fleith, M. Nardin, V. Ball, P. Lavalley, P. Marie, J. C. Voegel, P. Schaaf, *Langmuir* **2005**, *21*, 10328.
- [17] S. Minko, M. Muller, M. Motornov, M. Nitschke, K. Grundke, M. Stamm, *Journal of the American Chemical Society* **2003**, *125*, 3896.
- [18] Young, *Phil. Trans. R. Soc. London* **1805**, *95*, 65.
- [19] R. N. Wenzel, *Industrial and Engineering Chemistry* **1936**, *28*, 988.
- [20] D. H. Bangham, R. I. Razouk, *Transactions of the Faraday Society* **1937**, *33*, 1459.
- [21] G. A. P. Adamson A.W., *Physical Chemistry of Surfaces*, Willey Interscience, New-York, **1997**.
- [22] A. B. D. Cassie, *Discussions of the Faraday Society* **1948**, *3*, 11.
- [23] R. E. Johnson, R. H. Dettre, *Journal of Physical Chemistry* **1964**, *68*, 1744.
- [24] R. J. Good, *Journal of Adhesion Science and Technology* **1992**, *6*, 1269.
- [25] J. R. Henderson, *Physical Review E* **1994**, *50*, 4836.
- [26] R. J. Good, *Journal of Colloid and Interface Science* **1977**, *59*, 398.

- [27] D. Y. Kwok, A. W. Neumann, *Advances in Colloid and Interface Science* **1999**, *81*, 167.
- [28] A. Marmur, *Langmuir* **2004**, *20*, 3517.
- [29] A. Marmur, *Langmuir* **2003**, *19*, 8343.
- [30] C. W. Extrand, S. I. Moon, P. Hall, D. Schmidt, *Langmuir* **2007**, *23*, 8882.
- [31] R. H. Dettre, R. E. Johnson, *Journal of Physical Chemistry* **1965**, *69*, 1507.
- [32] K. Grundke, in *Handbook of Applied Surface and Colloid Chemistry : Wetting, Spreading and Penetration Vol. 2* (Ed.: K. Hilmberg), **2001**, pp. 119.
- [33] A. B. D. Cassie, S. Baxter, *Transactions of the Faraday Society* **1944**, *40*, 0546.
- [34] F. E. Bartell, J. W. Shepard, *Journal of Physical Chemistry* **1953**, *57*, 211.
- [35] A. W. Neumann, R. J. Good, *Journal of Colloid and Interface Science* **1972**, *38*, 341.
- [36] G. M. Nishioka, S. P. Wesson, Elsevier Science Bv, **1996**, pp. 247.
- [37] V. E. Smorodin, *Langmuir* **1994**, *10*, 2250.
- [38] W. A. Goedel, *Europhysics Letters* **2003**, *62*, 607.
- [39] S. Shibuichi, T. Onda, N. Satoh, K. Tsujii, *Journal of Physical Chemistry* **1996**, *100*, 19512.
- [40] T. Onda, S. Shibuichi, N. Satoh, K. Tsujii, *Langmuir* **1996**, *12*, 2125.
- [41] N. A. Patankar, *Langmuir* **2004**, *20*, 8209.
- [42] B. He, N. A. Patankar, J. Lee, *Langmuir* **2003**, *19*, 4999.
- [43] R. N. Wenzel, *Journal of Physical and Colloid Chemistry* **1949**, *53*, 1466.
- [44] J. Bico, C. Tordeux, D. Quere, *Europhysics Letters* **2001**, *55*, 214.
- [45] R. H. Dettre, C. Johnson, *Adv. Chem. Ser.* **1964**, *43*, 136.
- [46] F. Garbassi, M. Morre, E. Occhiello, *Langmuir* **1989**, *5*, 872.
- [47] S. Wu, *Polymer interface and adhesion*, M.Dekker, New York, **1982**.
- [48] N. A. Patankar, *Langmuir* **2003**, *19*, 1249.
- [49] S. Brandon, N. Haimovich, E. Yeger, A. Marmur, *Journal of Colloid and Interface Science* **2003**, *263*, 237.
- [50] F. E. Bartell, J. W. Shepard, *Journal of Physical Chemistry* **1953**, *57*, 455.
- [51] C. W. Extrand, *Langmuir* **2003**, *19*, 3793.
- [52] W. Chen, A. Y. Fadeev, M. C. Hsieh, D. Oner, J. Youngblood, T. J. McCarthy, *Langmuir* **1999**, *15*, 3395.
- [53] J. P. Youngblood, T. J. McCarthy, *Macromolecules* **1999**, *32*, 6800.
- [54] D. Oner, T. J. McCarthy, *Langmuir* **2000**, *16*, 7777.
- [55] L. C. Gao, T. J. McCarthy, *Langmuir* **2009**, *25*, 7249.
- [56] S. R. Holmesfarley, R. H. Reamey, R. Nuzzo, T. J. McCarthy, G. M. Whitesides, *Langmuir* **1987**, *3*, 799.
- [57] T. L. Sun, G. J. Wang, L. Feng, B. Q. Liu, Y. M. Ma, L. Jiang, D. B. Zhu, *Angewandte Chemie-International Edition* **2004**, *43*, 357.
- [58] F. J. Holly, *Journal of Biomedical Materials Research* **1975**, *9*, 315.

- [59] S. H. Lee, E. Ruckenstein, *Journal of Colloid and Interface Science* **1987**, *117*, 172.
- [60] S. H. Lee, E. Ruckenstein, *Journal of Colloid and Interface Science* **1987**, *120*, 529.
- [61] J. Hopken, M. Moller, *Macromolecules* **1992**, *25*, 2482.
- [62] K. Senshu, S. Yamashita, H. Mori, M. Ito, A. Hirao, S. Nakahama, *Langmuir* **1999**, *15*, 1754.
- [63] A. Vaidya, M. K. Chaudhury, *Journal of Colloid and Interface Science* **2002**, *249*, 235.
- [64] V. V. Tsukruk, I. Luzinov, K. Larson, S. Li, D. V. McGrath, *Journal of Materials Science Letters* **2001**, *20*, 873.
- [65] E. B. Zhulina, C. Singh, A. C. Balazs, *Macromolecules* **1996**, *29*, 6338.
- [66] E. B. Zhulina, C. Singh, A. C. Balazs, *Macromolecules* **1996**, *29*, 8254.
- [67] B. Zhao, W. J. Brittain, *Journal of the American Chemical Society* **1999**, *121*, 3557.
- [68] A. Sidorenko, S. Minko, K. Schenk-Meuser, H. Duschner, M. Stamm, *Langmuir* **1999**, *15*, 8349.
- [69] P. Uhlmann, L. Ionov, N. Houbenov, M. Nitschke, K. Grundke, M. Motornov, S. Minko, M. Stamm, *Progress in Organic Coatings* **2006**, *55*, 168.
- [70] S. Khongtong, G. S. Ferguson, *Journal of the American Chemical Society* **2001**, *123*, 3588.
- [71] U. Makal, K. J. Wynne, *Langmuir* **2005**, *21*, 3742.
- [72] U. Makal, N. Uslu, K. J. Wynne, *Langmuir* **2007**, *23*, 209.
- [73] J. D. Ferry, *Viscoelastic Properties of Polymers*, Wiley, New York, **1980**.
- [74] T. Tanaka, L. O. Hocker, G. B. Benedek, *Journal of Chemical Physics* **1973**, *59*, 5151.
- [75] S. H. Gehrke, *Advances in Polymer Science* **1993**, *110*, 81.
- [76] J. L. Drury, D. J. Mooney, *Biomaterials* **2003**, *24*, 4337.
- [77] X. C. Xiao, L. Y. Chu, W. M. Chen, J. H. Zhu, *Polymer* **2005**, *46*, 3199.
- [78] W. Lin, Y. S. Zhou, Y. Zhao, Q. S. Zhu, C. Wu, *Macromolecules* **2002**, *35*, 7407.
- [79] H. J. Kim, J. H. Lee, M. Lee, *Angewandte Chemie-International Edition* **2005**, *44*, 5810.
- [80] S. M. Kuo, G. C. C. Niu, S. J. Chang, C. H. Kuo, M. S. Bair, *Journal of Applied Polymer Science* **2004**, *94*, 2150.
- [81] M. R. Rekha, C. P. Sharma, *Journal of Controlled Release* **2009**, *135*, 144.
- [82] J. I. Lee, H. S. Kim, H. S. Yoo, *International Journal of Pharmaceutics* **2009**, *373*, 93.
- [83] S. J. Rendevski, A. N. Andonovski, *Polymer Bulletin* **2005**, *54*, 93.
- [84] D. Bulone, P. L. S. Biagio, *Biophysical Journal* **1990**, *57*, A256.
- [85] D. M. R. Mateus, S. S. Alves, M. M. R. da Fonseca, *Biotechnology and Bioengineering* **1999**, *63*, 625.
- [86] N. Mohmeyer, H. W. Schmidt, *Chemistry-a European Journal* **2007**, *13*, 4499.
- [87] S. Meyer, W. Richtering, *Macromolecules* **2005**, *38*, 1517.

- [88] C. Wu, X. H. Wang, *Physical Review Letters* **1998**, *80*, 4092.
- [89] V. V. A. Fernandez, N. Tepale, J. C. Sanchez-Diaz, E. Mendizabal, J. E. Puig, J. F. A. Soltero, *Colloid and Polymer Science* **2006**, *284*, 387.
- [90] K. Makino, H. Agata, H. Ohshima, *Journal of Colloid and Interface Science* **2000**, *230*, 128.
- [91] S. Nayak, L. A. Lyon, *Chemistry of Materials* **2004**, *16*, 2623.
- [92] A. Fernandez-Nieves, M. Marquez, *Journal of Chemical Physics* **2005**, *122*.
- [93] K. Lee, S. A. Asher, *Journal of the American Chemical Society* **2000**, *122*, 9534.
- [94] H. Hirose, M. Shibayama, *Macromolecules* **1998**, *31*, 5336.
- [95] T. Tanaka, D. J. Fillmore, *Journal of Chemical Physics* **1979**, *70*, 1214.
- [96] E. S. Matsuo, T. Tanaka, *Journal of Chemical Physics* **1988**, *89*, 1695.
- [97] K. Takahashi, T. Takigawa, T. Masuda, *Journal of Chemical Physics* **2004**, *120*, 2972.
- [98] E. Karadag, D. Saraydin, *Polymer Bulletin* **2002**, *48*, 299.
- [99] H. Kawaguchi, K. Fujimoto, Y. Mizuhara, *Colloid and Polymer Science* **1992**, *270*, 53.
- [100] M. Rasmusson, B. Vincent, N. Marston, *Colloid and Polymer Science* **2000**, *278*, 253.
- [101] L. C. Dong, A. S. Hoffman, *Journal of Controlled Release* **1991**, *15*, 141.
- [102] P. W. Zhu, D. H. Napper, *Langmuir* **2000**, *16*, 8543.
- [103] J. H. Holtz, S. A. Asher, *Nature* **1997**, *389*, 829.
- [104] I. J. Suarez, B. Sierra-Martin, A. Fernandez-Barbero, **2009**, pp. 30.
- [105] I. J. Suarez, A. Fernandez-Nieves, M. Marquez, *Journal of Physical Chemistry B* **2006**, *110*, 25729.
- [106] W. McPhee, K. C. Tam, R. Pelton, *Journal of Colloid and Interface Science* **1993**, *156*, 24.
- [107] J. Musch, S. Schneider, P. Lindner, W. Richtering, *Journal of Physical Chemistry B* **2008**, *112*, 6309.
- [108] Y. Maeda, T. Nakamura, I. Ikeda, *Macromolecules* **2001**, *34*, 1391.
- [109] H. M. Crowther, B. R. Saunders, S. J. Mears, T. Cosgrove, B. Vincent, S. M. King, G. E. Yu, *Colloids and Surfaces a-Physicochemical and Engineering Aspects* **1999**, *152*, 327.
- [110] C. S. Brazel, N. A. Peppas, *Macromolecules* **1995**, *28*, 8016.
- [111] V. T. Pinkrah, M. J. Snowden, J. C. Mitchell, J. Seidel, B. Z. Chowdhry, G. R. Fern, *Langmuir* **2003**, *19*, 585.
- [112] S. Kazakov, M. Kaholek, D. Kudasheva, I. Teraoka, M. K. Cowman, K. Levon, *Langmuir* **2003**, *19*, 8086.
- [113] L. Nabzar, D. Duracher, A. Elaissari, G. Chauveteau, C. Pichot, *Langmuir* **1998**, *14*, 5062.
- [114] E. Rodriguez, I. Katime, *Journal of Applied Polymer Science* **2003**, *90*, 530.
- [115] M. A. Barakat, N. Sahiner, *Journal of Environmental Management* **2008**, *88*, 955.

- [116] M. J. Snowden, B. Z. Chowdhry, B. Vincent, G. E. Morris, *Journal of the Chemical Society-Faraday Transactions* **1996**, 92, 5013.
- [117] R. H. Pelton, P. Chibante, *Colloids and Surfaces* **1986**, 20, 247.
- [118] H. Senff, W. Richtering, *Journal of Chemical Physics* **1999**, 111, 1705.
- [119] Y. Ogawa, K. Ogawa, B. L. Wang, E. Kokufuta, *Langmuir* **2001**, 17, 2670.
- [120] C. D. H. Alarcon, S. Pennadam, C. Alexander, *Chemical Society Reviews* **2005**, 34, 276.
- [121] V. C. Lopez, J. Hadgraft, M. J. Snowden, *International Journal of Pharmaceutics* **2005**, 292, 137.
- [122] Z. Guo, H. Sautereau, D. E. Kranbuehl, *Macromolecules* **2005**, 38, 7992.
- [123] S. Q. Xu, J. G. Zhang, C. Paquet, Y. K. Lin, E. Kumacheva, *Advanced Functional Materials* **2003**, 13, 468.
- [124] B. Brugger, W. Richtering, *Advanced Materials* **2007**, 19, 2973.
- [125] L. Bromberg, M. Temchenko, T. A. Hatton, *Langmuir* **2003**, 19, 8675.
- [126] H. G. Stevin, in *Advances in Polymer Science, Vol. 110*, Springer Verlag, Berlin/Heidelberg, **1993**.
- [127] B. R. Saunders, B. Vincent, *Advances in Colloid and Interface Science* **1999**, 80, 1.
- [128] M. J. Serpe, C. D. Jones, L. A. Lyon, *Langmuir* **2003**, 19, 8759.
- [129] V. Nerapusri, J. L. Keddie, B. Vincent, I. A. Bushnak, *Langmuir* **2006**, 22, 5036.
- [130] C. D. Sorrell, L. A. Lyon, *Langmuir* **2008**, 24, 7216.
- [131] N. Singh, A. W. Bridges, A. J. Garcia, L. A. Lyon, *Biomacromolecules* **2007**, 8, 3271.
- [132] T. Sakai, Y. Takeoka, T. Seki, R. Yoshida, *Langmuir* **2007**, 23, 8651.
- [133] S. B. Quint, C. Pacholski, *Journal of Materials Chemistry* **2009**, 19, 5906.
- [134] S. Tsuji, H. Kawaguchi, *Langmuir* **2005**, 21, 8439.
- [135] S. Schmidt, T. Hellweg, R. von Klitzing, *Langmuir* **2008**, 24, 12595.
- [136] F. Di Benedetto, A. Biasco, D. Pisignano, R. Cingolani, Iop Publishing Ltd, **2005**, pp. S165.
- [137] M. Kumoda, Y. Takeoka, M. Watanabe, *Langmuir* **2003**, 19, 525.
- [138] D. Biswal, H. D. Chirra, J. Z. Hilt, *Biomedical Microdevices* **2008**, 10, 213.
- [139] Y. Lu, D. F. Wang, T. Li, X. Q. Zhao, Y. L. Cao, H. X. Yang, Y. Y. Duan, *Biomaterials* **2009**, 30, 4143.
- [140] J. B. Ciolino, T. R. Hoare, N. G. Iwata, I. Behlau, C. H. Dohlman, R. Langer, D. S. Kohane, *Investigative Ophthalmology & Visual Science* **2009**, 50, 3346.
- [141] L. L. Li, G. Li, Y. Wang, J. M. Jiang, *Applied Surface Science* **2009**, 255, 7734.
- [142] D. Bontempo, N. Tirelli, G. Masci, V. Crescenzi, J. A. Hubbell, *Macromolecular Rapid Communications* **2002**, 23, 418.
- [143] Y. Osada, J. P. Gong, *Progress in Polymer Science* **1993**, 18, 187.
- [144] K. L. Wang, J. H. Burban, E. L. Cussler, *Advances in Polymer Science* **1993**, 110, 67.

- [145] G. Binnig, C. F. Quate, C. Gerber, *Physical Review Letters* **1986**, 56, 930.
- [146] T. R. Matzelle, G. Geuskens, N. Kruse, *Macromolecules* **2003**, 36, 2926.
- [147] M. E. Harmon, D. Kucking, C. W. Frank, *Langmuir* **2003**, 19, 10660.
- [148] N. C. Woodward, M. J. Snowden, B. Z. Chowdhry, P. Jenkins, I. Larson, *Langmuir* **2002**, 18, 2089.
- [149] A. Suzuki, M. Yamazaki, Y. Kobiki, H. Suzuki, *Macromolecules* **1997**, 30, 2350.
- [150] S. Schmidt, H. Motschmann, T. Hellweg, R. von Klitzing, *Polymer* **2008**, 49, 749.
- [151] International Standart, ISO 13321, *Methods for Determination of Particle Size Distribution Part 8: Photon Correlation Spectroscopy*, International Organisation for Standardisation (ISO), **1996**.
- [152] B. E. Dahneke, *Measurement of Suspended Particles by Quasielastic Light Scattering*, Wiley, **1983**.
- [153] D. Li, A. W. Neumann, *Applied Surface Thermodynamics*, Marcel Dekker, New York, **1996**.
- [154] Adamson A.W., *Physical Chemistry of Surfaces*, Wiley, New York, **1990**.
- [155] R. J. Hunter, N. Ekdawi, *Colloids and Surfaces* **1986**, 18, 325.
- [156] J. H. Conway, N. J. A. Sloane, *Sphere Packings, Lattices and Groups*, 3 ed., Springer Verlag, Berlin, **1999**.
- [157] L. H. Lee, *Journal of Polymer Science Part a-2-Polymer Physics* **1967**, 5, 1103.
- [158] P. J. Flory, N. Rabjohn, M. C. Shaffer, *Journal of Polymer Science* **1949**, 4, 225.
- [159] X. Yunshu, S. Heri, Y. Fumio, M. Keizo, *Journal of Applied Polymer Science* **1997**, 66, 113.
- [160] D. M. Preiss, W. M. Sawyer, W. C. Simpson, *Journal of Applied Polymer Science* **1963**, 7, 1803.
- [161] E. G. Kent, F. B. Swinney, *I&EC Product Research and Development* **1966**, 5, 134.
- [162] Y. Miyamoto, H. Yamao, K. Sekimoto, *Macromolecules* **2003**, 36, 6462.
- [163] Y. H. Park, J. H. Han, K. D. Suh, *Macromolecular Chemistry and Physics* **2008**, 209, 938.
- [164] C. D. Jones, L. A. Lyon, *Macromolecules* **2000**, 33, 8301.
- [165] W. Borchard, A. Emberger, J. Schwarz, *Angewandte Makromolekulare Chemie* **1978**, 66, 43.
- [166] T. Tanaka, D. Fillmore, S. T. Sun, I. Nishio, G. Swislow, A. Shah, *Physical Review Letters* **1980**, 45, 1636.
- [167] M. F. Refojo, *Abstracts of Papers of the American Chemical Society* **1975**, 170, 71.
- [168] H. Inomata, K. Nagahama, S. Saito, *Macromolecules* **1994**, 27, 6459.
- [169] K. G. Wiese, *Journal of Cranio-Maxillofacial Surgery* **1993**, 21, 309.

- [170] A. Moulton, J. Grosjean, G. Owen, *The Moulton Formulae and Methods - directly usable for calculations in mechanical engineering*, Wiley, London, **2005**.
- [171] M. Horecha, V. Senkovskyy, M. Stamm, A. Kiriy, *Macromolecules* **2009**, *42*, 5811.
- [172] L. Ionov, N. Houbenov, A. Sidorenko, M. Stamm, I. Luzinov, S. Minko, *Langmuir* **2004**, *20*, 9916.
- [173] F. Hoffman, K. Delbruch, in *Farbenfabriken Bayer*, Germany, **1909**.
- [174] W. Bauer, H. Lauth, in *Rohm and Haas*, Germany, **1931**.
- [175] M. Munzer, E. Trommsdorff, *Polymerization Processes*, Wiley, New York, **1977**.
- [176] G. E. Molau, *Abstracts of Papers of the American Chemical Society* **1969**, PO30.
- [177] P. Perrin, *Langmuir* **1998**, *14*, 5977.
- [178] B. Jakobs, T. Sottmann, R. Strey, J. Allgaier, L. Willner, D. Richter, *Langmuir* **1999**, *15*, 6707.
- [179] W. C. Griffin, *Journal of the Society of Cosmetic Chemists* **1949**, *1*, 312.
- [180] G. Riess, C. Labbe, *Macromolecular Rapid Communications* **2004**, *25*, 401.
- [181] P. J. Dowding, B. Vincent, E. Williams, *Journal of Colloid and Interface Science* **2000**, *221*, 268.
- [182] B. Yildiz, B. Isik, M. Kis, *European Polymer Journal* **2002**, *38*, 1343.
- [183] D. E. Owens, Y. Jian, J. E. Fang, B. V. Slaughter, Y.-H. Chen, N. A. Peppas, *Macromolecules* **2007**, *40*, 7306.
- [184] C.-H. Choi, J.-H. Jung, D.-W. Kim, Y.-M. Chung, C.-S. Lee, *Lab Chip* **2008**, *8*, 1544
- [185] Q. Sun, Y. Deng, *Journal of the American Chemical Society* **2005**, *127*, 8274.
- [186] L. S. Zha, Y. Zhang, W. L. Yang, S. K. Fu, *Advanced Materials* **2002**, *14*, 1090.
- [187] F. M. Winnik, M. F. Ottaviani, S. H. Bossmann, W. S. Pan, M. Garciagaribay, N. J. Turro, *Macromolecules* **1993**, *26*, 4577.
- [188] K. Zhang, W. Wu, K. Guo, J. Chen, P. Zhang, *Langmuir*.
- [189] R. Pelton, *Advances in Colloid and Interface Science* **2000**, *85*, 1.
- [190] T. Gilanyi, I. Varga, R. Meszaros, G. Filipcsei, M. Zrinyi, *Physical Chemistry Chemical Physics* **2000**, *2*, 1973.
- [191] Q. S. Zhang, L. S. Zha, J. H. Ma, B. R. Liang, *Journal of Applied Polymer Science* **2007**, *103*, 2962.
- [192] J. R. Tauro, R. A. Gemeinhart, *Journal of Biomaterials Science-Polymer Edition* **2005**, *16*, 1233.
- [193] A. Z. Pich, H. J. P. Adler, *Polymer International* **2007**, *56*, 291.
- [194] H. Feil, Y. H. Bae, F. J. Jan, S. W. Kim, *Macromolecules* **1993**, *26*, 2496.
- [195] C. Erbil, A. T. Gokceoren, Y. O. Polat, *Polymer International* **2007**, *56*, 547.
- [196] C. K. Chiklis, Grasshof.Jm, *Journal of Polymer Science Part a-2-Polymer Physics* **1970**, *8*, 1617.

- [197] E. C. Muniz, G. Geuskens, **2001**, pp. 879.
- [198] Y. Yamamoto, M. V. Sefton, *Journal of Applied Polymer Science* **1996**, *61*, 351.
- [199] L. H. Zhang, G. S. Kauffman, J. A. Pesti, J. G. Yin, *Journal of Organic Chemistry* **1997**, *62*, 6918.
- [200] A. Elachari, X. Coqueret, A. Lablachecombier, C. Loucheux, *Makromolekulare Chemie-Macromolecular Chemistry and Physics* **1993**, *194*, 1879.
- [201] J. D. Debord, L. A. Lyon, *Journal of Physical Chemistry B* **2000**, *104*, 6327.
- [202] S. B. Debord, L. A. Lyon, *Journal of Physical Chemistry B* **2003**, *107*, 2927.
- [203] L. Zha, J. Hu, C. Wang, S. Fu, A. Elaissari, Y. Zhang, *Colloid and Polymer Science* **2002**, *280*, 1.
- [204] X. Wu, R. H. Pelton, A. E. Hamielec, D. R. Woods, W. McPhee, *Colloid and Polymer Science* **1994**, *272*, 467.
- [205] H. G. Schild, *Progress in Polymer Science* **1992**, *17*, 163.
- [206] K. H. Kim, J. Kim, W. H. Jo, *Polymer* **2005**, *46*, 2836.
- [207] H. Mackova, D. Kralova, D. Horak, *Journal of Polymer Science Part a-Polymer Chemistry* **2007**, *45*, 5884.
- [208] W. Zhu, B. B. Wang, Y. Zhang, J. D. Ding, *European Polymer Journal* **2005**, *41*, 2161.
- [209] Z. X. Zhao, Z. Li, Q. B. Xia, E. Bajalis, H. X. Xi, Y. S. Lin, *Chemical Engineering Journal* **2008**, *142*, 263.
- [210] F. Meunier, A. Elaissari, C. Pichot, *Polymers for Advanced Technologies* **1995**, *6*, 489.
- [211] G. Zhang, D. Y. Wang, Z. Z. Gu, J. Hartmann, H. Mohwald, *Chemistry of Materials* **2005**, *17*, 5268.
- [212] I. Horcas, *Rev.Sci.Instrum.* **2007**, *78*.
- [213] S. Hofl, L. Zitzler, T. Hellweg, S. Herminghaus, F. Mugele, *Polymer* **2007**, *48*, 245.
- [214] A. Fernandez-Barbero, A. Fernandez-Nieves, I. Grillo, E. Lopez-Cabarcos, *Physical Review E* **2002**, *66*.
- [215] B. R. Saunders, *Langmuir* **2004**, *20*, 3925.
- [216] B. E. Rodriguez, M. S. Wolfe, M. Fryd, *Macromolecules* **1994**, *27*, 6642.
- [217] M. L. Christensen, K. Keiding, *Colloids and Surfaces a-Physicochemical and Engineering Aspects* **2005**, *252*, 61.
- [218] S. Rimmer, C. Johnson, B. Zhao, J. Collier, L. Gilmore, S. Sabnis, P. Wyman, C. Sammon, N. J. Fullwood, S. MacNeil, *Biomaterials* **2007**, *28*, 5319.
- [219] A. Sosnik, M. V. Sefton, *Biomacromolecules* **2006**, *7*, 331.
- [220] H. Kasgoz, *Polymer Bulletin* **2006**, *56*, 517.
- [221] R. K. Mishra, M. Datt, K. Pal, A. K. Banthia, *Journal of Materials Science-Materials in Medicine* **2008**, *19*, 2275.
- [222] H. Tanaka, *Journal of Polymer Science Part a-Polymer Chemistry* **1979**, *17*, 1239.

- [223] H. Kawaguchi, H. Hoshino, Y. Ohtsuka, *Journal of Applied Polymer Science* **1981**, *26*, 2015.
- [224] R. J. Eldridge, *Abstracts of Papers of the American Chemical Society* **1979**, 31.
- [225] L. H. Zhang, G. S. Kauffman, J. A. Pesti, J. G. Yin, *Journal of Organic Chemistry* **1998**, *63*, 10085.
- [226] R. H. Boutin, G. M. Loudon, *Journal of Organic Chemistry* **1984**, *49*, 4277.
- [227] M. Ghasemi, M. Minier, M. Tatouliau, F. Arefi-Khonsari, *Langmuir* **2007**, *23*, 11554.
- [228] J. H. Moon, J. W. Shin, S. Y. Kim, J. W. Park, *Langmuir* **1996**, *12*, 4621.
- [229] E. S. Matsuo, T. Tanaka, *Nature* **1992**, *358*, 482.
- [230] K. Makino, K. Suzuki, Y. Sakurai, T. Okano, H. Ohshima, *Journal of Colloid and Interface Science* **1995**, *174*, 400.
- [231] A. Fernandez-Nieves, A. Fernandez-Barbero, B. Vincent, F. J. de las Nieves, *Macromolecules* **2000**, *33*, 2114.
- [232] R. Mills, *The Journal of Physical Chemistry* **1973**, *77*, 685.
- [233] K. Makino, J. Hiyoshi, H. Ohshima, *Colloids and Surfaces B: Biointerfaces* **2000**, *19*, 197.
- [234] D. J. Gan, L. A. Lyon, *Journal of the American Chemical Society* **2001**, *123*, 8203.
- [235] I. Berndt, W. Richtering, *Macromolecules* **2003**, *36*, 8780.
- [236] Y. Lu, A. Wittemann, M. Ballauff, M. Drechsler, *Macromolecular Rapid Communications* **2006**, *27*, 1137.
- [237] M. Bradley, B. Vincent, *Langmuir* **2008**, *24*, 2421.
- [238] N. Dingenouts, C. Norhausen, M. Ballauff, *Macromolecules* **1998**, *31*, 8912.
- [239] V. Lapeyre, C. Ancla, B. Catargi, V. Ravaine, *Journal of Colloid and Interface Science* **2008**, *327*, 316.
- [240] X. Li, J. Zuo, Y. L. Guo, X. H. Yuan, *Macromolecules* **2004**, *37*, 10042.
- [241] K. E. Christodoulakis, M. Vamvakaki, *Langmuir* **2009**.
- [242] D. Schmaljohann, *Advanced Drug Delivery Reviews* **2006**, *58*, 1655.
- [243] Q. Wu, Z. Q. Wang, X. F. Kong, X. D. Gu, G. Xue, *Langmuir* **2008**, *24*, 7778.
- [244] J. A. Balmer, S. P. Armes, P. W. Fowler, T. Tarnai, Z. Gaspar, K. A. Murray, N. S. J. Williams, *Langmuir* **2009**, *25*, 5339.
- [245] D. Benoit, E. Harth, P. Fox, R. M. Waymouth, C. J. Hawker, *Macromolecules* **2000**, *33*, 363.
- [246] Y. Miura, K. Miyake, *Journal of Polymer Science Part a-Polymer Chemistry* **2005**, *43*, 6153.
- [247] N. S. DeSilva, I. Ofek, E. C. Crouch, *American Journal of Respiratory Cell and Molecular Biology* **2003**, *29*, 757.
- [248] H. Tokuyama, N. Ishihara, S. Sakohara, *Polymer Bulletin* **2008**, *61*, 399.
- [249] N. Khanduyeva, V. Senkovskyy, T. Beryozkina, M. Horecha, M. Stamm, C. Urich, M. Riede, K. Leo, A. Kiriya, *Journal of the American Chemical Society* **2009**, *131*, 153.

- [250] T. Beryozkina, K. Boyko, N. Khanduyeva, V. Senkovskyy, M. Horecha, U. Oertel, F. Simon, M. Stamm, A. Kiriya, *Angewandte Chemie-International Edition* **2009**, *48*, 2695.
- [251] R. Li, X. L. Yang, G. L. Li, S. N. Li, W. Q. Huang, *Langmuir* **2006**, *22*, 8127.
- [252] S. A. F. Bon, S. Cauvin, P. J. Colver, *Soft Matter* **2007**, *3*, 194.
- [253] S. U. Pickering, *Journal of the Chemical Society* **1907**, *91*, 2001.
- [254] S. Melle, M. Lask, G. G. Fuller, *Langmuir* **2005**, *21*, 2158.
- [255] Y. X. Li, D. P. Yin, Z. Q. Wang, B. Li, G. Xue, *Colloids and Surfaces a-Physicochemical and Engineering Aspects* **2009**, *339*, 100.
- [256] S. Sadasivan, G. B. Sukhorukov, *Journal of Colloid and Interface Science* **2006**, *304*, 437.
- [257] O. J. Cayre, P. F. Noble, V. N. Paunov, *Journal of Materials Chemistry* **2004**, *14*, 3351.
- [258] W. Kangwansupamonkon, C. M. Fellows, D. J. Lamb, R. G. Gilbert, S. Kiatkamjornwong, *Polymer* **2004**, *45*, 5775.
- [259] D. D. Jiang, G. F. Levchik, S. V. Levchik, C. Dick, J. J. Liggat, C. E. Snape, C. A. Wilkie, *Polymer Degradation and Stability* **2000**, *68*, 75.
- [260] B. Jurkowski, B. Jurkowska, **1998**, pp. 135.
- [261] A. Rolland, J. Omullane, P. Goddard, L. Brookman, K. Petrak, *Journal of Applied Polymer Science* **1992**, *44*, 1195.
- [262] F. Ziaee, H. S. Mobarakeh, M. Nekoomanesh, *Polymer Degradation and Stability* **2009**, *94*, 1336.
- [263] M. P. Anachkov, S. K. Rakovsky, G. E. Zaikov, *Journal of Applied Polymer Science* **2007**, *104*, 427.
- [264] X. R. Zeng, T. M. Ko, *Journal of Applied Polymer Science* **1998**, *67*, 2131.
- [265] J. L. Valentin, A. Fernandez-Torres, P. Posadas, A. Marcos-Fernandez, A. Rodriguez, L. Gonzalez, *Journal of Polymer Science Part B-Polymer Physics* **2007**, *45*, 544.
- [266] K. Ishizu, K. Kuwahara, *Journal of Polymer Science Part a-Polymer Chemistry* **1993**, *31*, 661.
- [267] J. Glazer, J. H. Schulman, *Journal of Polymer Science* **1954**, *14*, 169.
- [268] G. J. Liu, Z. Li, X. H. Yan, *Polymer* **2003**, *44*, 7721.
- [269] T. W. Ebbesen, H. J. Lezec, H. F. Ghaemi, T. Thio, P. A. Wolff, *Nature* **1998**, *391*, 667.
- [270] C. Genet, T. W. Ebbesen, *Nature* **2007**, *445*, 39.

Acknowledgements

This work would not have been possible without the support, help and everyday effort of a large number of people.

First of all I highly appreciate Prof. Dr. Manfred Stamm for the opportunity to make my PhD work in IPF and his guidance, advices and countenance throughout this work.

I want to express my heartfelt gratitude to my supervisor Dr. Volodymyr Senkovskyy for his recommendations and for everyday support, for his great effort to make our collaborative work the most enjoyed and efficient as possible. It was an exciting pleasure for me to work with him, whose passion and enthusiastic about the science motivated me to continuously grow in knowledge and experience. I am proud that I had a great opportunity to be advised by wonderful chemist and to learn a lot of him.

I am also grateful to D. Anton Kiriy, he was always open for discussions and new ideas. His wide knowledge, advices and constant encouragement provided a good basis for my dissertation.

This work required a lot of various techniques and equipment. For help with this I would like to show my appreciation to many people working at IPF. I gratefully acknowledge Dr. Petr Formanek who helped me to perform SEM and TEM investigations, Andreas Janke for support in AFM measurements, Dr. Ulrich Örtel who measured and helped in interpretation of UV-vis spectra, Dr. Alla Synytska for Z-potential measurements, Dr. Simona Schwarz, Mandy Mende and Dr. Viktoria Dutschk for assistance in DLS and contact angle measurements, Dr. Konrad Schneider for mechanical experiments, Gudrun Adam for FTIR

spectra measurements, Petra Treppe for GPC and Kerstin Arnhold for TGA analysis of polymers.

I thank to the secretaries of department of Nanostructures Materials Janett Forkel and Claudia Nöh for the excellent assistance in many different ways.

I would like also to thank my friends Dr. Vera Bocharova, Dr. Natalia Khanduyeva, Dr. Roman Tkachov, Dr. Konstantin Demidenok, Ksenia Boyko, Katja Svetushkina and all my colleagues at IPF for cooperation, friendliness and willingness to help.

Especially I would like to thank my husband, Andriy Horechyy, for his endless patience, kindness and understanding. He helped me a lot in my work, supported me wholeheartedly and without his inspiration and regular encouragement it would be much more difficult for me to stay here.

My hearty thanks are to my family in Ukraine, my parents and sister for always being there for me, for their love and worry about me that make me feel close to home wherever I am. To all my friends who strongly believed in my success and supported me in difficult moments.

This research was made possible through the financial support from IPF Dresden and German Research Foundation (Deutsche Forschungsgemeinschaft, SPP 1259/1 and 1259/2 “Intelligente hydrogele”).

LIST OF PUBLICATIONS

1. **Horecha M.**, Senkovskyy V., Schneider K., Kiriy A and Stamm M. Swelling behaviour of PNIPAM-polyisoprene core-shell microgels at surfaces. *Colloid and Polymer Science* **2010**, DOI: 10.1007/s00396-010-2312-9
2. **Horecha M.**, Senkovskyy V., Synytska A., Stamm M., Chervanyov A. and Kiriy A. Ordered surface structures from PNIPAM-based loosely packed microgel particles. *Soft Matter* **2010**, 6, 5980-5992.
3. Tkachov R., Senkovskyy V., Oertel U., **Horecha M.**, Synytska A and Kiriy A. Microparticle-Supported Conjugated Polyelectrolyte Brushes Prepared by Surface-Initiated Kumada Catalyst Transfer Polycondensation for Sensor Application. *Macromolecular Rapid Communications* **2010**, 31, 2146-2150
4. Tkachov R., Senkovskyy V., **Horecha M.**, Oertel U., Stamm M and Kiriy A. Surface-initiated Kumada catalyst-transfer polycondensation of poly(9,9-dioctylfluorene) from organosilica particles: chain-confinement promoted β -phase formation *Chemical Communications* **2010**, 46, 1425-1427
5. Senkovskyy V., Tkachov R., Beryozkina T., Komber H., Oertel U., **Horecha M.**, Bocharova V., Stamm M., Gevorgyan S.A., Krebs F.C. and Kiriy A. "Hairy" Poly(3-hexylthiophene) Particles Prepared via Surface-Initiated Kumada Catalyst-Transfer

- Polycondensation *Journal of the American Chemical Society* **2009**, 131, (45), 16445-16453
6. **Horecha, M.**; Senkovskyy, V.; Stamm, M.; Kiriya, A. One-Pot Synthesis of Thermoresponsive PNIPAM Hydrogel Microcapsules Designed to Function in Apolar Media. *Macromolecules* **2009**, 42, (15), 5811-5817
7. Beryozkina, T.; Boyko, K.; Khanduyeva, N.; Senkovskyy, V.; **Horecha, M.**; Oertel, U.; Simon, F.; Stamm, M.; Kiriya, A. Grafting of Polyfluorene by Surface-Initiated Suzuki Polycondensation. *Angewandte Chemie-International Edition* **2009**, 48, (15), 2695-2698
8. Khanduyeva, N.; Senkovskyy, V.; Beryozkina, T.; **Horecha, M.**; Stamm, M.; Uhrich, C.; Riede, M.; Leo, K.; Kiriya, A. Surface Engineering Using Kumada Catalyst-Transfer Polycondensation (KCTP): Preparation and Structuring of Poly(3-hexylthiophene)-Based Graft Copolymer Brushes. *Journal of the American Chemical Society* **2009**, 131, (1), 153-161

CONTRIBUTION TO THE CONFERENCES

Horecha M., Senkovskyy V., Synytska A., Kiriya A., and Stamm M. *Systems with Inverse-Switching Behavior: Experimental Prove of a Concept*, 239th ACS National Meeting and Exposition, San Francisco CA, 2010.

Synytska A., Ionov L., Berger S., **Horecha M.**, Senkovskyy V., Kiriya A., Stamm M. *Stimuli-responsive hybrid particles with polymer*

brushes 238th ACS National Meeting, Washington, DC, August 16-20, 2009

Horecha, M.; Senkovskyy, V.; Kiriya, A.; Stamm, M. *Synthesis and Characterization of Hydrogel Microcapsules and Microparticles stable in organic solvents*, 8th International Conference on Advanced Polymers via Macromolecular Engineering, Dresden, 2009.

Horecha, M.; Senkovskyy, V.; Stamm, M. *Atomic Force Microscopy Investigation of the Surface-Immobilized Hydrogel Particles*, Workshop, SPP 1259 "Intelligente Hydrogele", Karlsruhe, 2009.

Horecha, M.; Senkovskyy, V.; Kiriya, A.; Stamm, M. *Preparation of Hydrogel Microcapsules and Microparticles stable in organic solvents*, *Frontiers in Polymer Science*, Mainz, 2009.

Senkovskyy, V.; **Horecha, M.;** Stamm, M. *Synthesis of the Core-Shell Hydrogel Particles*, Workshop SPP 1259 "Intelligente Hydrogele", Aachen, 2009.

Senkovskyy, V.; **Horecha, M.;** Stamm, M. *Coatings with Inverse Switching Behavior: New Application of Core-Shell Hydrogel Particles*, Workshop SPP 1259 "Intelligente Hydrogele", Frankfurt am Main, 2008.

Senkovskyy, V.; **Horecha, M.;** Stamm, M. *Coatings with Inverse Switching Behavior: New Application of Core-Shell Hydrogel Particles*, Workshop, SPP 1259 "Intelligente Hydrogele", Aachen, 2007; Aachen, 2007.

CURRICULUM VITAE

MARTA HORECHA

PERSONALIEN	
Name	Horecha (geboren Okpysh)
Vorname	Marta
Geburtsdatum/ -ort	04. August 1976 in Lviv, Ukraine
Staatsangehörigkeit	Ukraine
Familienstand	Verheiratet

AUSBILDUNG	ZEITRAUM
Studium	
Technische Universität Dresden, Fakultät Mathematik und Naturwissenschaft Institut für Polymerforschung, Dresden	Promotion Studium im Fach Polymerchemie, Betreuer: Prof. Dr. M. Stamm, Gastwissenschaftlerin 2006 - 2010
Leder Fabrik „Yurok Plus GmbH“, Lviv, Ukraine	Finanzmanagerin 2000-2006
Fakultät Wirtschaftswissenschaft, Nationale Universität “Lvivska Polytechnika“, Ukraine	Weiterbildung im Fach Ökonomie, Master/Diplom. 1999-2001
Abteilung Physikalische Chemie, Lviver Staatliche Universität, Ukraine	Promotion Studium in Fach Physikalische Chemie 1998 - 1999
Lviver Staatliche Universität, Ukraine, Fakultät Chemie.	Studium im Fach Chemie, Master/Diplom mit Auszeichnung 1993 - 1998
Schulbildung	
Allgemeinbildende Schule No78 Lviv, Ukraine	1983 - 1993

Versicherung

Hiermit versichere ich, dass ich die vorliegende Arbeit ohne unzulässige Hilfe Dritter und ohne Benutzung anderer als der angegebenen Hilfsmittel angefertigt habe; die aus fremden Quellen direkt oder indirekt übernommenen Gedanken sind als solche kenntlich gemacht. Die Arbeit wurde bisher weder im Inland noch im Ausland in gleicher oder ähnlicher Form einer anderen Prüfungsbehörde vorgelegt.

Die vorliegende Arbeit wurde unter der wissenschaftlichen Betreuung von Prof. Dr. Manfred Stamm an dem Leibniz-Institut für Polymerforschung Dresden e.V. angefertigt. Keine frühere erfolglose Promotionsverfahren statt gefunden haben. Die Promotionsordnung der Technischen Universität Dresden der Fakultät Mathematik und Naturwissenschaft erkenne ich an.

Dresden,.....

Marta Horecha

